



HAL
open science

VEGA 1 and VEGA 2 entry probes: An investigation of local UV absorption (220-400 nm) in the atmosphere of Venus (SO₂ aerosols, cloud structure)

Jean-Loup Bertaux, Thomas Widemann, Alain Hauchecorne, V. Moroz, A. Ekonomov

► To cite this version:

Jean-Loup Bertaux, Thomas Widemann, Alain Hauchecorne, V. Moroz, A. Ekonomov. VEGA 1 and VEGA 2 entry probes: An investigation of local UV absorption (220-400 nm) in the atmosphere of Venus (SO₂ aerosols, cloud structure). *Journal of Geophysical Research. Planets*, 1996, 101 (E5), pp.12709-12745. 10.1029/96JE00466. insu-03132206

HAL Id: insu-03132206

<https://insu.hal.science/insu-03132206>

Submitted on 5 Feb 2021

HAL is a multi-disciplinary open access archive for the deposit and dissemination of scientific research documents, whether they are published or not. The documents may come from teaching and research institutions in France or abroad, or from public or private research centers.

L'archive ouverte pluridisciplinaire **HAL**, est destinée au dépôt et à la diffusion de documents scientifiques de niveau recherche, publiés ou non, émanant des établissements d'enseignement et de recherche français ou étrangers, des laboratoires publics ou privés.

VEGA 1 and VEGA 2 entry probes: An investigation of local UV absorption (220–400 nm) in the atmosphere of Venus (SO₂, aerosols, cloud structure)

Jean-Loup Bertaux, Thomas Widemann, and Alain Hauchecorne

Service d'Aéronomie du Centre National de la Recherche Scientifique, Verrières-le-Buisson, France

V. I. Moroz and A. P. Ekonomov

Space Research Institute, Moscow, Russia

Abstract. In 1985 the VEGA 1 and VEGA 2 spacecraft dropped two descent probes into the nightside of Venus. On board was the French-Russian ISAV ultraviolet spectroscopy experiment, consisting of a UV light source absorbed by atmospheric constituents circulating freely into a tube attached outside the pressurized modules. ISAV generated a wealth of absorption spectra in the 220- to 400-nm range with an unprecedented vertical resolution (60–170 m) from 62 km of altitude down to the ground. On the basis of known instrument properties and a careful examination of the light curves recorded in 13 wavelength intervals in the UV, we show that most of the recorded differential absorption (at each wavelength with respect to 394 nm) can be explained by a combination of gaseous SO₂ absorption and absorption by aerosols deposited on the mirrors during the crossing of Venus' lower cloud. The spectral signature of this absorber, termed X, was obtained, thanks to an unexpected shock on VEGA 1 which removed this absorber from the mirrors at 18 km of altitude. The UV spectral signature of X resembles that of croconic acid, C₅O₅H₂, whose absorbing power as a contaminant of H₂SO₄ droplets at 2.5% dilution is compatible with the observations. However, the nonidentity of the spectral signature, together with stability arguments, makes this identification less plausible. Whatever its nature, the relevance of this new absorber X is discussed in connection with the albedo of Venus and the IR variable leak windows. If this absorber X detected by ISAV in the lower cloud were also present in the upper cloud, it would be a good candidate to explain the UV part ($\lambda < 400$ nm) of the Venus albedo. Three layers of absorbing material, called b, c, and d, are identified in the data of both ISAV 1 and 2 in the altitude range 49–43 km. The higher layer b is inside the lower cloud identified by the nephelometer of Pioneer Venus, while the two other layers are well below the lower cloud boundary as measured by Pioneer Venus. The SO₂ profile (from 60 km down to 10 km) is characterized for ISAV 1 by a double peak of the mixing ratio (150 ppmv at 51.5 km, 125 ppmv at 42.5 km) separated by a deep trough at 30 ppmv at 45.6 km. For ISAV 2 there is a single peak at 43 km. Both SO₂ profiles are quite compatible with recent ground-based measurements, showing 130 ± 40 ppmv in the altitude range of 35–45 km [Bézard *et al.*, 1993]. Below the clouds the measured SO₂ mixing ratio decreases steadily on both probes, down to 25 ± 2 ppmv at 10 km for ISAV 1, which is lower than previously reported values from gas chromatograph measurements (shown to be incompatible with ISAV measurements). The variation of SO₂ mixing ratio with altitude implies a strong vertical transport which is given as a function of altitude, showing the source and sink regions of SO₂ from 10 to 60 km of altitude. These data should impose severe constraints on future chemical models of the atmosphere of Venus, occurring after volcanic episodes or impact cratering events. The total SO₂ column density (0–60 km) was measured to be 4×10^{22} molecules cm⁻² or 4.2 g cm⁻², a factor of 5 below previous estimates. With an average reaction rate of 4.6×10^{10} molecules cm⁻² s⁻¹ with calcite, CaCO₃, estimated by Fegley and Prinn [1989], it would take only 27,000 years to get rid of SO₂ and associated H₂SO₄ droplets if calcite were present all over the surface of Venus. Therefore SO₂ and its associated ubiquitous cloud cover may only be transient phenomena in the life of Venus.

1. Introduction

Before their encounter with comet Halley in March 1986, the two Soviet interplanetary spacecraft VEGA 1 and VEGA

2 flew by planet Venus in June 1985. They released two floating balloons and two atmospheric probes which were designed to conduct both atmospheric in situ measurements and soil analysis, similar to previous Venera missions. The two probes were identical, and each carried a new type of instrument, the ISAV, a spectrometer designed to measure the local atmospheric absorption and its detailed spectrum in the UV range (220–

Copyright 1996 by the American Geophysical Union.

Paper number 96JE00466.

0148-0227/96/96JE-00466\$09.00

400 nm). In the following, ISAV 1 designates the instrument on board the probe launched from VEGA 1, and correspondingly, ISAV 2 was on the probe launched from Vega 2.

The flyby geometry at Venus was constrained by the desire to encounter comet Halley later on, and as a result, the atmospheric probes were released on the nightside of Venus. This was an ideal situation to conduct an "active spectroscopy" experiment like ISAV, in which the UV spectrum of an artificial light source was continuously measured through a gas cell of 1.70-m path length, in which was circulated the ambient atmosphere all along the descent down to the ground.

Useful measurements were collected from 62.5 km altitude down to the ground, with an unprecedented vertical resolution (from 40 to 180 m), thanks to the relatively high sampling rate (one spectrum every 4 s). This was the first time such an instrument was flown in an extraterrestrial planet, and we do not expect to have new opportunities to repeat it in the foreseeable future. Among other reasons, this character of uniqueness compels us to present a critical analysis of the actual data and our interpretation of these data in terms of vertical distribution of UV gaseous absorption (SO_2 and other gases) and aerosol absorption spectrum.

A first analysis of these data was published earlier in the Soviet literature [Bertaux *et al.*, 1987] (also with an uncontrolled translation in English as indicated by the orthograph of the authors names, Berto *et al.*, in which the local UV absorption was assigned to SO_2 (which was expected to be significant) and tentatively to another gas, elemental sulfur, S_8 , because SO_2 alone could not account for the observed spectral shape of the absorption.

In this paper we present a new analysis of the ISAV 1 and ISAV 2 data, characterized by the following changes and improvements.

1. We have a better understanding of the way the instrument behaved in flight, and in particular, we capitalized on a serendipitous event during ISAV 1 descent: a strong mechanical shock was synchronous of a sharp decrease of absorption (increase of received light), that we interpret as the result of the detachment of aerosol particles (or their contaminant) from the mirrors of the instrument, where they deposited during the crossing of the Venus clouds.

2. We disregard S_8 as an important absorber because the quantity that was inferred in the early analysis would imply an absorption of solar light in the blue part of the spectrum (400–500 nm), incompatible with previous measurements of the vertical profile by Venera 11 and 12.

3. The method of analysis was also modified. Instead of trying to obtain for each spectrum a global fit by a combination of several absorbers altogether, we preferred to take advantage of the fact that each absorber considered has a strong spectral signature, with some wavelengths being strongly absorbed and others not at all. In such a case, it was found more practical to determine the quantity of each absorber in successive steps, one after the other (for each altitude where a spectrum was recorded). As will be explained further, we will rely more on spectral differential absorption (variation of absorption with wavelength) than on the absolute value of the absorption, because of some instrumental difficulties.

As a result of these new efforts, we present in this paper more complete and accurate vertical profiles of SO_2 than in our earlier paper [Bertaux *et al.*, 1987], as well as a somewhat detailed discussion about the rapidly increasing absorption during the crossing of the lower cloud deck (52–47 km). We

interpret this feature as due to the deposition of cloud particles on the mirrors of the absorption cell, containing a contaminant for which we determine the UV absorption spectral signature. The results that we present here are quite relevant to a number of important new features which have emerged in the overall knowledge of planet Venus since 1987.

1. Hartley *et al.* [1989] have proposed that croconic acid, $\text{C}_5\text{O}_5\text{H}_2$, a polymer of carbon monoxide, if diluted as a minor contaminant in sulfuric acid droplets, could explain the spectral albedo of Venus in the wavelength region 350–450 nm. Indeed we found in ISAV data an aerosol contaminant with a UV spectral signature bearing some resemblance to that of croconic acid. However, it is fair to say here that there are arguments against the existence of croconic acid in the atmosphere of Venus.

2. The superb radar mapping of Magellan revealed clear signs of past volcanic activity but, to the best of our knowledge, no signs of present volcanic activity. The concentration of SO_2 near the ground of Venus is a crucial test of a state of equilibrium or nonequilibrium in the chemical reactions of SO_2 with the rocks (CaCO_3), a nonequilibrium value being potential evidence for injection of SO_2 in the atmosphere through recent volcanic activity or impact cratering.

3. The discovery of near-infrared (NIR) windows in the nightside of Venus by Allen and Crawford [1984] allows scientists to probe the gaseous chemical composition below the clouds, as discussed extensively by Pollack *et al.* [1993], and useful comparisons can be made with the in situ ISAV measurements. In addition, it is now generally admitted that the leakage of IR thermal emission generated below the clouds from some areas of the cloud cover is connected to a decrease of the lower cloud optical thickness or number of particles [Kamp and Taylor, 1990; Carlson *et al.*, 1991], in an altitude region where most of the aerosols' UV absorption was collected by ISAV also on the nightside of Venus.

We are aware that some of the results that we present here rely on some assumptions that we had to make about the behavior of the instrument (and the descent probe) during its course to the ground. This is not a unique situation in space research, where it is not trivial to repeat an experiment. However, there is a great similarity between the results of ISAV 1 and ISAV 2, which makes us confident that our assumptions are quite reasonable. In any case, we present both the primary data and our interpretations, along with a detailed discussion of the assumptions involved, in such a way that the readers may be able to establish their own opinions about the data and our conclusions.

Section 2 contains a somewhat detailed description of the instrument, in order that the reader may have a better understanding of the data collected by both instruments. The (almost) raw data are presented in section 3, in the form of light curves for each wavelength (artificial light intensity recorded as a function of time during the descent). A detailed discussion of these light curves allows one to discriminate between purely instrumental effects and atmospheric effects (section 3). Various atmospheric regions linked mainly to the cloud structure can be identified on the basis of this discussion, and the ISAV 1 shock event is discussed. In section 5, an estimate is made of the quantity of H_2SO_4 droplets which could have been accumulated on the mirrors during the descent, compatible with the measured absorption, and it is shown that croconic acid is a good candidate, as far as its absorbing power is concerned. In section 6 the connection of ISAV UV X absorber collected in

the aerosols, with the UV albedo, UV markings, and near-IR leakage of the upper atmosphere is discussed. Section 7 is devoted to a discussion of the vertical structure comparison between ISAV 1 and ISAV 2. Some comparisons with other experiments on Pioneer Venus, Venera, and VEGA descent probes are spread over sections 5–7. Finally, section 8 is devoted to SO₂ results: structure of the vertical profile, estimate of vertical transport flux, equilibrium with surface reactions, and relevance to recent volcanism.

2. ISAV Instrument and Mission Profile

Concept of ISAV

A first version of the ISAV spectrometer was designed in the mid-1970s to fly on board a large balloon floating at an altitude of 54 km or 500-mbar pressure for several days, in order to analyze the solar radiation at this altitude in the spectral range 200–800 nm. This large balloon, designed by Centre National d'Etudes Spatiales (CNES), was an important item of the so-called Venera 83 mission, but it was canceled in 1981 when Halley's comet became the prime target of the space mission, renamed Venera-Halley or VEGA. Instead of two large balloons and two orbiters, the new mission consisted of two flyby probes, taking advantage of the gravity of Venus for a later encounter with comet Halley and dropping two descent probes for the analysis of the atmosphere and the soil of Venus, and two small balloons to study dynamics and properties of the middle cloud layer.

The geometry of the VEGA flyby probes of Venus on their trajectory to Halley's comet in 1985 imposed a flight over the night hemisphere of Venus, and the descent probes were launched in dark night conditions. It was therefore no longer possible to analyze the solar radiation, and therefore the instrument was completely redesigned to analyze the ultraviolet absorption of atmospheric gaseous constituents with "active spectrometry." This term means that the instruments, diving into the nightside of the atmosphere, were equipped with an artificial UV light source. A cylindrical tube, through which the atmospheric gases would flow freely during the descent, was attached outside the pressurized module [Bertaux *et al.*, 1987], and the absorption of the artificial UV light would be recorded as a function of altitude and wavelength in the range 200–400 nm. This method of active spectrometry was used for the first time during this VEGA mission. Using a path length of the order of 1 m, instead of several kilometers when the solar radiation is used, this method of measuring the local absorption is obviously less sensitive, but in return, can measure strong absorbers (particularly in the UV) at depths where the solar radiation is totally extinguished, and allows a much finer vertical resolution of the absorbers.

The primary scientific objective of the experiment was the vertical distribution of atmospheric gases characterized by a strong absorption in the range 200–400 nm, i.e., SO₂ first identified in 1979 [Barker, 1979] and possibly other constituents. Before the 1985 flight, it was assumed that in this spectral region, SO₂ would be the main absorbing gas in the atmosphere of Venus. Preflight calibrations were then conducted with SO₂. However, the spectral range was also chosen to detect and possibly identify the so-called UV absorber, i.e., the substance (or any group of substances) responsible for the single albedo decrease with wavelength at various altitudes, resulting in the unexplained spectral dependence of Venus spherical albedo from $\lambda \approx 320$ to 500 nm.

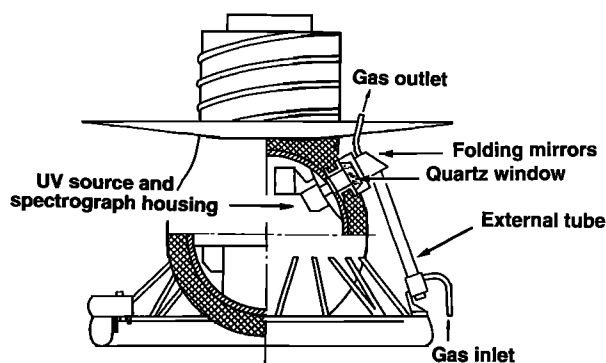


Figure 1. The ISAV instrument mounted on the VEGA 1 and VEGA 2 Venusian landers of the joint Venus-Halley Soviet mission of 1985–1986 were operated from an altitude of 64 km to the ground level, on the night hemisphere of the planet. The instrument consisted of a UV grating spectrometer operating in the range 220–400 nm with an onboard ultraviolet source, a xenon flash. The light, originating from the pressurized, thermally insulated descent module, was directed through a 4-cm quartz window into an external, 85.0 × 5.0 cm cylindrical tube in which atmospheric gases circulated freely once the lower thermal shield of the probe was released after main parachute deployment. Atmospheric gases and aerosols penetrated from an intake located at its base, with its opening directed vertically downward. The hydrodynamic pressure gradient between inlet and outlet pipes allowed gases to cross the tube at the same velocity as the descent probe.

The ISAV spectrometer was a part of the optical instrumentation flown on board the two VEGA descending probes, together with the ISAV-A equipment dedicated to the aerosol cloud particles, results of which have been reported elsewhere [Moshkin *et al.*, 1986; Gnedych *et al.*, 1987]. In previously published papers [Bertaux *et al.*, 1986, 1987], the ISAV spectrometer was referred as ISAV-S; here we will refer as ISAV 1 and ISAV 2, the two UV instruments doing local absorption spectral measurements, launched from VEGA 1 and VEGA 2, respectively.

Experimental Flight Conditions

Both landers dropped in the atmosphere during the VEGA 1 and VEGA 2 flybys were insulated by two heat protection hemispheres. Their overall design was similar to Venera 13 and Venera 14 landers which flew in March 1982 (Figure 1). Each shield had a diameter of 2.4 m and consisted of two hemispheres nonhermetically joined. The release of the landers protected inside followed a complex sequence described elsewhere with more details [Deryugin *et al.*, 1987; Moroz, 1987]. At an altitude of 65 km, a pilot parachute slowed the probe and, after pyrotechnical separation, the aft hemisphere was moved upward away from the lander at an altitude of 64.5 km. In this aft hemisphere were located the crucial deployment system of the Venus balloons and their scientific equipment. Each balloon was programmed to release itself from the upper hemisphere, to deploy a two-stage parachute, then to unfold and inflate.

Simultaneously, the main braking parachute of the probe was deployed to decelerate the remaining part of the lander. Four seconds later, at an altitude of 64.2 km, the inferior hemisphere of the thermal shield was finally jettisoned. This altitude corresponds to the starting of data acquisition by

Table 1. Chronology of Descent Phases for VEGA 1 and VEGA 2 Venus Landers With Events Related to ISAV Instrument Acquisition

Mission	VEGA 1	VEGA 2
Launch	Dec. 15, 1984	Dec. 21, 1984
Venus encounter	June 11, 1985	June 15, 1985
Atmospheric entry (Moscow time)	0459:49	0459:30
Incidence angle	18.23°	19.08°
Entry velocity	10.75 km s ⁻¹	10.80 km s ⁻¹
Begin parachute descent	0500:27	0500:05
Release of upper hemisphere, deployment of braking parachute		
Time	0500:38	0500:16
Altitude	64.5 km	64.5 km
Release of lower hemisphere	0500:42	0500:20
Begin ISAV acquisition	64.23 km	64.23 km
Release of braking parachute	0509:37	0509:15
Begin aerobraking	47.00 km	47.00 km
Landing	0602:54	0600:50
Landing site		
Latitude	7.5°N	8.5°S
Longitude	177.7°	164.5°
Altitude	-0.6 km	+0.1 km
Pressure	95 atm	91 atm
Temperature	740 K	736 K
Solar zenith angle z_0	169.3°	164.5°

Altitudes are calculated with reference to the mean planetary radius. The landing site altitude must be subtracted to retrieve the absolute probe altitude to the ground [adapted from *Deryugin et al., 1987*].

ISAV instruments, though they were switched on 40 s before the bottom shield was jettisoned. It also determines the altitude at which atmospheric gases start flowing through the external tube once their bottom admission pipe was exposed. Then, 9 min later, at an altitude of 47.0 km, in a sequence similar to many previous Soviet Venera missions and also to Pioneer-Venus large probe operations in 1978, the main parachute was released (Table 1). The landers started their free fall under aerobraking conditions, controlled with drag devices to minimize vibrations and spin and to ensure stability. A toroidal

system of the same design as Venera 13 and Venera 14 absorbed the impact on landing [*Deryugin et al., 1987*].

In the following sections, ISAV 1 designates the ISAV instrument on board the lander released by VEGA 1, or lander 1, and ISAV 2 the ISAV instrument on board the lander released by VEGA 2, or lander 2. Flight characteristics for both descent modules and landing sites are summarized in Table 1. Landing sites are shown in Figure 2.

ISAV Parts

Optical layout. The grating spectrometer of ISAV, the ultraviolet source, the 512-pixel detector, and its proximity electronics were located inside the pressurized section of the landers, heavily thermally insulated (Figure 1). In contrast, the external tube through which the atmosphere of Venus was forced to circulate and acting as the absorption cell was outside the pressurized section, and a thick quartz window was integrated into the container structure to let the light in and out (Figure 3). The UV source was a Soviet-made xenon flashlamp of the type ISK-20 designed for commercial stroboscopic equipment, operated at 100 flashes/s. The xenon was chosen for its strong ultraviolet emission lines in the range 200–400 nm (mainly 247, 253, 260.5, 311, and 365 nm) in addition to a continuum emitted by the plasma at a temperature of 10,000 K, both to be absorbed by atmospheric constituents flowing through the external tube. A small diaphragm was placed in front of the flash light, and the beam was collected by a 25-mm quartz objective lens to form an almost parallel beam of 20 mm diameter. After crossing the 4-cm-thick quartz window, this beam was reflected by a first plane mirror ($3.4 \times 2.3 \text{ cm}^2$) along the external tube opposite to the flow of atmospheric gas and down to a concave spherical mirror. There the light was reflected back along the tube to another plane mirror adjacent to the first one, forming also a slight, $2^\circ 9'$ angle with the normal to the beam.

The diaphragm was conjugated through the quartz lens to the spherical mirror located at the bottom end of the external tube, in a quasi-Littrow optical layout (Figure 3). The light

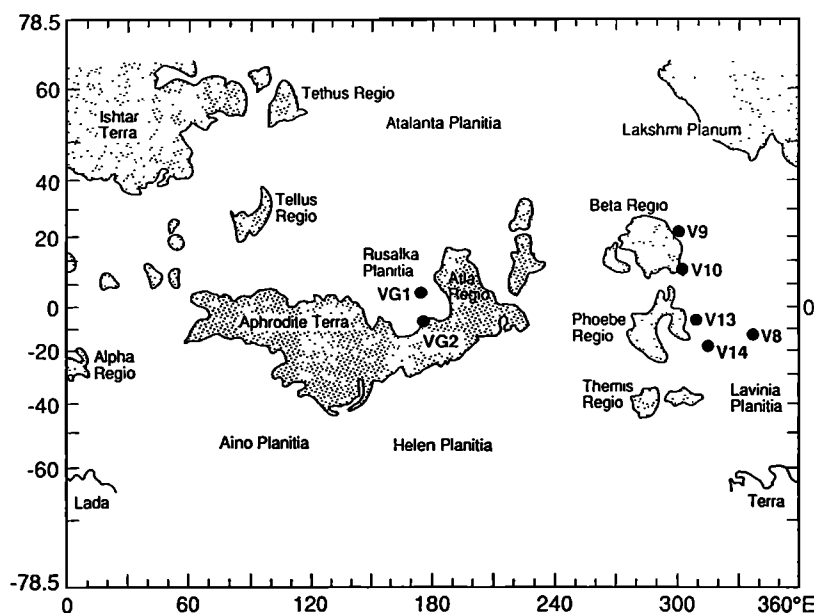


Figure 2. Landing sites for VEGA 1 (177.7°, 7.5°N) and VEGA 2 (164.5°, 8.5°S) Venusian landers (VG1 and VG2). The horizontal distance between the two probes is 2100 km [after *Weitz and Basilevsky, 1993*].

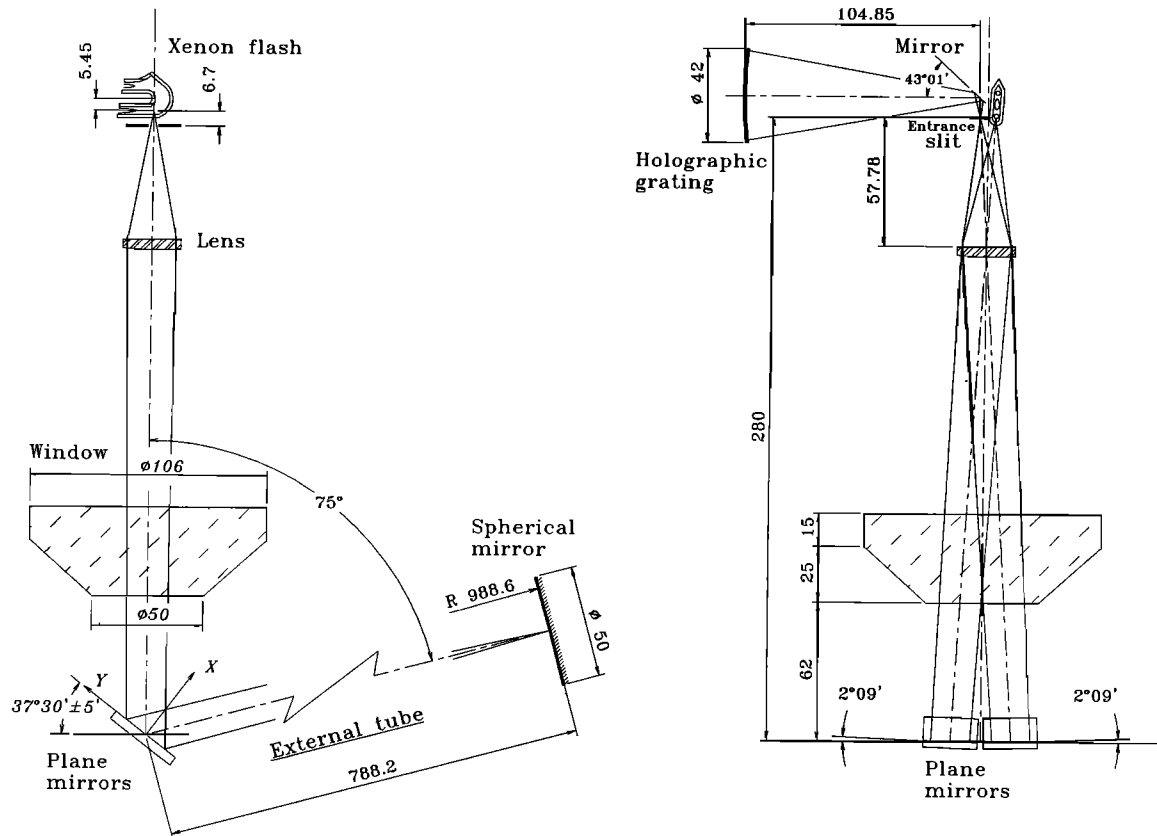


Figure 3. Optical layout of ISAV spectrometer, quartz window, and optical path in the external tube. The UV light is directed from the pressurized vessel through a thick quartz window into the external tube. A spherical, 5-cm-diameter mirror is located near the tube lower end. After absorption by atmospheric constituents in the range 200–400 nm, the beam is redirected into the pressurized module through the quartz window with a plane mirror, to the entrance slit of the grating spectrograph. The total surface of mirrors exposed to atmospheric flow is 35 cm², and the optical path length for absorption is 170 cm. In the “short spectra” survey mode, detector pixels are summed by groups of 32 consecutive pixels and read every 4 s, at a coarse spectral resolution but high vertical resolution (170–65 m).

reflected by the second plane mirror forming the slight angle 2°9' with the outgoing beam, crossed the quartz window inward and was focused by the same quartz objective lens to the entrance slit of the spectrograph. The entrance slit of the spectrograph is 0.02 × 2 mm², and the optical layout magnifies 10-fold the UV flash diaphragm. Inside the spectrograph a small plane mirror deflected the light to a 475 grooves/mm spherical concave holographic diffraction grating designed by C. Taulemesse at Service d'Aéronomie and made by Jobin et Yvon to provide a spectrum of the entrance slit with a good resolution between 200 and 400 nm on the flat area of the multipixel detector described below.

External tube. The external tube consisted of a cylindrical, 85-cm-long, 5-cm-wide tube attached to the pressurized module and exposed to atmospheric conditions. An admission pipe of 16 mm diameter, directed vertically downward, is located at the bottom end of the external tube close to the spherical mirror (Figure 1). It has an inner diameter of 27.5 mm. Atmospheric gases flow through the tube during the descent by differential hydrodynamic pressure and are evacuated through an outlet of the same size at the top end near the two plane mirrors. Light from the ultraviolet light is reflected at the bottom end of the tube, close to the admission pipe, and runs twice the distance between the spherical and the plane mirrors

before being directed back to the spectrograph through the quartz window inside the pressurized vessel. The length of “useful” optical path measuring ultraviolet atmospheric absorption is then 2 × 85 = 170 cm.

The opening of the gas intake (admission pipe) was located in such a way that, in principle, materials outgassed by the disintegration of the heat shield of the descending probe could not enter the cell of the system. The outlet pipe of the cell was located in the low-pressure region behind the aerodynamic draft of the descending probe. As measured by aerodynamic tests in a wind tunnel and on a descending craft, the gas velocity through the cell is about 1 m/s, and accordingly, the time of gas renewal in the absorption cell is about 1 s.

Detector. The detector chip was a unidimensional array of 512 photodiodes (or pixels). Each photodiode had a size 2.5 × 0.025 mm² fitted as the geometric image of the entrance slit of the spectrograph after its reflection on the holographic grating. The physical length of the detector was 12.8 mm in the grating focal plane. The barrette readout frequency was 10 Hz, corresponding to light received from 10 consecutive flashes, as the UV flash was operated as a succession of 6 μs impulses emitted at a frequency of 100 Hz. Each photodiode readout was made through a capacitor, and the corresponding voltage was pro-

Table 2. Operational Description of Survey (Short Spectra) and High-Resolution (Long Spectra) Acquisition Modes for ISAV 1 and ISAV 2 Experiments on Board VEGA 1 and VEGA 2 Landers

Period	UV Flash Period, ms	Acquisition Mode 1	Acquisition Mode 2	Spectral Resolution
<i>VEGA 1 and ISAV 2</i>				
Group of 45 short spectra of 4-s exposure on a time interval of $45 \times 4 = 180$ s (3 min). At the end of each period, 20 s of telemetry; total of period + telemetry = 200 s.	10	Three cycles of 15 short spectra corresponding to one long spectrum; 1 cycle = $15 \times 4 = 60$ s; 45 short spectra and three long spectra per period.	Five cycles of nine short spectra corresponding to one long spectrum; 1 cycle = $9 \times 4 = 36$ s; 45 short spectra and five long spectra per period.	Each spectral resolution element includes $10 \times 60 = 600$ (mode 1) or $10 \times 36 = 360$ (mode 2) exposure readouts for long spectra, and $10 \times 4 = 40$ readouts of 16 groups of 32 pixels for short spectra in both mode.
<i>VEGA 2 and ISAV 2</i>				
Same	10	same	same	same
		ISAV 1	ISAV 2	
Number of short spectra		584	594	
Unused short spectra		1–7	1–6	
Reference short spectrum		8	7	
Remaining short spectra		576	587	

portional to the number of photoelectrons created inside the diode since the last readout.

Each readout, converted in volts, was directed through a sampling/holding system scheme to the 12-bit analog-to-digital converter (ADC) input and next to the data processing and storage electronics, controlled by an onboard microprocessor similar to a RCA 1804. Encapsulated under vacuum conditions, the array of photodiodes was cooled by a Peltier junction at its operating temperature of -20°C in order to reduce the dark current. The hot end of the Peltier cooler was held at a constant temperature by heat transfer into a liquefaction heat accumulator, a salt of $\text{LiNO}_3 \cdot 3\text{H}_2\text{O}$ with a melting temperature of about 30°C .

Data acquisition sequence. The high data rate output from the detector ($12 \times 512 \times 10 = 61.4$ kbits/s) was not possible to be transmitted to the ground, and two data compression schemes were implemented in parallel within the software of the microprocessor. In one mode, all spectra were added together, with one memory for each of the 512 pixels, during a specified time (60 s above 25 km, 36 s below 25 km, the altitude at which some other instruments were no longer operated and more telemetry was available). In this “high-spectral resolution mode,” a full spectrum between 200 and 400 nm of the xenon light attenuated by absorption in the cell was obtained with a moderate vertical resolution depending on the vertical velocity (and hence the altitude), and ranging from 0.6 to 2.3 km. Each full spectrum was the average of 600 or 360 individual spectra, the digital data being transmitted on 16 bits per spectral pixel, 4 bits for the order and 12 bits for the mantissa. At the same time, the same digital numbers coming out from the ADC were also summed in a different scheme. The numerical integration time was only 4 s, providing a much better vertical resolution (from 40 to 180 m, depending on the altitude), at the expense of a much coarser spectral resolution, since blocks of 32 consecutive spectral pixels were added together to give 16 spectral sampling elements, of each 12.5-nm bandwidth between 200 and 400 nm.

Those survey spectra were also called “short spectra” for their few resolution elements. (Actually only 14 are useful,

since there was no light from the xenon flash in the range 200–212.5 nm and very little in the range 212.5–225 nm). The characteristics of the two different modes are summarized in Table 2.

Every 200 s the flash lamp was stopped for about 20 s, during which the microprocessor organized a data package for sending to the telemetry system of the lander, containing three (or five below 25 km) full spectra and 45 “survey mode” spectra. Then the flash lamp was reactivated, and the data acquisition scheme was repeated, until several minutes after the lander did touch the ground. In the present paper, we focus essentially on the “survey” mode spectra because several experimental features, which deviated from an expected nominal behavior, are easier to understand with the high vertical (and time) resolution of this survey mode, as will be explained in the next section.

Instrumental noise. Here we discuss several contributors to the instrumental noise and indicate briefly how it was possible to get rid of most of them.

Shot noise: According to preflight calibrations of the detectors, one unit of the ADC output (one digital number (DN)) for a single readout corresponds to about 10^4 electrons created in the photodiode. Therefore the electron shot noise for a signal giving a reading of n DN is $100 n^{1/2}$. Since the maximum level of n was $2^{12} = 4096$, the maximum electron shot noise was 6400, always less than 1 DN, to be compared to a typical signal of several hundreds of DN. The shot noise is therefore negligible.

Dark current: For an integration time of 0.1 s and an operating temperature of the detector of -20°C maintained by the Peltier cooler and the associated phase-change chemical reservoir of $\text{LiNO}_3 \cdot 3\text{H}_2\text{O}$, the Dark Current was known to be also smaller than 1 DN. However, a “zero” voltage offset was provided to the reading electronics of the detectors, in such a way that in the absence of any light, the output voltage was still well above the zero voltage level of the ADC, to provide only positive DN readings.

Spectral fixed pattern noise: The most obvious effect in the raw data (not shown here) comes from the fact that even

and odd spectral pixels have completely separated driving electronics, with different zero offsets and gains. An intercalibration of odd and even pixels can be made from the raw data but will not be discussed here, since we concentrate on the 16 spectral bins, in which an average of odd and even pixels is obtained.

Still, when there was no more light coming to the detector after touch down, there were small and systematic differences between the levels of the 16 spectral bins representing differences of dark current + offset levels. An average of several “survey mode” spectra acquired after touch down were therefore subtracted from all the data, leveling off the small differences along one survey mode spectra, and taking care of the dark current + offset correction to a first approximation.

Time fixed pattern noise: More surprising was the finding that the average level of one survey mode spectrum was displaying recurrent time variations, even when no more light was coming to the detector after touch down. This was traced back to a periodic variation of the actual voltage of the reference zero level of the ADC, linked to the various blocks of RAM memory activated in turn during the data acquisition and summing processes. The spectral bin dedicated to 200–212.5 nm, receiving no light from the flash lamp, displayed all along the descent such a periodic variation. It was used to correct for the above mentioned effect by subtracting its value from all the other spectral bins, spectrum by spectrum.

Once all these raw data corrections were made, the data became very smooth, as demonstrated by the small scattering of points representing the variations as a function of time of the light recorded within each spectral bin, forming a set of 16 “curves of light” for each ISAV, which are displayed in Figures 5 and 6 and will serve as the basis of our analysis and understanding of the experiment throughout the whole atmosphere of Venus below 64 km.

3. Light Curves

Behavior

A total of 584 short spectra were acquired for ISAV 1 and 594 for ISAV 2 during the flights, at a constant rate of one every 4 s (except for a small interruption every 200 s for 20 s). The signal does not raise to a satisfactory level before the eighth spectrum of ISAV 1, and the seventh spectrum of ISAV 2, so the total number of exploitable spectra is 576 (ISAV 1) and 587 (ISAV 2) (Table 2). Practically, the signal emitted by the ultraviolet source disappears below 6–8 km and is not exploited below. The pixel values below these altitudes were used to determine the noise pattern for every pixel.

The altitude in the atmosphere between two low-resolution spectra varies from 170 m initially to 40 m according to the variable vertical descent velocity. This vertical resolution has never been reached in previous in situ analyses of gaseous absorbers in Venus or any planetary atmosphere. The altitude in the atmosphere of Venus was related to the time, thanks to the descent profile determined for Vega 2 by *Linkin et al.* [1987] and assumed to be identical for Vega 1 as a function of descent time.

We define as λ_j the central wavelength of each group of 32 pixels in the low-resolution mode. The first spectral bin centered on 206.25 nm, grouping pixels 0–31 and ranging from 200.0 to 212.5 nm, receives no light from the xenon flash and is used as a reference for dark current and fixed pattern noise correction. The second spectral bin (pixels 32–63) contains

little signal and, in practice, is discarded in the analysis, which we start at $\lambda_3 = 231.25$ nm. The central wavelength for each remaining spectral bin of 32 consecutive pixels is $206.25 + (j - 1)12.5$ nm, for $j = 3$ –16. The last spectral bin, grouping pixels 479–511, ranges from 387.5 to 400 nm and is centered on $\lambda_{16} = 393.75$ nm or, in short, 394 nm. All the data points for one given spectral bin j form a so-called light curve $I_{or}(\lambda_j, z)$ at a constant wavelength λ_j and various altitudes z . Wavelength intervals and central wavelengths in short are indicated in Figure 5.

In fact, it is the variation of light curves from one wavelength to the other which contains information about the spectral UV opacity of the atmosphere of Venus. Therefore we have normalized all light curves to 1 for the average of spectra 8–11 for ISAV 1 and similarly for ISAV 2, at the beginning of useful measurements when atmospheric absorption can be assumed to be minimal. This average of spectra (Figure 4) represents the xenon UV spectra energy distribution combined with the spectral efficiency of the instrument, in the presence of a minimal atmospheric absorption. This reference spectrum $I_{or}(\lambda_j, z_{ref})$ is somewhat different for ISAV 1 and ISAV 2.

All normalized light curves $I(\lambda_j, z)$ are represented in Figure 5 for ISAV 1 and Figure 6 for ISAV 2, for λ_j varying from 231 to 394 nm, as a function of altitude above the landing point. The spread of the individual points along a light curve is representative of the total instrumental noise and is, in most cases, quite small. Except for this noise, the variations of intensity displayed by the light curves are either instrumental or atmospheric in origin. There are three features which can be seen on Figures 5 and 6 which are obviously of instrumental origin.

1. The first measurements of the xenon flash lamp were obtained when the heat shield hemispheres of the spacecraft began to be jettisoned, at 64.2 km, an altitude where no atmospheric absorption was expected. Nonetheless, the signal was very low for a few seconds both for ISAV 1 and ISAV 2 (the first few points of Figures 5–6), until it rose sharply at an altitude of 62.5 km. We interpret the first low readings as due to an unexpected delay before the xenon flash lamp reached its nominal discharge regime.

2. The two first times the xenon flash is switched on again, after having been interrupted at the end of an acquisition sequence of three long spectra of 60 s, the intensity is slightly higher than before the interruption, then returns to the same level after ≈ 30 s. This effect is more pronounced for ISAV 1 than for ISAV 2 and affects only the shortest wavelengths (i.e., $\lambda_j = 281$ nm) and may amount to 15% at most. However, we should be aware of this effect on the spectra at the altitudes of 57 and 51 km, during their subsequent analysis. Below, it is practically absent (except, curiously, for $\lambda_j = 394$ nm below 10 km).

3. A sharp increase of the intensity at an altitude of 18 km is experienced by ISAV 1 and not by ISAV 2 (Figure 5). We interpret this feature as the result of a mechanical shock which kicked off from the mirrors of the absorption cell some absorbing material deposited during the descent. This hypothesis will be discussed further below. Here, it is enough to say that it is a proven fact that there was indeed a shock on the VEGA 1 landing probe, since one spacecraft subsystem, which was supposed to detect the shock of the landing, was unfortunately triggered prematurely precisely at the very same time.

This shock does not exist on ISAV 2. However, except for this important difference, the overall behavior of the light

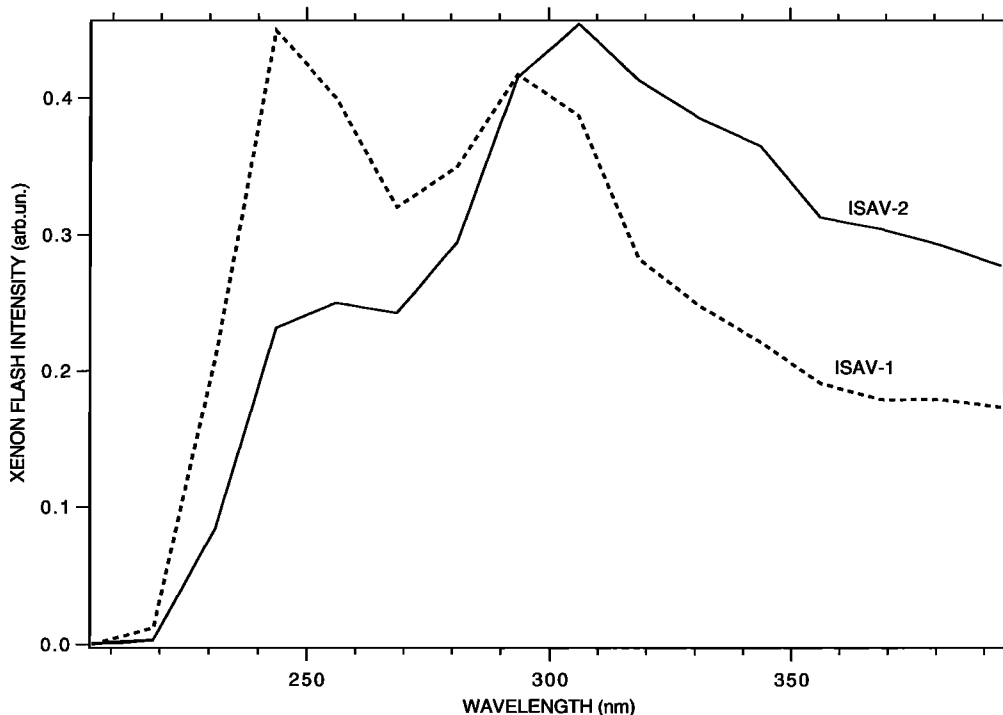


Figure 4. Spectrum of the xenon flash as observed by ISAV 1 and ISAV 2 taken at the altitude of 62 km for ISAV 1, where all light curves were normalized and where absorption is supposedly minimal.

curves of both instruments is quite similar. The behavior of the light curves changes with altitude, and it was found convenient to distinguish five different altitude regions characterized by a specific pattern, as displayed in Figures 5 and 6. In the following, the boundary altitudes are given from ISAV 2 curves, but they are nearly identical for ISAV 1.

Region 1 (62.5–56.5 km). All light curves for all wavelengths show a nearly monotonous increase of the light received by the spectrometer. This is interpreted as an increase of the xenon flash light after a long period of rest.

Region 2 (56.5–51 km). Some wavelengths show a monotonous increase of the light ($\lambda_{16} = 394$ nm, $\lambda_{15} = 381$ nm for ISAV 2), whereas shorter wavelengths show rather a monotonous decrease of light. This is interpreted as the continuation of the increase of light from the xenon flash, combined with the appearance of some absorbing material in the cell tube absorbing preferentially at short wavelengths ($\lambda < 300$ nm).

Region 3 (51–42.8 km). The signal drops at all wavelengths below 356 nm. In the short UV range (below ≈ 300 nm) there is a change of slope at ≈ 48 km with a sharper decrease below, whereas longer wavelengths display a clear vertical structure with three dips separated by peaks, well reproduced on both ISAV 1 and ISAV 2 (Figures 6 and 7) and corresponding most likely to a vertical cloud structure common to both landing sites of VEGA 1 and VEGA 2, separated by 2100 km.

Region 4 (42–32.3 km). The signal slightly increases at all wavelengths.

Region 5 (32.3–0 km). The signal decreases at all wavelengths, except for the ISAV 1 event at 18 km, at which the signal is sharply increases. The signal vanishes at a lower altitude for ISAV 1 than for ISAV 2. A quasi-periodic wiggle can be seen on curve 7 (281 nm) and to a lesser degree on curve 4 (244 nm) of ISAV 2, which is probably of nonatmospheric origin, but still unidentified.

The variations of intensities displayed by these light curves may have several origins, the most likely being (1) the changing absorption by the atmosphere contained in the tube cell, (2) a variation of the flash intensity, and (3) the deposition of cloud particles on the reflecting mirrors contained in the tube cell, or its removal (partial or total), as explained further below at the time of the ISAV 1 event at 18 km.

We can attempt to discriminate the various causes affecting the variation of light by a careful examination of the normalized light curves. However, the discussion will be clearer when their variations are compared with the boundaries of the three cloud layers, upper, middle, and lower, as determined by Pioneer Venus probes [Knollenberg and Hunten, 1980]. Figures 7 and 8 are an enlargement of Figures 5 and 6, restricted to the cloud region for better clarity.

The first region, where all light curves increase with decreasing altitudes, coincides with the upper cloud layer. Here, we interpret this increase of the light as an instrumental effect rather than a decrease of atmospheric opacity. Indeed, the intensities $I_{or}(\lambda_j, z_{ref})$ lie well below the last lamp spectrum taken before launch, about 9 months before VEGA encounters with Venus in June 1985, although they present the same overall spectral shape. This is probably due to the long time off for the xenon flash, and we interpret the signal increase in the first few kilometers as a recovery of the flash up to a stationary regime.

In the second region, which coincides with the middle cloud layer, the longest wavelength light curve, $\lambda_j = 394$ nm, increases the most, whereas shorter wavelength light curves either increase less, or even decrease strongly. The logical interpretation is that the light intensity of the xenon flash is still increasing, whereas there is some absorption occurring from the Venus atmosphere (or from the deposit of cloud particles) affecting the various wavelengths of the light source differently.

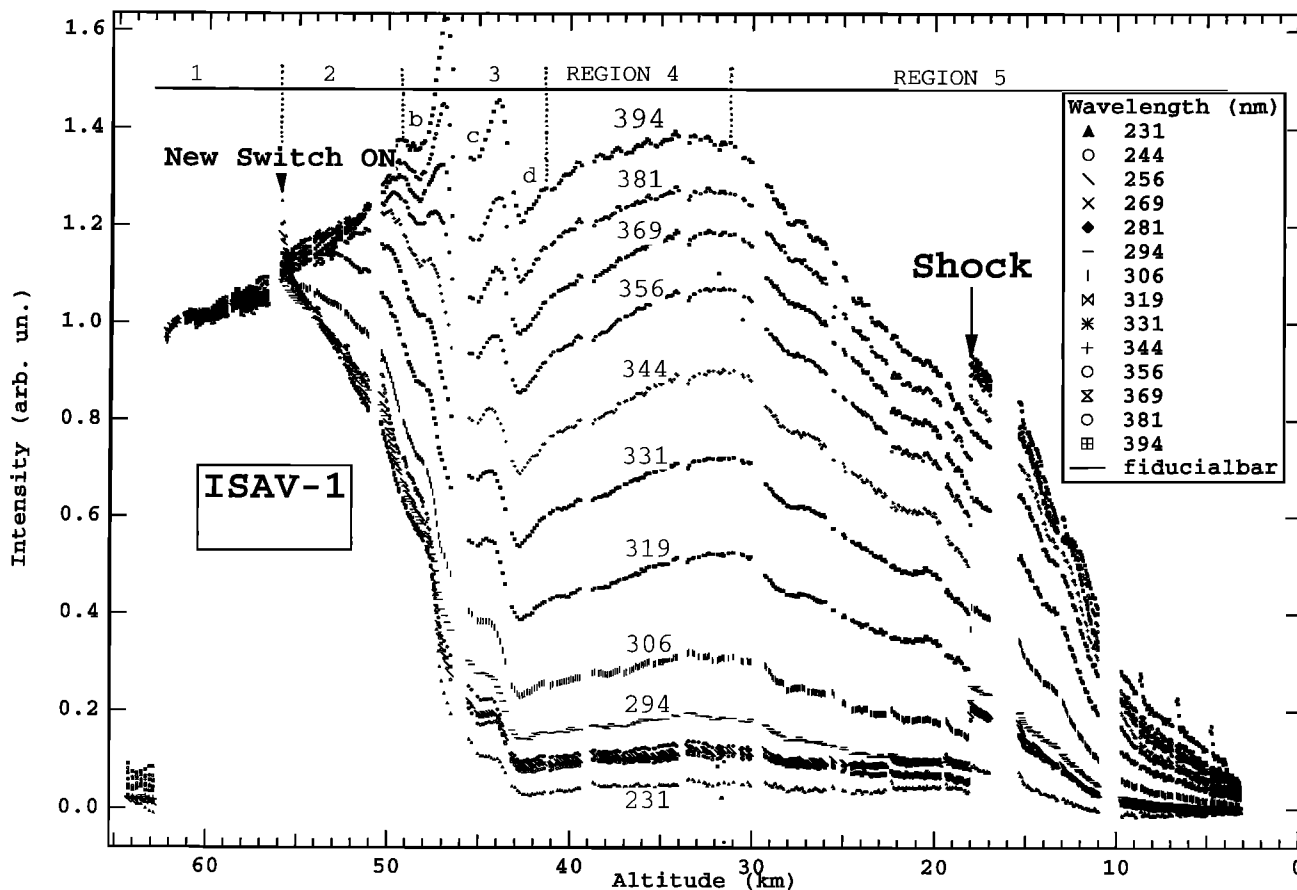


Figure 5. ISAV 1 data as a function of altitude in the atmosphere of Venus. All light curves for different wavelengths have been normalized to 1 at 62.5 km. In the region 20–40 km the light curves are in increasing order of wavelength (394 nm at top). The event at 18 km, where all light curves suddenly increase, is interpreted as a shock that released Venus aerosols collected on ISAV optics at higher altitudes. Around 56 km (also at 50 km), several wavelengths show a sharp increase, which disappears in ≈ 20 s, interpreted as a spurious instrumental effect happening just after a new switch-on of the xenon flash. Five different regions are identified to describe the overall variation of all light curves (see text for discussion), and narrow absorbing layers identified in the curve 394 nm are labeled b, c, and d.

This differential absorption will serve as the basis of the interpretation of the ISAV results. In order to make a quantitative analysis, we have to assume that the flash spectrum shape did not change during the entire descent, though its overall intensity was changing as stated above. This assumption is supported by ground tests of the ISAV instrument made at various levels of the integration of the instrument.

The differential absorption analysis implies to select one wavelength as a reference. The obvious choice is to take $\lambda_{16} = 394$ nm as the reference wavelength, since the light curves of both ISAV 1 and 2 demonstrate the smallest intensity decrease overall, as shown in Figures 5 and 6.

Region 3 (51–42.8 km), the upper boundary of which is close to that of the lower cloud as experienced by Pioneer Venus probes, displays the most complex vertical structure, as shown in Figures 7 and 8. The ISAV 2 curve for the reference wavelength, $\lambda_{16} = 394$ nm, shows four episodes of decreasing intensity (increasing absorption) separated by episodes of increasing light. These can be interpreted as the presence of four discrete layers of absorbing material in this lower cloud level, labeled a–d in Figures 7 and 8. The absorption found on layer a is quite small for ISAV 2 and, in fact, does not exist in the

ISAV 1 curve for $\lambda_{16} = 394$ nm, whereas layers b–d can be clearly identified on the ISAV 1 curves, though they are found at slightly lower altitudes, as indicated in Table 3. The thickness of the absorbing layers indicated in Table 3 have been measured on the light curves $\lambda_{16} = 394$ nm by the distance separating the adjacent intensity peaks.

It can be noted that the decrease of light at the top half of layer c is much more pronounced for ISAV 2 than for ISAV 1, amounting to -44% and -19% , respectively. Except for this difference and in spite of the complexity of the vertical structure of the light curves, there is a great similarity of ISAV 1 and ISAV 2 results, indicating a quite satisfactory self-consistency and parallelism of the vertical cloud structure at the two landing sites separated by 2100 km.

Quite important for the understanding of region 3 is the strong difference of behavior for the light curves of various wavelengths, notably in the lower half of layer b, where the intensity for wavelengths shorter than 350 nm decreases, whereas it increases for $\lambda > 350$ nm.

From 42 to 32.3 km, region 4 is located below the lower cloud layer, and is characterized by an intensity varying little at all wavelengths, slightly decreasing or slightly increasing, de-

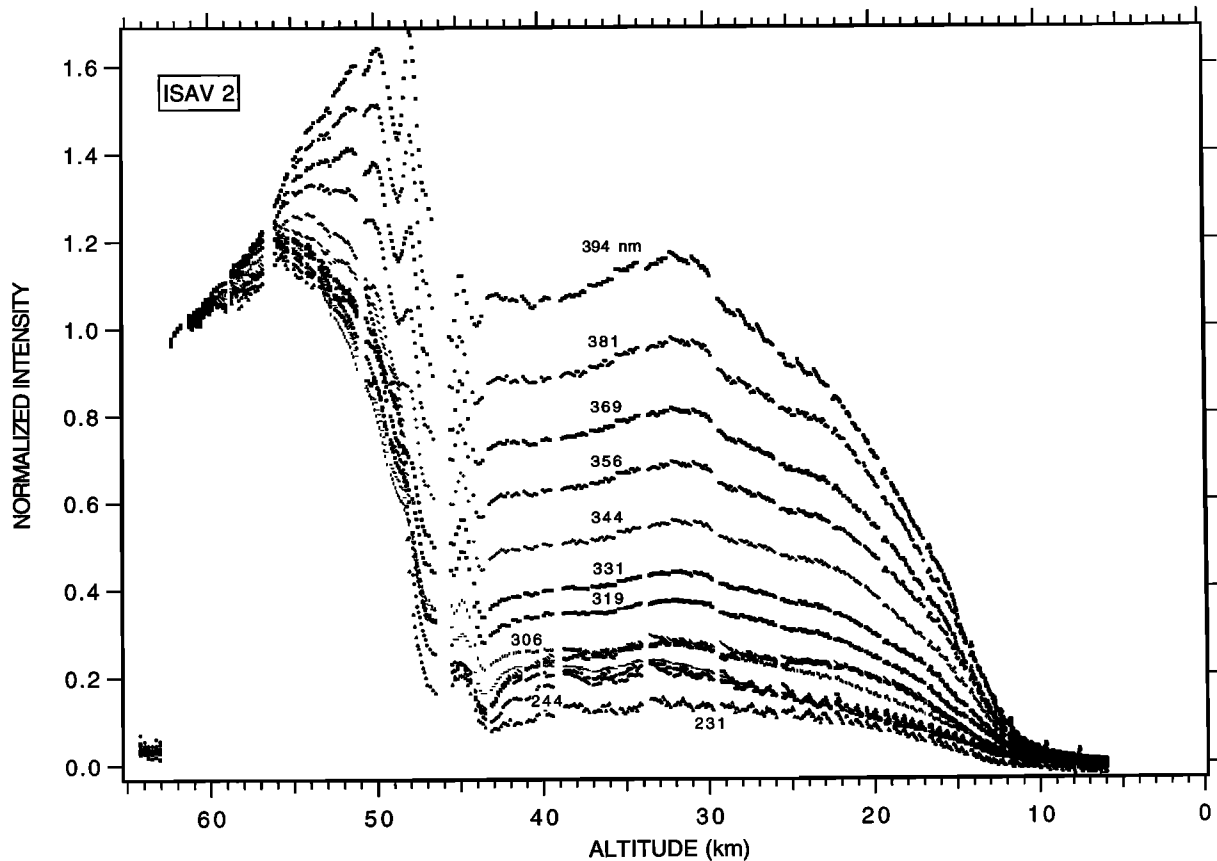


Figure 6. Same as Figure 5, but for ISAV 2.

pending on wavelength and altitude. Obviously, the atmosphere is rather clear in this region. Of course, it is quite possible that the increase of the xenon flash intensity, which is used to explain region 1 behavior, is still present, though to a much lesser extent, when approaching a stationary regime as suggested by the ISAV 1 light curve for $\lambda_{16} = 394$ nm.

In region 5, below 32 km, the intensity is always decreasing at all wavelengths for both instruments, except for the ISAV 1 event at 18 km, which is discussed below. There is no obvious reason to relate this overall decrease to a peculiar instrumental behavior (at variance with the ISAV 1 event), and accordingly, it is likely the sign of the increasing atmospheric opacity at all wavelengths below 400 nm. It cannot be SO_2 , which has a vanishingly small absorption cross section at 394 nm (Figure 9). The differential absorption analysis of the next section will allow one to determine the SO_2 vertical profile.

ISAV 1 Event

All the light curves show a sudden signal increase at the altitude of 18.0 km on ISAV 1 data (except for $\lambda_1 = 206$ and $\lambda_2 = 219$ nm, where there was no signal). This sharp increase is certainly of instrumental origin, and we interpret it in the present paper as the sudden removal, under the effect of a mechanical shock, of an absorbing deposit (liquid or solid) laid on the experiment mirrors, collected somewhere above 18 km during the descent through the atmosphere of Venus.

We know for sure that the VEGA 1 lander suffered a mechanical shock during its descent in the Venus atmosphere. At $z = 18.0$ km, precisely at the time of signal variation ($t_s = 1876$ s), an accelerometer, under operation to detect contact

with the ground, was accidentally triggered. It caused the deployment of a soil drilling mechanism of another on-board instrument, the X ray fluorescence spectrometer, which could not be operated after landing in consequence of its early deployment. This unexpected motion may have caused a major shake on board, with an important consequence for this analysis: the sudden removal of an absorber accumulated on the mirrors. Alternately, the shock triggering the accelerometer might have been produced by the external tube of the ISAV 1 experiment itself. The tube lower end was attached to the pressurized module, so that its thermal dilatation should be compensated by a mechanical degree of freedom of its bottom end inside a small guide rail. An excess of screw tightening might have blocked longitudinal dilatation, possibly causing a sudden release at $t = t_s$. However, a crude estimate shows in that case that the intensity of vibration induced by uncontrolled dilatation was too small to reach the triggering threshold for the on-board accelerometer. We are rather leaning toward another possible explanation, in which the shock was due to a pressure accident, activating the accelerometer, deploying the drilling arm of the X ray fluorescence spectrometer and removing the deposited material out of the ISAV 1 mirrors.

The VEGA landers were equipped with an upper compartment containing instruments other than ISAV, and were stopping their operation around the pressure level of 17 bars. This is, by the way, why more data telemetry was available for ISAV below this altitude. This upper compartment is built to withstand an external pressure of ≈ 17 bars, a level at which a valve was supposed to allow a gradual income of Venus air to avoid the crush of this compartment. This valve might have not

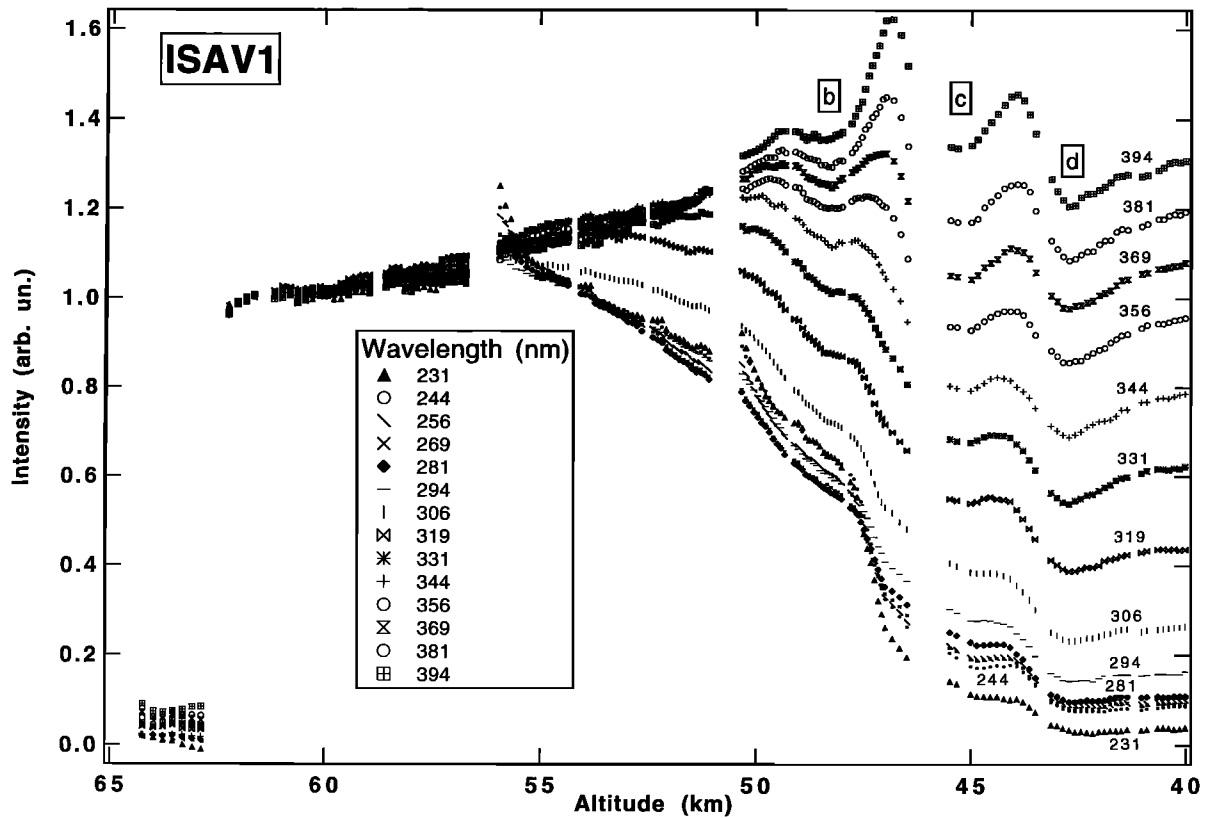


Figure 7. Enlargement of Figure 5 for ISAV 1 in the altitude range 65–40 km. Several absorbing layers, labeled b, c, and d, are indicated along the light curve at 394 nm, showing a strong structure in the cloud layer.

operated, leading to the implosion of this compartment at the altitude of 18 km (26 bars). Or perhaps the valve stuck down to the level of 18 km, and suddenly released, the shock being in this case the result of the sudden invasion of the high-pressure atmosphere into the upper compartment.

Whatever the exact origin of this shock, which indeed existed as proven by the accelerometer, we interpret the ISAV 1 light event at 18 km as the removal of an absorber, called X in this paper, deposited earlier during the descent. The relative increase of light at the time of the shock varies with λ , and gives an essential clue to the spectral signature of the removed absorber.

ISAV 1 data can be used to evaluate the spectral signature of this absorber X. By dividing the spectral intensity of low-resolution data spectrum 352, before the shock ($t = 1868$ s, $z = 18.11$ km), by data spectrum 354, immediately after the shock ($t = 1880$ s, $z = 17.95$ km), we obtain a ratio of intensities I_{352}/I_{354} , for which the inverse logarithm $\tau_x = -\log I_{352}/I_{354}$ is the optical thickness of the absorber X kicked out from the mirrors at the shock. Its wavelength signature is shown in Figure 10. In the following, “log” means the natural logarithm.

The absorber X spectral signature shows a maximum absorption at 280 nm and $\tau_x(\lambda)$ larger than 1 in the range 260–310 nm. A monotonous decrease is observed toward both longer and shorter wavelengths, except at 230 nm, where a significant increase is present. As explained in more detail in the next section, the 14 $\tau_x(\lambda)$ values are multiplied by a concentration factor $\alpha_x(z)$ varying with altitude, and deter-

mined to fit the observed signal extinction along with other absorbers in ISAV 1 data.

We anticipate here on the results of the next section to say that the vertical profile of $\alpha_x(z)$ (Figure 13) shows that this absorber is (1) gradually collected into the optical path during the cloud descent, mainly in the middle (56.5–50.5 km) and lower (50.5–47.5 km) cloud region, then (2) stable, and then (3) suddenly removed at 18 km from the ISAV 1 optical path. Early in ISAV data analysis (1985), we considered a different interpretation for the signal increase of ISAV 1 at 18 km. We thought that, due to thermal dilatation, a possible mechanical distortion of instrument optics might have modified the measured spectrum of the lamp by the spectrometer (though no clear mechanism could be proposed for that), then suddenly relaxed at 18 km. However, if it were so, we would expect the spectral signature of X building up all along the descent, down to 18 km; on the contrary, the results show that the spectral signature of X did build up in a rather limited range of altitude, in which the temperature changed only by ≈ 70 K, and nearly stopped at ≈ 47 km, whereas thermal dilatation did continue below. We feel confident this “mechanical distortion” explanation must be discarded; furthermore, the fact that the X spectral signature builds up in the clouds of Venus is an obvious support for the aerosol deposition hypothesis.

As a conclusion of this section, in which the ISAV light curve results were discussed qualitatively, in connection with what was known already of the vertical structure of the Venus cloud layers, there are two points which must be emphasized: (1) in spite of significant differences between ISAV 1 and ISAV 2

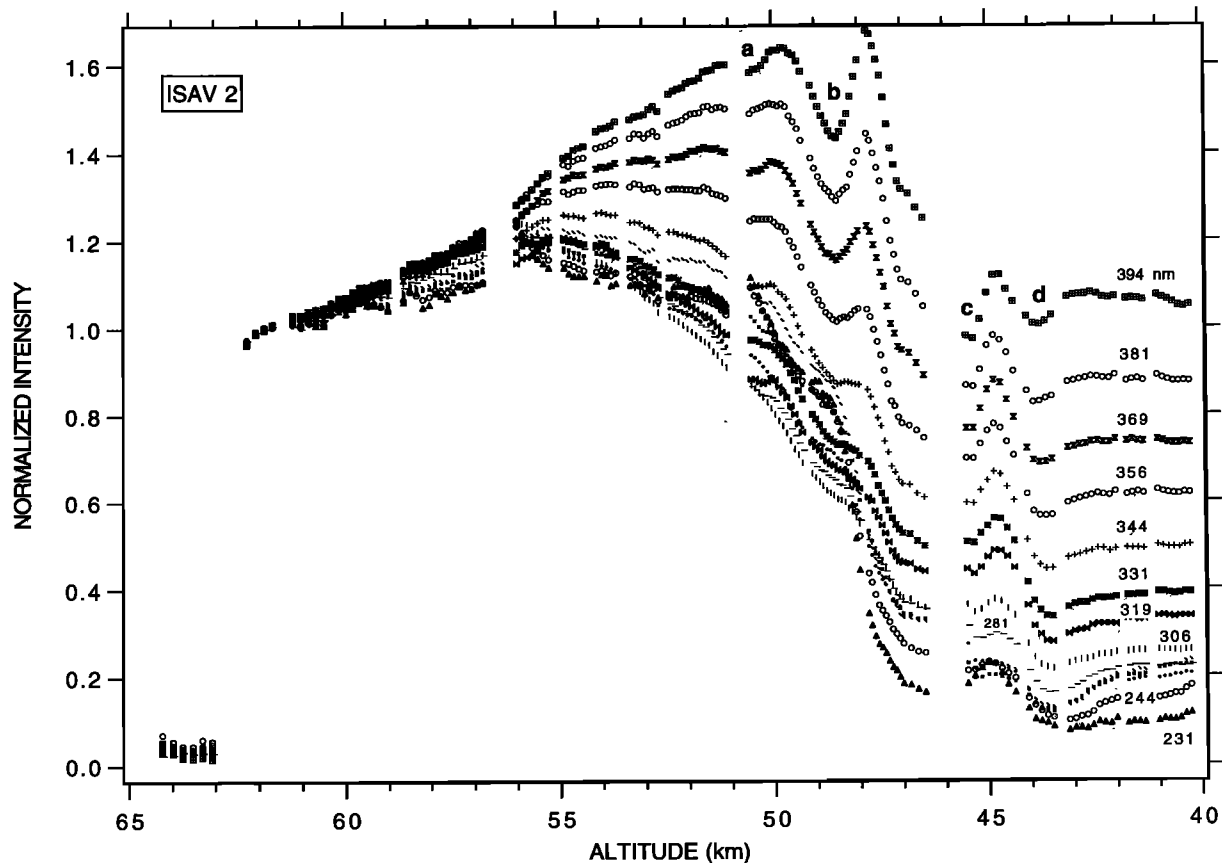


Figure 8. Same as Figure 7, but for ISAV 2. An additional absorbing layer, labeled a, is present between 50 and 51 km, not visible for the ISAV 1 data.

results, there is a great similarity of behavior, even in the detailed vertical structure; and (2) clearly the episode of strongest and most complex variation of signal is connected with the crossing of the lower cloud layer, with a much clearer atmo-

sphere below the clouds. This double consistency (internal and external to the ISAV experiment) increases our confidence in the quality of the ISAV measurements and in the quantitative analysis presented in the next section.

Table 3. Altitude Boundaries of the Various Regions Identified in the ISAV Data Compared With the Cloud Boundaries as Determined by Previous Experiments

	ISAV 1			ISAV 2		
	Upper Boundary	Lower Boundary	Thickness	Upper Boundary	Lower Boundary	Thickness
Region 1*	62.5	56.5	6.0	62.5	56.5	6.0
Upper cloud†	66	56	10			
Region 2	56.5	49.6	6.9	56.5	51	5.5
Middle cloud	56	50	6			
Region 3	49.6	41.3	8.3	51	43.1	7.9
Lower cloud	50	47	3			
Layer a				51.1	49.8	1.3
Layer b	49.5	47.0	2.5	49.8	47.8	2.0
Layer c	47.0	43.9	3.1	47.8	44.7	3.1
Layer d	43.8	41.0	2.8	44.7	43.1	1.6
Region 4	41.3	31.3	10	42	32.3	9.7
Event‡	18.0	18.0	NA	NA	NA	NA
Region 5	31.3	0	31.3	32.3	0	32.3

All altitudes and thicknesses are in kilometers. NA, not applicable.

*Boundary altitudes of ISAV regions and absorbing layers are visually defined on the plot light of curves (Figures 5–8).

†Boundaries of Venus clouds are quoted from the night probe of Pioneer Venus.

‡Altitude of mechanical event ISAV 1 light curve.

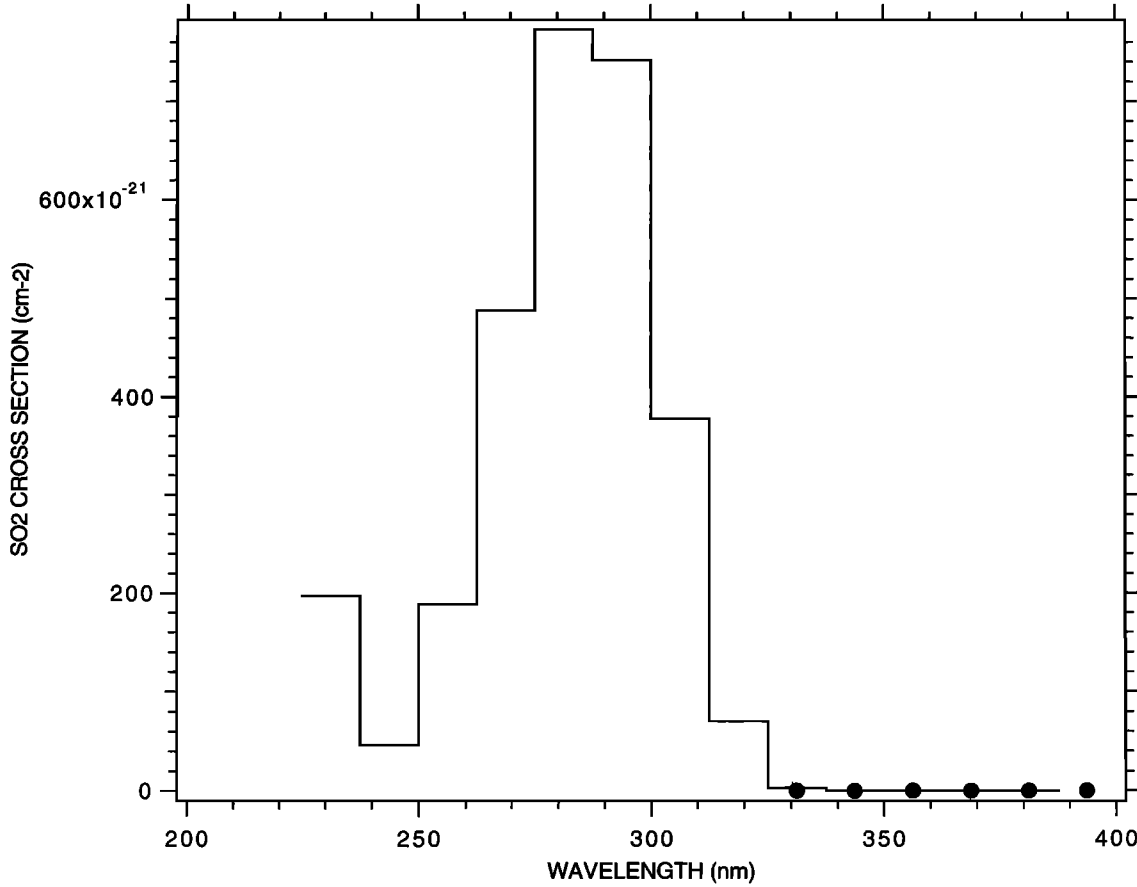


Figure 9. Cross section of gaseous SO₂ averaged over wavelength intervals corresponding to each of the 16 wavelengths bins of ISAV (each 12.5 nm wide). It peaks at 269–281 nm and is very small above 340 nm, allowing a safe determination by differential absorption. The large black dots mark the six upper wavelength bins (331–394 nm) selected to determine the quantity of absorber X because SO₂ absorption is negligible.

4. Quantitative Spectral Data Analysis

Let $I_{or}(\lambda_j, z_k)$ be the spectrum intensity measured at wavelength λ_j at altitude z_k , and $I_0(\lambda_j, z_k)$ be the intensity which would be measured under vacuum conditions in the cell tube, and in the absence of cloud particle deposition on the reflecting mirrors. The absorption by various species inside the tube and deposited on the mirrors is characterized by the optical thickness $\tau(\lambda_j, z_k)$ present at altitude z_k :

$$I_{or}(\lambda_j, z_k) = I_0(\lambda_j, z_k) e^{-\tau(\lambda_j, z_k)} \quad (1)$$

$$\tau(\lambda_j, z_k) = -\log \frac{I_{or}(\lambda_j, z_k)}{I_0(\lambda_j, z_k)} \quad (2)$$

Under ideal conditions, $I_0(\lambda_j, z_k)$ would have been constant in time during the entire descent (at all z_k), and would have been equal to the last spectrum taken before launch on the ground, because absorption by air in the range 200–400 nm is negligible.

Unfortunately, the intensities $I_{or}(\lambda_j, z_k)$ lie well below this last spectrum, which is probably due to the long time that the xenon flash is off (9 months between the last ground experiments and the VEGA encounters with Venus in June 1985). We therefore interpret the signal increase in the first few kilometers as a recovery of the flash up to a stationary regime.

Based on experience acquired during ground testing of the

ISAV instrument, we will assume in the following that the flash spectrum shape did not change during the entire descent, though the overall intensity may have changed in an unknown manner. Therefore the altitude dependence of the shape of $I_0(\lambda_j, z_n)$ can be dropped and (2) rewritten as

$$\tau(\lambda_j, z_k) = -\log \frac{I_{or}(\lambda_j, z_k)}{I_0(\lambda_j) \varepsilon(z)} \quad (3)$$

in which $\varepsilon(z)$ is a multiplicative factor indicating the variation of the whole spectrum $I_0(\lambda_j, z_k)$ applied to a reference spectrum $I_0(\lambda_j)$.

Let us assume for clarity that the optical thickness in the path light is zero at the altitude of reference, $z_{ref} = 62.5$ km, where light curves have been normalized. This assumption can be expressed by

$$\tau(\lambda_j, z_{ref}) = 0 \quad I_0(\lambda_j) = I_{or}(\lambda_j, z_{ref}) \quad \varepsilon(z_{ref}) = 1$$

Using the definition of our normalized light curves,

$$I(\lambda_j, z_k) = \frac{I_{or}(\lambda_j, z_k)}{I_0(\lambda_j)},$$

(3) can be rewritten as

$$\tau(\lambda_j, z_k) = -\log I(\lambda_j, z_k) + \log \varepsilon(z) \quad (4)$$

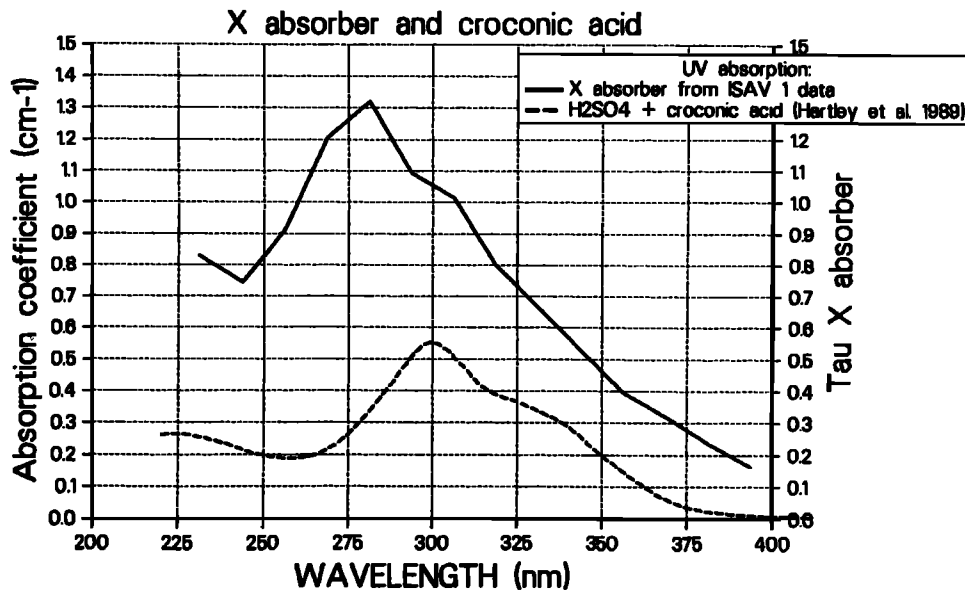


Figure 10. The solid line represents the wavelength dependence (spectral signature) of the optical depth for the unknown absorber removed from ISAV 1 at 18 km during the shock. The absorption coefficient measured by *Hartley et al.* [1989] in a 1-cm cell containing a solution of sulfuric acid concentrated at 84% and contaminated with 2×10^{-5} croconic acid mole per liter of sulfuric acid is reproduced for comparison (dotted line). The two spectral signatures are similar, but not identical.

Equation (4) is in fact a set of 16 equations, one for each wavelength λ_j and, in particular, can be written for $j = 16$, $\lambda_j = 394$ nm:

$$\tau(\lambda_{16}, z_k) = -\log I(394, z_k) + \log \varepsilon(z) \quad (5)$$

Equation (5) can be subtracted from all equations (4) for $j = 1-15$ to yield

$$\tau(\lambda_j, z_k) - \tau(\lambda_{16}, z_k) = -\log \frac{I(\lambda_j, z_k)}{I(394, z_k)} \quad (6)$$

where the right-hand term is composed of the normalized ISAV measurements presented in Figures 5 and 6. In practice, we have only 13 equations (6) because of the inadequate light for $j = 1$ and 2.

The left-hand term is the differential optical thickness: it is the difference of optical thickness at all wavelengths $\lambda < 394$ nm with the wavelength at $\lambda = 394$ nm.

The choice of the reference wavelength $\lambda_{\text{ref}} = 394$ nm seems logical in view of its smallest variation as indicated by its light curve. It is possible to use (4) or (6) with two nearby altitudes z_k and $z_{k'}$, to examine in a small-altitude region the spectral signature of additional absorbers, with the hope that a small number of substances (one, preferably) will show up in a limited altitude range. This is, for instance, the obvious case of the ISAV 1 event.

We have assumed above for clarity that there was no absorption at the reference altitude z_{ref} , the highest altitude where a correct spectrum is found: 62.25 km for ISAV 1 and 62.04 km for ISAV 2. We expect a minimal and likely negligible absorption at this altitude. In the following, we shall indeed neglect this absorption, which is only a small, but unknown constant which would have to be added to the results obtained. It can be noted that whatever is neglected at z_{ref} will not prevent one from obtaining the spectral shape of additional absorbing substances as appearing at lower altitudes.

Therefore, in spite of the difficulty concerning the unknown variation of $I_0(\lambda_j, z_k)$, ISAV measurements allow us to detect the increase of differential optical thicknesses, respective to the reference altitude z_{ref} and the wavelength λ_{ref} . Keeping in mind that we put aside the unknown absorption at z_{ref} , we will often neglect it in the following for simplicity.

At any given altitude z_k , the optical thickness $\tau(\lambda_j, z_k)$ is the sum of gaseous absorption and of absorption by substances deposited on the mirrors during the descent:

$$\tau(\lambda_j, z_k) = \sum_{i'} \alpha_{i'}(z_k) \tau_{i'}(\lambda_j) + \sum_{i''} \sigma_{i''}(\lambda_j) L n_{i''}(z_k) \quad (7)$$

where $i = i' + i''$ is the total number of absorbers. For i'' indexed species, the gaseous absorption cross section $\sigma_{i''}(\lambda_j)$ is multiplied by the column density $L n_{i''}(z_k)$ inside the tube of length $L = 170$ cm, $n_{i''}(z_k)$ being the concentration of the absorbing gas in cm^{-3} . For i' indexed species, which are solid or liquid phases deposited on the mirrors, the proportionality factor $\alpha_{i'}$ describes the abundance with altitude, relative to an altitude at which the optical thickness spectrum of this species is $\tau_{i'}(\lambda_j)$. The same description applies to differential optical thickness either in wavelength or in altitude.

As stated in the previous section, we interpret the ISAV 1 event at 18.0 km as the kick-off from the mirrors of one substance called X deposited earlier during the descent. The optical thickness $\tau_X(\lambda_j)$ of this substance X shown in Figure 10 is present at all wavelengths, including $\lambda = 394$ nm, where it is smallest. Nevertheless, we will consider also its differential optical thickness $\tau_X(\lambda_j) - \tau_X(394)$ in the following.

In our analysis, we are going to try to describe the ISAV results with the minimum possible number of absorbing substances and gases. For ISAV 1, we will first determine the opacity of substance X, then we will determine SO_2 that we know is surely present in the atmosphere of Venus, and then

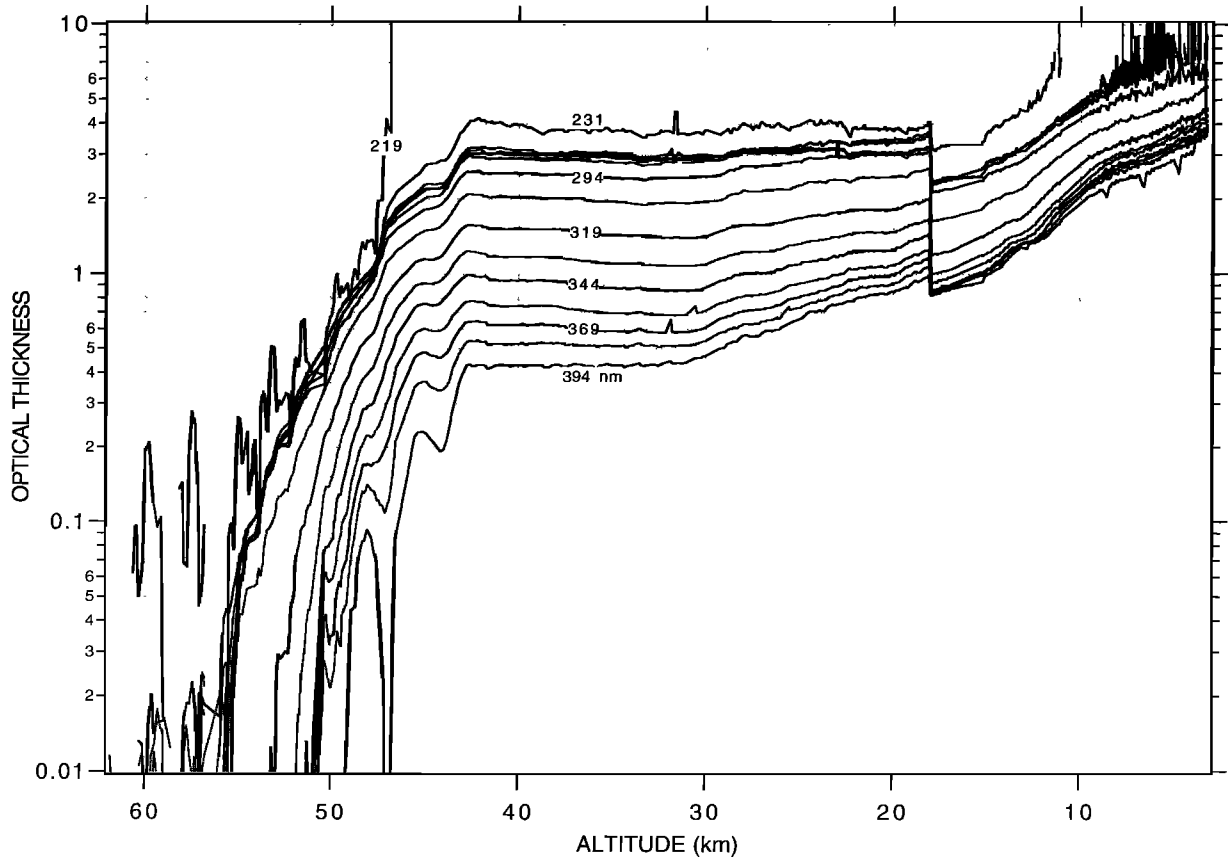


Figure 11. Optical thickness measured by ISAV 1 as a function of altitude for various wavelengths. Optical thickness increases when wavelength decreases, particularly obvious in the plateau in the region 45–18 km. The effect of the shock at 18 km is clearly apparent. The absorption becomes stronger below 15 km at all wavelengths, but this trend seems to begin at 30 km altitude.

examine what spectral signature is left in the remaining differential optical thickness.

Though we will rely entirely on the approach of differential optical thickness (with respect to 394 nm) in our quantitative analysis, it is useful to try an estimate of the optical thickness built up at 394 nm. For this purpose, a model of the curve I_0 (394 nm), which would have been measured in the absence of all absorption, was built as explained in section 7. It represents the intrinsic variation of the xenon flash intensity, not only at 394 nm, but also at all wavelengths, since the shape of the xenon flash spectrum is assumed to be constant. The optical thickness at all λ_j can be computed with respect to I_0 (394 nm) and is displayed in Figure 11 as a function of altitude. Figure 12 shows the spectrum of this optical thickness $\tau(\lambda_j, z)$ for various altitudes.

For the numerical analysis, we prefer to use the differential optical thickness respective to 394 nm. The optical thickness at 394 nm is subtracted from all data of Figure 12, therefore alleviating any error which could have been made in the choice of assumptions necessary to build the model curve I_0 (394 nm).

The differential optical thickness b_j measured by ISAV 1, respective to the reference altitude z_{ref} and to $\lambda_{\text{ref}} = 394$ nm, for various altitudes z is therefore

$$\begin{aligned} \tau(\lambda_j, z_k) - \tau(\lambda_{16}, z_k) &= -\log \frac{I(\lambda_j, z_k)}{I(394, z_k)} \\ &= b_j \end{aligned} \quad (8)$$

Of course, all measured differential optical thicknesses b_j vanish for $\lambda_j = 394$ nm. The six large black dots in Figure 9 indicate the five spectral bins that are selected to retrieve at each altitude the quantity $\alpha(z)$ of X absorber. They were selected because we do not expect a significant SO_2 absorption in this wavelength domain, as can be seen in Figure 9. We assume also that all differential absorption in this wavelength domain can be attributed to absorber X.

At each altitude z , we have therefore a set of five linear equations ($\lambda_j = 11-15$) and only one unknown $\alpha(z)$:

$$\begin{aligned} b_{11} &= \alpha[\tau_X(\lambda_{11}) - \tau_X(394)] \\ &\vdots \\ b_{15} &= \alpha[\tau_X(\lambda_{15}) - \tau_X(394)] \end{aligned} \quad (9)$$

Calling $a_i = \tau_X(\lambda_i) - \tau_X(394)$, the least squares solution of this overdetermined system gives

$$\alpha = \frac{\sum a_i b_i}{\sum a_i^2} \quad i = 11, 15 \quad (10)$$

The value of α is plotted in Figure 13 and will be discussed further in the next section. For each altitude and λ_j ($j = 3, 15$), the differential optical thickness due to absorber X was computed:

$$b'_j = \alpha[\tau_X(\lambda_j) - \tau_X(394)]$$

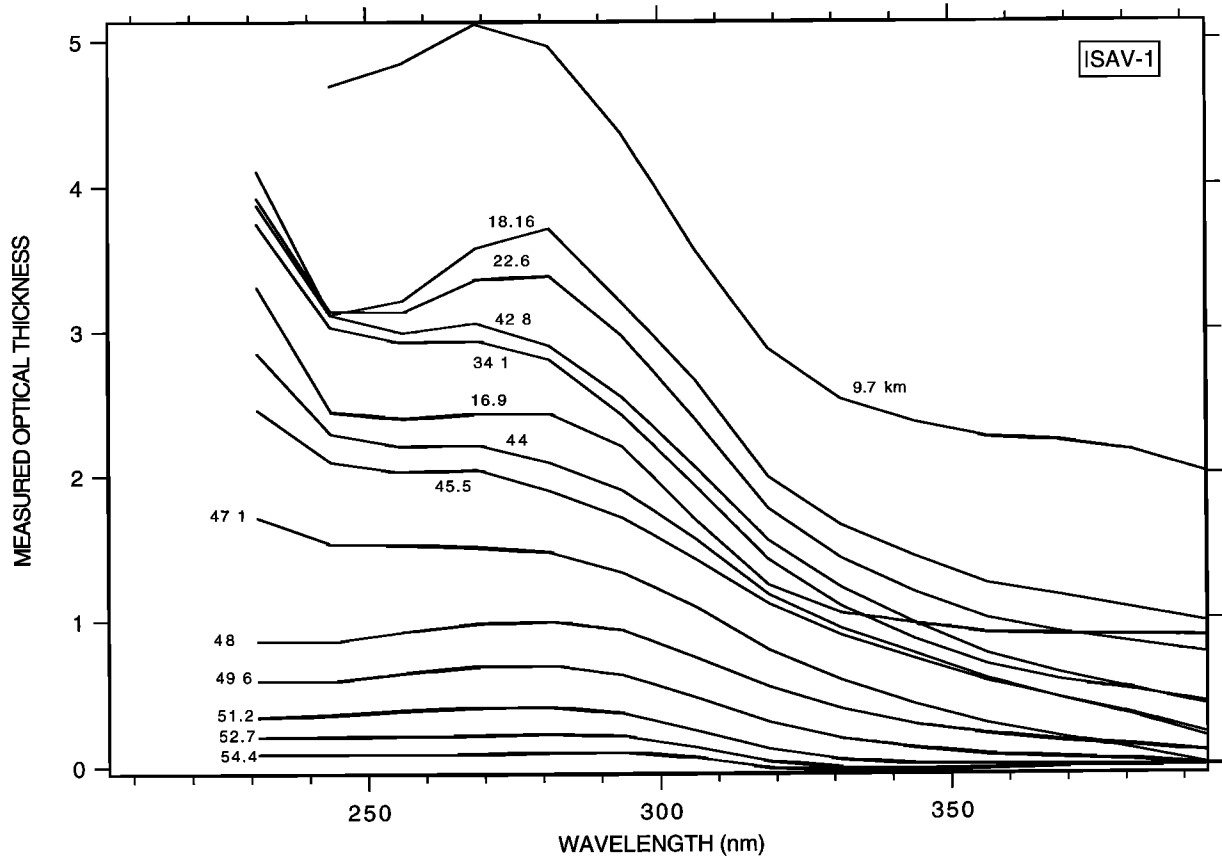


Figure 12. Spectrum of optical thickness $\tau(\lambda, z)$ for various altitudes. The measured differential optical thickness is obtained by subtracting $\tau(394, z)$ from all other wavelengths. The result of the subtraction is not shown here. The observed variation of optical thickness in the six upper wavelength bins (331–394 nm), indicated by black dots in Figure 9, are used in the following to determine the quantity of absorber X, because SO_2 absorption is negligible.

and then subtracted from measurements b_j to yield the remaining optical thickness c_j other than that due to X:

$$c_j = b_j - b'_j$$

The values c_j are plotted as a function of j for various altitudes in Figure 14. It remains small for wavelengths 331–394 nm, showing that most of the differential absorption in this domain can indeed be explained by the deposition of absorber X on the mirrors of ISAV 1. The remaining optical thickness is significant only below 331 nm, and is due to SO_2 and other absorbers. Based on this remark, we have next determined the SO_2 optical thickness necessary to explain the data of Figure 13 with the five wavelength bins 7, 8, 9, 10, 11 at 281, 294, 306, 319, and 331 nm, respectively, where the SO_2 cross sections, averaged over 12.5-nm line are indicated in Figure 9, allowing again a differential absorption analysis. Here again, we assume that all differential absorption on these bins (after subtraction of X absorber contribution) is due to SO_2 only.

A system of equations similar to (8) can be written for each altitude:

$$\begin{aligned} c_7 &= 170[\sigma_{\text{SO}_2}(\lambda_7) - \sigma_{\text{SO}_2}(\lambda_{11})]n_{\text{SO}_2} \\ &\vdots \\ c_{10} &= 170[\sigma_{\text{SO}_2}(\lambda_{10}) - \sigma_{\text{SO}_2}(\lambda_{11})]n_{\text{SO}_2} \end{aligned} \quad (11)$$

This system of four equations with only one unknown, the number density n_{SO_2} , is overdetermined and its least squares solution is similar to (9). Solved at each altitude z , it provides the SO_2 absolute concentration vertical profile which is indicated in Figure 15, and will be discussed in more detail in section 7. Then the optical thickness of SO_2 in the 170-cm light path was computed for each wavelength and each altitude, and was subtracted from c_j , to obtain the remaining optical thickness d_j plotted in Figure 16. Clearly, there is a remaining signal confined to the shortest wavelengths of the spectral domain which will deserve future studies.

5. Deposition Process on Mirrors of Instrument Observations

It should be well understood, first, that the typical optical thickness of cloud aerosols is $\approx 10^{-3}$ in the tube, and therefore unmeasurable. It is only because they accumulated on the reflecting mirrors that they could be measured.

The general vertical distribution of absorber X (Figure 13) is in agreement with the hypothesis of an absorber laid on the ISAV external optical surfaces, exposed to the flow of Venus atmosphere, i.e., the outer side of the quartz window and the three mirrors in the cell tube of ISAV experiment. Absorber X is gradually collected into the optical path when the spacecraft

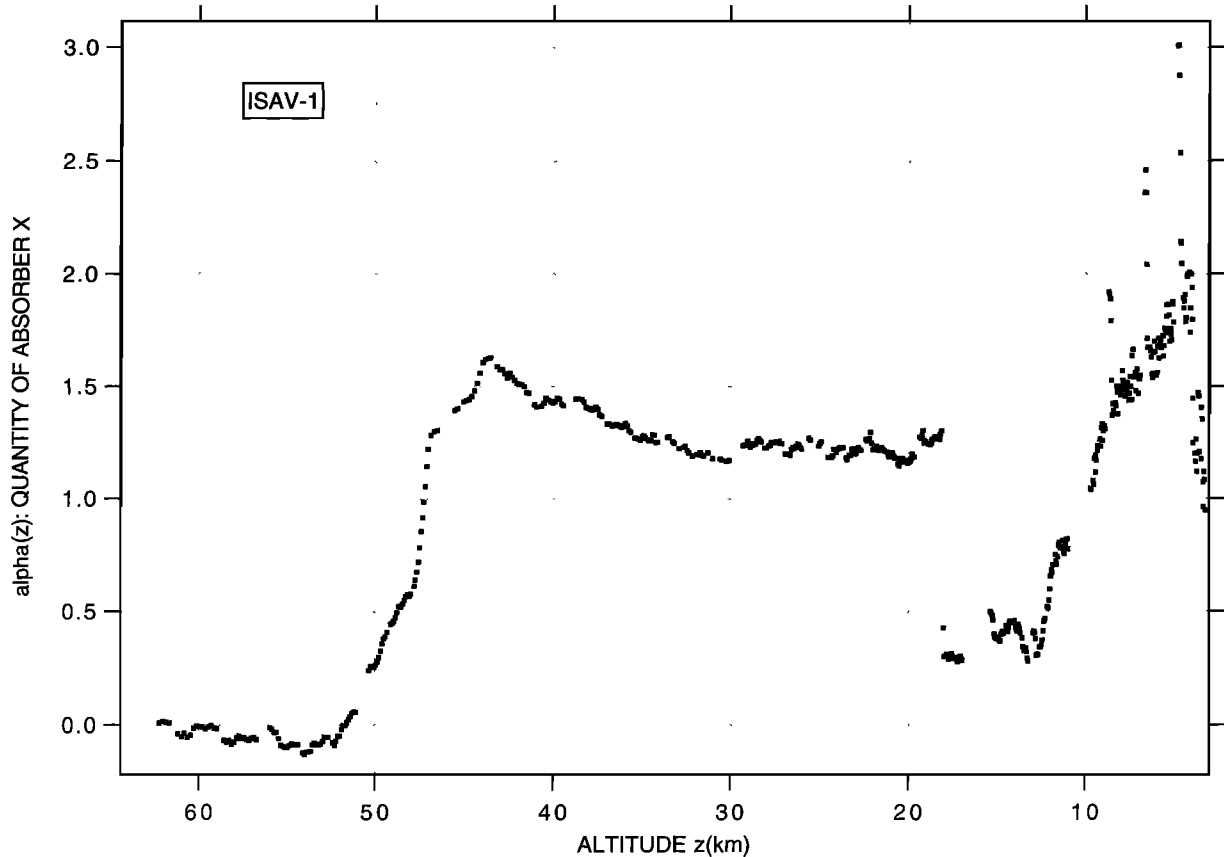


Figure 13. Coefficient $\alpha_X(z)$ to opacity $\tau_X(\lambda_i)$ for absorber X in ISAV 1 obtained at each altitude z to fit differential absorption data in the wavelength bins 331–394 nm, where SO_2 absorption is negligible. For ISAV 1, X absorber accumulates in the optical path from the middle cloud level (≈ 53 km) to the bottom of the lower cloud at 47.5 km. Absorber is suddenly released out of the optical path at $z = 18.0$ km.

crosses the cloud deck. Its spectral signature becomes apparent once the descent module passes through the lower middle cloud region, near 52 km, where the density of mode 1 particles of H_2SO_4 is 300 cm^{-3} and their mean radius is $0.3 \mu\text{m}$, and mode 2 particles, of mean radius $1.2 \mu\text{m}$, have a density of 50 cm^{-3} . While crossing the lower cloud region (50.5–47.5 km), its opacity at 281 nm grows rapidly from 0.2 to 1.7, in a range of altitude among the cloud deck which contains, in addition to mode 1 and mode 2 particles, larger particles called mode 3, with a mean radius of $7.2 \mu\text{m}$ [Knollenberg and Hunten, 1980]. These mode 3 particles contain the bulk of the cloud mass loading but may be an extension of the mode 2 population, as discussed by several authors later on.

As calculated by Krasnopolsky and Pollack [1994], the atmospheric profile of Venus is such that H_2SO_4 cannot exist under the liquid form below ≈ 48 km, which is then identified as the bottom of the lower cloud deck (lower cloud boundary, LCB). In addition, gaseous H_2SO_4 should disappear below ≈ 40 km in the reverse thermochemical reaction $\text{H}_2\text{SO}_4 \rightarrow \text{H}_2\text{O} + \text{SO}_3$ ($T \approx 430 \text{ K}$, $p \approx 4$ bars). Indeed, absorber X stops increasing very fast at ≈ 47 km (Figure 13), coinciding with the position of LCB, both predicted by theory [Krasnopolsky and Pollack, 1994], and observed by Pioneer Venus probes. As shown in Figure 11, all opacities increase below 32 km, maybe as a consequence of the absorption by sulfur-bearing molecules (SO_3 , S_3 , S_4 , etc.).

The absorber X is then suddenly removed at 18 km (Figure

12), and the opacity does not return to zero but rather to 0.4. There remains after the shock some absorber X on the ISAV external optics. However, the variation of α at 18 km is $\Delta\alpha = 1$, which is not surprising, as the two spectra used for the X spectral signature determination are the low-resolution spectra immediately before the shock ($t = 1868 \text{ s}$, $z = 18.11 \text{ km}$) and immediately after the shock ($t = 1880 \text{ s}$, $z = 17.95 \text{ km}$). We note that the X absorber is not detected in the upper cloud region. Assuming that X is a contaminant of aerosols, absorbing ultraviolet in the range 230–400 nm, dissolved in mode 1, mode 2, and perhaps mode 3 H_2SO_4 droplets, this absence of buildup of opacity while the probe passes through the upper cloud region indicates that mode 1 particles at higher altitudes may be free of this contaminant or that the collection of aerosols in this region is negligible. The opacity coefficient $\alpha_X(z)$ of $\tau_X(\lambda_i)$, as calculated and shown in Figure 13, starts to increase at 52 km, in the middle cloud region ($50.5 < z < 56.5$ km), then continues to increase in the lower cloud region ($47.5 < z < 50.5$ km), where particles have maximum mass and size, according to Toon *et al.* [1984] and Knollenberg [1984], up to a maximum value reached once the main cloud deck is cleared at 47 km. Further below, the increase of opacity for X is stopped, and its absorption remains roughly constant. The absorption coefficient decreases sharply at $z = 18.0$ km, where $\tau_X(\lambda_i)$ has been determined (Figure 10). Should the absorber be brought into the optical path by H_2SO_4 liquid droplets, as a contaminant dissolved in sulfuric acid, those droplets would eventually

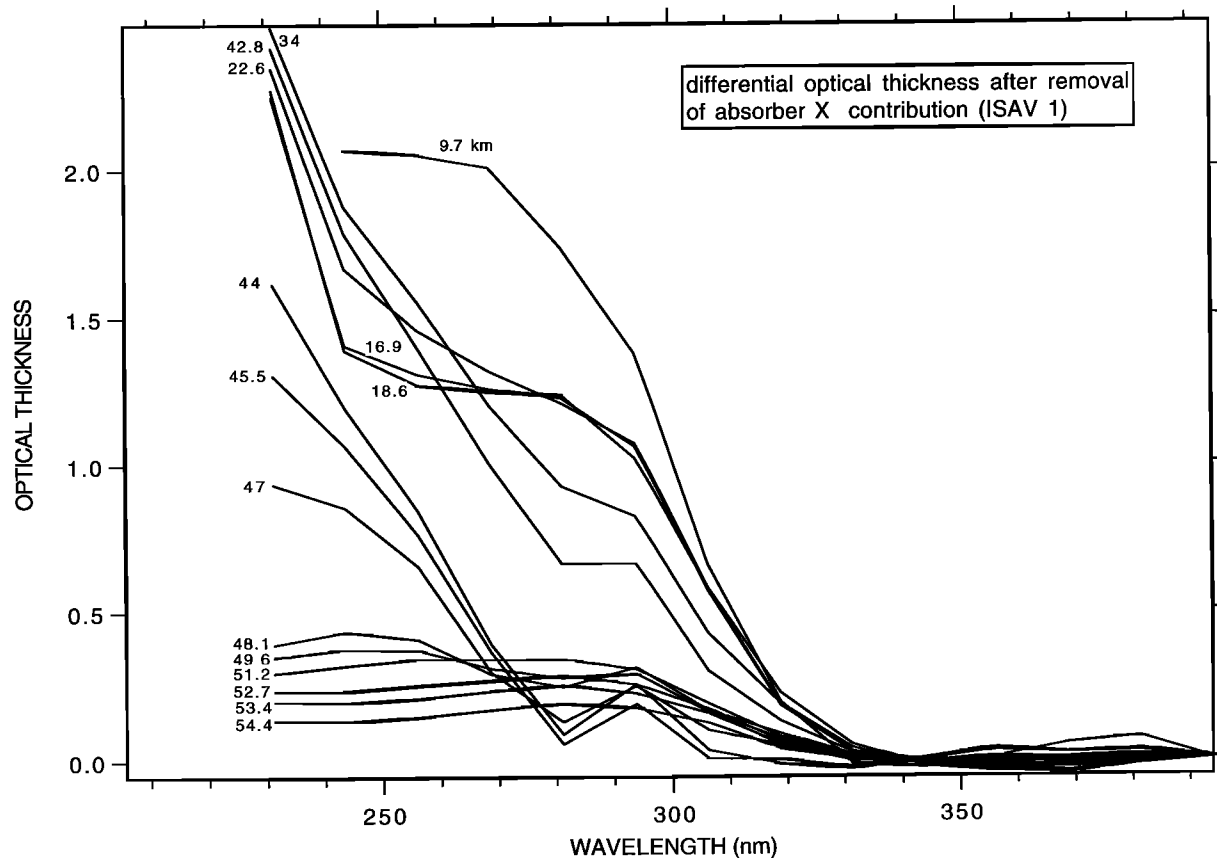


Figure 14. Residual differential optical thickness once the contribution of absorber X has been removed at all wavelengths and all altitudes, according to its spectral signature of Figure 10 and its distribution of Figure 13. Four spectral bins have been used to determine the SO₂ quantity of Figure 15, for which absorption was then removed from all wavelengths to yield the residual absorption in the short UV range as displayed in Figure 16.

evaporate below the main cloud deck, leaving on the mirrors a residue of contaminants absorbing in the UV, resisting the higher temperatures met below 30 km. The apparent growth of the absorber below 13 km in Figure 13 is an artifact of the method. What happens in actuality is that the UV absorption does increase again, at all wavelengths (Figures 11 and 18). However, the X absorber spectral signature does not fit at all the observed absorptions. Still, the numerical method tries to fit this absorption “as best as possible,” with the only absorber considered in the exercise: absorber X. Therefore the large absorption below 15 km must be attributed to other UV absorbers, like elemental sulfur, S₂, S₃, S₄, and possibly SO₃. A detailed discussion is beyond the scope of this paper.

Quantitative Study of H₂SO₄ Droplets

We rely heavily on the analysis of cloud particle distribution by *Knollenberg and Hunten* [1980] from the Pioneer Venus large probe cloud particle spectrometer (LCPS) to investigate the deposition on the mirrors of the external tube of H₂SO₄ droplets hypothetically contaminated with absorber X. We first make an estimate of the quantity of aerosol which passed through the tube during the cloud crossing, knowing that the admission pipe of the external tube has a circular section of 2.75 cm diameter. We note that while mode 1 and mode 2 particles, which are H₂SO₄ droplets, are the most numerous, the mode 3 particles, which are largest, by far dominate the

mass loading, with a columnar mass in each of the three modes of 1.5×10^{-4} , 18.7×10^{-4} , and 1.6×10^{-2} g cm⁻², respectively [*Knollenberg and Hunten*, 1980, p. 8052]. Assuming that most of the aerosol particles entering the 6 cm² admission pipe entrance will splash on one of the mirrors with area 11 cm², it will produce a layer with a uniform thickness of 0.4, 5, and 44 μm for mode 1, 2, and 3 particles, respectively (assuming a density of 2 g cm⁻³ for all particles). We note that if the deposition were spread among the three mirrors, the layers would be 3 times thinner but the resulting absorption would be approximately the same. If the sediment were spread all over the surface inside the tube, the layers would be 10–20 times thinner. However, this hypothesis is probably not realistic, since the walls of the tube are parallel to the aerodynamic flow, while the mirrors are perpendicular to the flow.

Hypothesis of Diluted Croconic Acid

We can compare our absorption spectral signature by X with the absorption effect of H₂SO₄ droplets contaminated with croconic acid, the carbon monoxide polymer (C₅O₅H₂) studied by *Harley et al.* [1989] as a potential contributor to Venus UV albedo in the wavelength range showing a still unexplained absorption (Figure 10). It shows the croconic acid opacity measured at the laboratory by these authors using a 1-cm cell containing a concentrated (84%) sulfuric acid solution contaminated with 2×10^{-5} croconic acid mole per liter (or a mixing

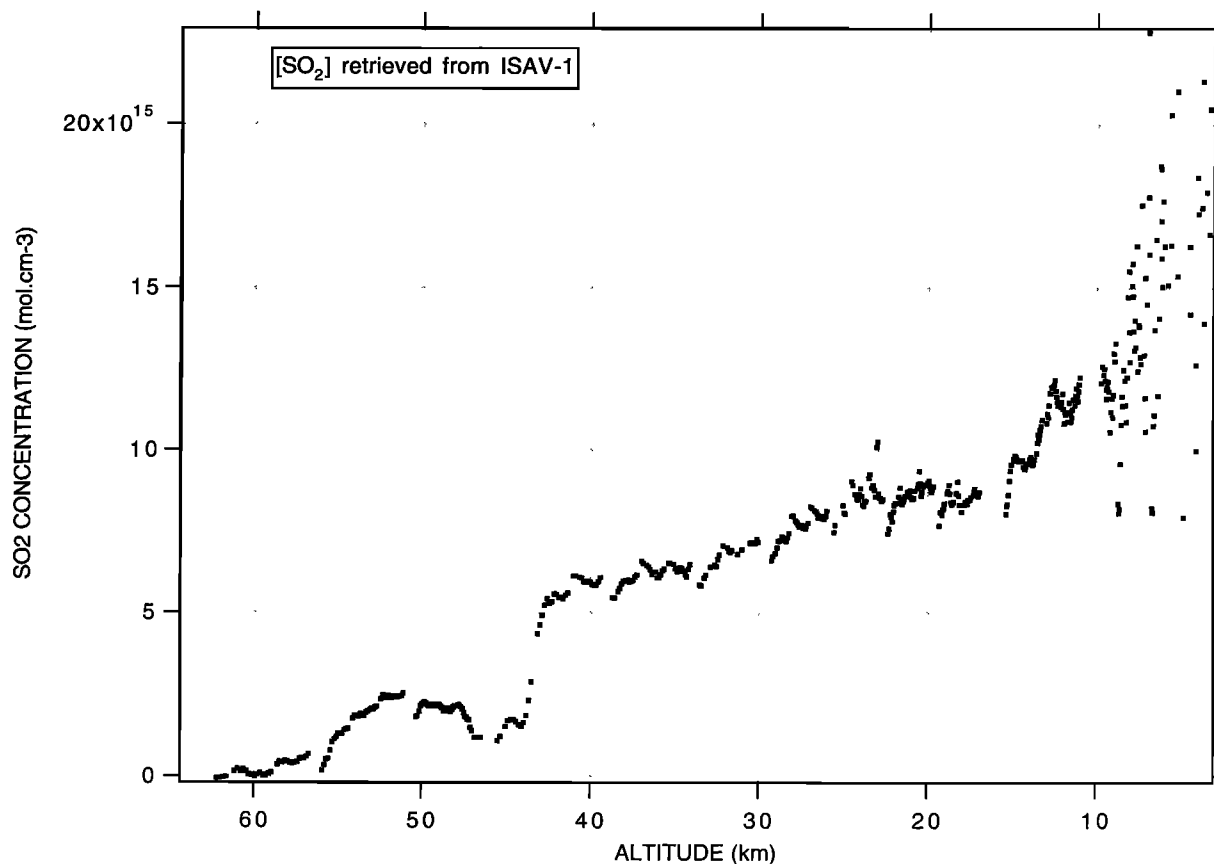


Figure 15. Vertical profile of the SO_2 concentration n_{SO_2} (cm^{-3}) retrieved by differential absorption from ISAV 1 measurements of optical thickness in the tube. The scatter of individual data points gives an idea of the uncertainty of the retrieval and instrumental errors. There is a significant decrease in the range 48–44 km. Below 10 km, the data scatter is larger due to a strong absorption and weak remaining signal. There is no variation at 18 km, the place of the ISAV shock event, which is what should be expected for SO_2 gaseous absorption.

ratio of 6.5×10^{-7}), together with the spectral signature of absorber X. The shapes are somewhat similar. We can now estimate what should be the concentration of croconic acid in H_2SO_4 droplets which would be needed in order to produce the observed ISAV 1 absorption. At 306 nm the differential optical thickness (with respect to 394 nm) of absorber X which is kicked off the mirrors is 0.83; however, not all absorber X is removed at this time, and the maximum value of α found at ≈ 44 km is 1.65. Therefore the differential optical thickness of absorber X deposited at 44 km (below the cloud deck) is $1.65 \times 0.83 = 1.37$. Given the layer thickness calculated above, the corresponding absorption coefficient is, for the three mode particles, 3.4×10^4 , 2.7×10^3 , and $3.1 \times 10^2 \text{ cm}^{-1}$ (assuming that only one of the modes at a time contribute to the absorption). When compared to the laboratory measurement of 0.55 cm^{-1} at 306 nm for a dilution of 6.5×10^{-7} , it would indicate a concentration of croconic acid in the H_2SO_4 droplets of Venus of 4%, 0.3%, and 0.037% in the mode 1, 2, and 3 particles, respectively. These values can be compared to the croconic acid concentration of 2.5%, which is called for by Hartley et al. [1989] to explain the UV albedo of Venus. If mode 1 particles were the only contributor to absorber X, they would have to be all collected on the mirrors and all contaminated with 4%. If mode 2 particles were the only contributor

with a concentration of 2.5% of croconic acid, a mirror collection efficiency of 12% would have been sufficient to produce the observed absorption, dropping to 1.5% efficiency for mode 3 particles alone.

As a conclusion of this subsection, we can state that indeed there is enough aerosol material in the clouds of Venus to have deposited a significant layer on the mirrors and that there is at least one potential contaminant, $\text{C}_5\text{O}_5\text{H}_2$, which has the right absorption coefficient in the UV to explain the observed absorption, though the observed spectral signature is not totally identical to that of $\text{C}_5\text{O}_5\text{H}_2$. It consolidates our proposed scenario, in which contaminated H_2SO_4 droplets are deposited in the clouds on the mirrors, provoking the observed absorption. This absorption could remain constant even after the droplets are submitted to evaporation into gaseous H_2SO_4 below 47 km because the contaminant does not evaporate.

However, croconic acid does evaporate and decompose at 150°C (39 km), as noted by referee V. A. Krasnopolsky, while absorber X is still present on the mirrors down to the surface (Figure 13). Therefore, despite some similarity in the absorption spectrum our measurements do not support the hypothesis of $\text{C}_5\text{O}_5\text{H}_2$ as the X absorber. It may be noted also that a scenario in which the absorber would not be contained in the

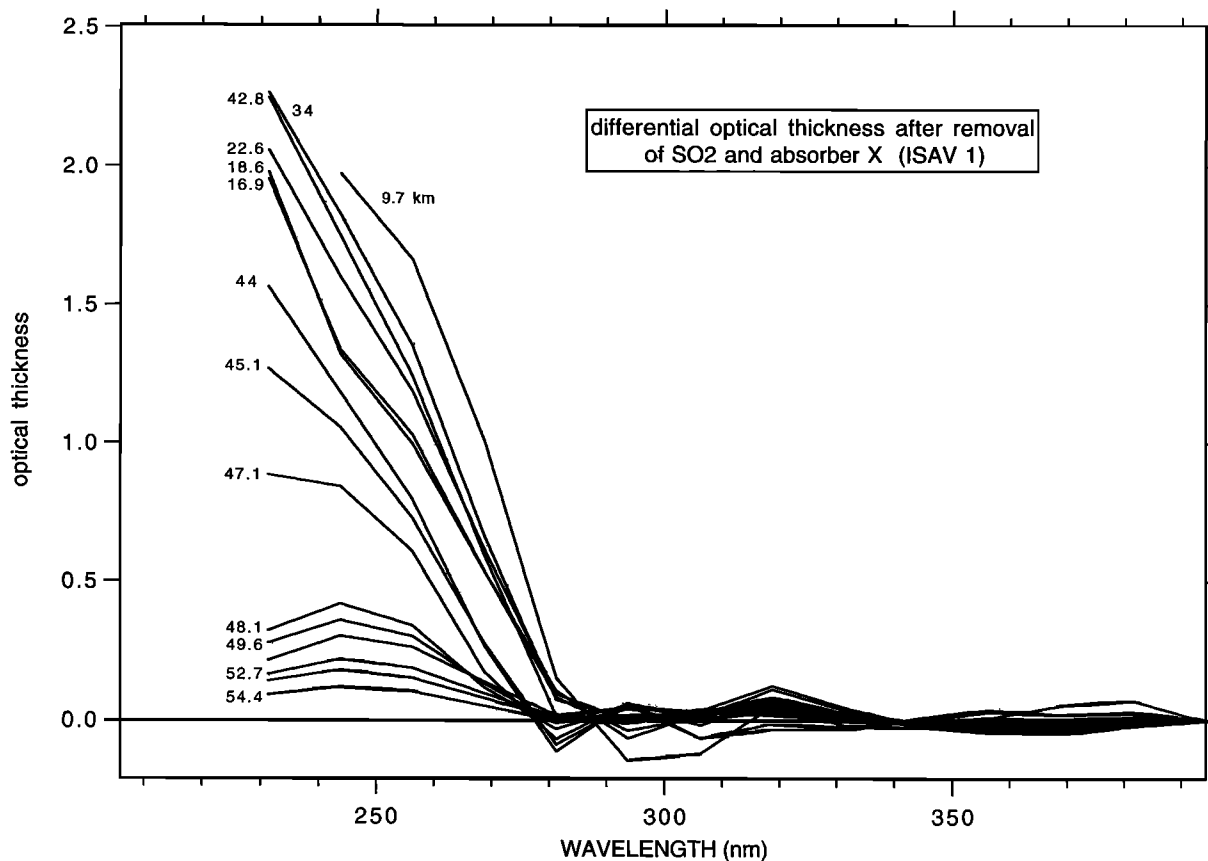


Figure 16. Residual differential optical thickness after removal of absorber X and SO₂. It is significant only below $\lambda < 281$ nm.

droplets, but would deposit directly on the mirrors, cannot be excluded either.

Comparison With Other VEGA Aerosol Measurements

A full discussion on the exact nature of the aerosol collected by ISAV is beyond the scope of this paper. It has a spectral signature in the UV which resembles that of C₅O₅H₂, but is not identical. Many other components have been proposed to explain the UV absorption in the albedo of Venus, like FeCl₃, elemental sulfur [Hapke and Nelson, 1975], amorphous sulfur [Toon et al., 1982], disulfurmonoxide, S₂O, and polysulfur oxide [Hapke and Graham, 1985] or ammonium pyrosulfite, (NH₄)₂S₂O₅ [Titov, 1983], and detailed comparisons with their spectral signatures should be pursued.

On board the same descending probes, VEGA 1 and VEGA 2, were two other experiments yielding information about the chemical nature of the aerosols. The IPF instrument studied by X ray fluorescence and absorption the aerosols collected on filters, and could determine some information about the elemental composition [Andreychikov et al., 1987]. Three elements were identified: sulphur, chlorine and phosphorus. Sulphur and chlorine in cloud particles were detected by the same kind of measurements done on previous Venera probes, but phosphorus was found for the first time during this flight. Some P-bearing substance can be important as a particle material in lower clouds. Distinct layers of differing composition were identified. Phosphoric acid H₃PO₄ is a likely candidate for this substance and phosphorous anhydride P₄O₆ for a gas responsible for its production [Andreychikov, 1987]. A critical review

of these data was given by Krasnopolsky [1989], who remarked that the lower subcloud boundary at about 33 km registered on VENERA 8 and Vega-1 and 2 [Gnedych et al., 1987] correlates well with the hypothesis of phosphoric acid particles dominating in subclouds.

A refractive index of 1.7 estimated for some of the particles registered in ISAV-A experiment (a particle size spectrometer/nephelometer, different from ISAV 1 and 2, [Gnedych et al., 1987]) can be understood if they consist of free condensed sulphur. Some evidences of the presence of free sulphur in clouds were obtained by the analysis of the VEGA SIGMA 3 (gas chromatographic analysis of particles [see Porshnev et al., 1987]) and IPF results. Therefore it is legitimate in the future to examine carefully the hypothesis that material collected on the ISAV mirrors could contain P- or Cl-bearing compounds or even free sulfur.

In section 8 the ISAV 2 results similarly show the possible deposition of one absorber, called Y in order not to impose the spectral signature of X in the analysis. It is interesting to correlate the buildup of absorber Y on ISAV 2 (Figure 22) with the amount of material collected on the filters of the IPF VEGA 2 X ray instrument, as shown by Andreychikov et al. [1987] or by Krasnopolsky [1989, Figure 1]. The materials containing Cl, S, and P atoms start to increase at ≈ 57 km, like absorber Y; there is a strong decrease of P atoms just above 47 km, explained by sublimation of the phosphorus-bearing aerosol, which is well correlated with the first level-off of absorber Y. Unfortunately, there are no data for the X ray instrument below 47 km.

Similarly, we note that the maximum concentration was found by the particle counter ISAV-A for VEGA 1, both for small and large particles in the altitude range 48–52 km [Gnedych et al., 1987]; this is exactly where the X absorber is building up for ISAV 1 (Figure 13).

6. Aerosols, Albedo of Venus, and Near-IR Features

In the previous sections we have shown that ISAV 1 and ISAV 2 data are consistent with the scenario of aerosol collection in the lower cloud, and a UV absorption spectral signature (220–400 nm) of such aerosols was obtained. Whatever is its exact nature, the contaminant collected in the aerosol droplets by ISAV, showing some UV absorption, should also be considered as a candidate for explaining a part of the UV albedo, as discussed below.

In this section we examine the relevance of this ISAV finding with various properties of the atmosphere of Venus and, in particular, its spectral albedo as seen from outside and the presence of so-called “UV markings.” The spectral albedo curve of Venus shows a steep decline at wavelengths between 500 and 300 nm. It can be explained only by the presence of some absorber(s) within the clouds of Venus, conventionally named “UV absorber,” although not only the UV part of the spectrum is affected and also not only one but several substances can contribute UV markings are detectable possibly because of horizontal variations of this absorber.

UV Optical Properties of the Atmosphere

It was shown convincingly that the material responsible for markings and spectral albedo (in addition to SO₂) is confined in the upper cloud of Venus [Pollack et al., 1980], and quite clearly the aerosols of the lower cloud (even if they were UV black) cannot have enough influence in the radiation field coming out of Venus in the UV part of the spectrum ($\lambda < 400$ nm), which comes from scattered solar radiation, to be responsible for the spectral albedo and markings.

Not very much was learned about the UV local opacity and pure absorption of the atmosphere of Venus below the upper cloud from Pioneer Venus probes. The nephelometer/radiometer of the Pioneer Venus sounding probes included a so-called “UV channel,” which showed a decrease of intensity down its trajectory [Ragent and Blamont, 1980]. However, it was suggested by Pollack et al. [1980] that, given the amount of UV absorber in the upper cloud necessary to explain the UV albedo, no UV radiation could penetrate below 63 km. The signal recorded by the UV radiometer therefore was assigned to the leak in the near-infrared of the filters, which was present in addition to the nominal UV bandwidth covering 300–400 nm [Ragent and Blamont, 1980, Figure 3]. Therefore these data cannot be used to infer anything about the UV properties of the atmosphere below 63 km.

The solar flux radiometer (LSFR) on the Pioneer Venus large probe had the capability to measure the net flux of solar scattered radiation through the atmosphere (the difference between downward and upward flux), and therefore to measure the pure absorption of the atmosphere [Tomasko et al., 1980]. The main region of absorption was found to be confined to the upper cloud, the lower cloud being conservative. However, the bandwidth of LSFR had no sensitivity at all in the UV $\lambda < 400$ nm [Tomasko et al., 1980, Figure 24].

After Pioneer Venus in 1978, there was only one in situ

experiment to study the vertical distribution of the UV absorber: a filter photometer on the Soviet descent probe Venera 14 (1982). It measured scattered solar fluxes in a bandpass of 70 nm centered at 350 nm from a few directions at altitudes between 62 and 48 km at significant levels (in spite of the above-mentioned suggestion of Pollack et al. [1980]). The analysis of the results [Ekonomov et al., 1983, 1984; Moroz, 1983] showed clearly the presence of two distinct components in the vertical distribution curve of the volume absorption coefficient. A first component dominates above 56 km, then the atmosphere is conservative (no local UV absorption between 56 and 53 km), then a second component absorbs below 53 km. This second component can be explained by SO₂ absorption, with a required mixing ratio value of 10 ppm at 53 km if a cross section of 10^{-22} cm² is used in the bandpass of the photometer.

In principle, the X absorber can be responsible for a part of the UV absorption detected as the second component below 56 km, through multiple scattering of light between aerosol particles in the atmosphere. But the SO₂ mixing ratio measured by ISAV is sufficient (Figure 24) to account for most, or for all of the absorption measured by Venera 14 in the UV below 53 km. However, it is not so easy to make quantitative comparisons between the ISAV UV absorption of aerosols accumulated over the mirrors over a large altitude range, and the UV opacity measured by Venera 14 from UV scattered solar light decreases. In particular, the fact that X absorber is observed only below 53 km (for ISAV 1) and 56 km (for ISAV 2), while the UV photometry found substantial absorption above 56 km, may be due to an inefficient collection of aerosol particles on the mirrors of ISAV in the upper atmosphere, or to the gaseous nature of the substance responsible for the UV albedo at high altitude.

We must point out here that the statement of Pollack et al. [1980] mentioned above (suggesting that, given the amount of UV absorber necessary to explain the UV albedo of Venus, no UV radiation could penetrate below 63 km) is contradicted by the results of the Venera 14 UV photometer, which actually measured UV radiation down to 46 km. Consequently, the Pioneer Venus signal seen by the UV radiometer might not have been fully contaminated by infrared leaks, and the problem of the validity of its results could be revisited.

ISAV Absorber, Venus Albedo, and UV Markings

It is somewhat confusing to refer to the UV absorber, meaning the material (in addition to SO₂) responsible for the planetary albedo and markings, since the material (or several materials) must have absorbing properties not only in the UV, but also at $\lambda > 400$ nm, up to 500–550 nm. Indeed, if the visible absorption must be confined to the upper cloud, as shown by LSFR results, these results do not preclude the presence of some UV absorbing material below the upper cloud, in addition to its existence in the upper cloud, since the LSFR had no sensitivity at all below 400 nm. This is true for SO₂ gas and also for the entire near-UV part of the “Venus absorber”). Statements found in the literature like “... the UV absorber of Venus is confined to the upper cloud region” [Crisp, 1986] are a little confusing. It may be true if it refers to the part of gas/aerosols which actually affects the solar radiation backscattered outside the atmosphere. It is not true if it designates the material, in a generic sense, which has UV absorbing properties. For instance, SO₂ affects the solar backscattered radiation in the UV and is certainly not confined to the upper cloud region. One must clearly distinguish, in this kind of discussion,

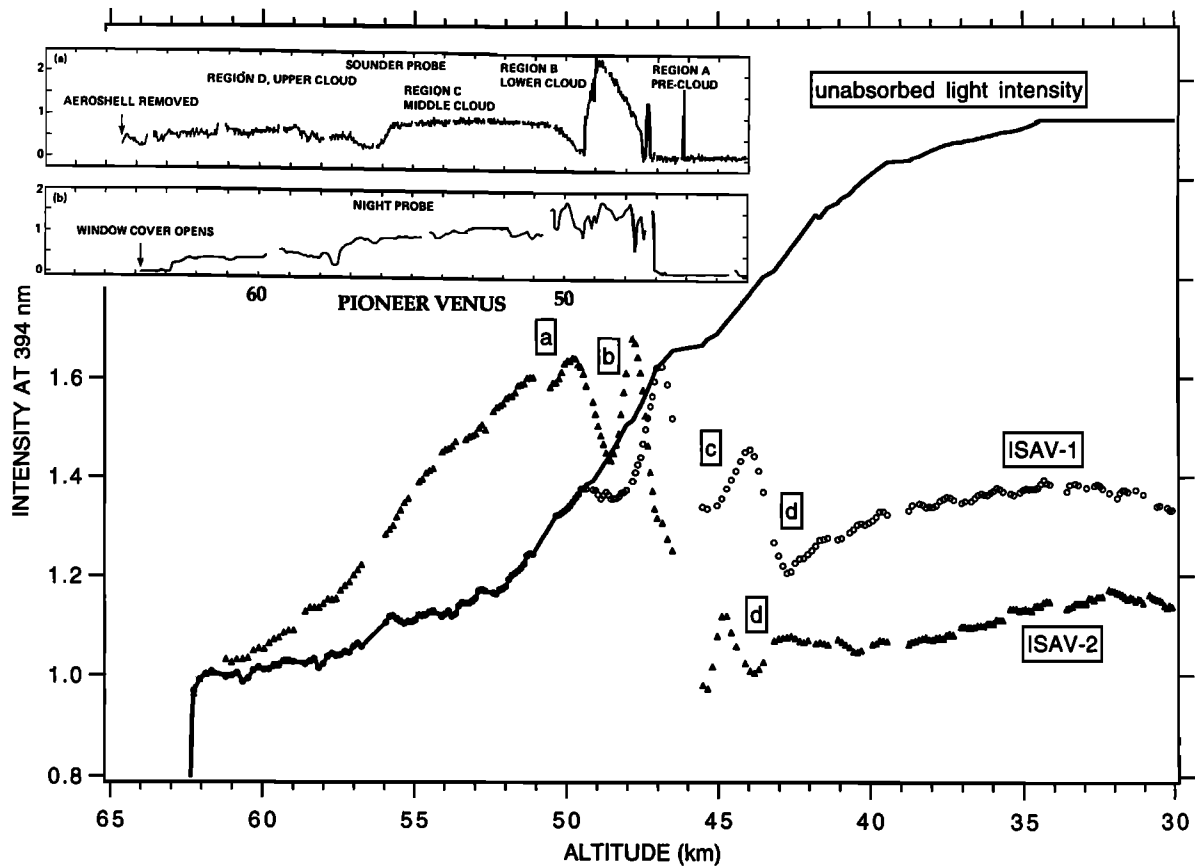


Figure 17. Measurements at 394 nm as a function of altitude for both ISAV 1 and ISAV 2. The solid line is a model of the variation of the xenon flash intensity at this wavelength, based on assumptions discussed in the text, and representing the light intensity that would be observed if there were no absorption in the path light. Four absorbing layers, labeled a–d are identified in the data of ISAV 2, with their counterparts b, c, and d clearly visible in ISAV 1 data, although at slightly lower altitudes. In the upper corner the cloud structure detected by the nephelometers of two probes of Pioneer Venus is indicated [Ragent and Blamont, 1980] on the same altitude scale, indicating a lower cloud boundary (LCB) at 47 km. While layers a and b for ISAV are experienced within the clouds, layers c and d are encountered well below the LCB.

three aspects: the vertical distribution of a material which has intrinsically optical absorbing properties, the vertical distribution of a material which actually absorbs the solar radiation, and the vertical distribution of a material which absorbs partially the solar radiation backscattered and observed from outside.

Therefore, it cannot be excluded that the same material found by ISAV in the particles of the lower cloud could also be present in the particles of the upper cloud and be responsible of the UV part ($\lambda < 400$ nm) of the albedo and UV markings. It must also be admitted that the present ISAV results give no compelling evidence that absorber X is present in the upper atmosphere.

Visible Part ($\lambda > 400$ nm)

If the ISAV material would also be present in the upper cloud to explain the UV part of the Venus albedo, it would require the existence of an additional material, in addition to SO_2 and X, to explain the visible part.

ISAV measurements being limited to $\lambda < 400$ nm, no conclusions can be drawn from ISAV about the problem of the visible part of the absorption affecting the upper atmosphere. Given the constraint of no pure absorption in the visible below 57 km as derived from the LSFRR data [Tomasko *et al.*, 1980] and Venera data [Moroz *et al.*, 1985], one would conclude that

only one single material would be responsible for the unexplained UV + visible albedo, and that this material would be present in the lower cloud. In that case, the ISAV absorber, though existing in the lower cloud, would not be the one responsible for the UV + visible part of the albedo.

It might be worthwhile, however, to reexamine in detail (but this is beyond the scope of this paper) the results of Tomasko *et al.* [1980] in view of the recent discovery of an important source of thermal emission leaking out from the nightside of Venus, in several windows (1.1, 1.7, and 2.3 μm), subject to intense modeling in a recent paper [Pollack *et al.*, 1993]. Measurements of the near-infrared mapping spectrometer (NIMS) instrument on board Galileo also show some radiation below 1 μm , extending at least down to 0.80 μm , as predicted by the radiative transfer model spectrum of Kamp and Taylor [1990]. Of course, this radiation field must also exist on the dayside, and according to its intensity, it might have influenced the data of the LSFRR radiometers. The narrowband radiometer of LSFRR is at a wavelength of 0.63 μm , which is above the visible spectral region of interest for the Venus absorber, and is probably at too short a wavelength to be influenced by the thermal emission. (We note, however, a small decrease of net flux measured by LSFRR just above the lower cloud, at 50 km.)

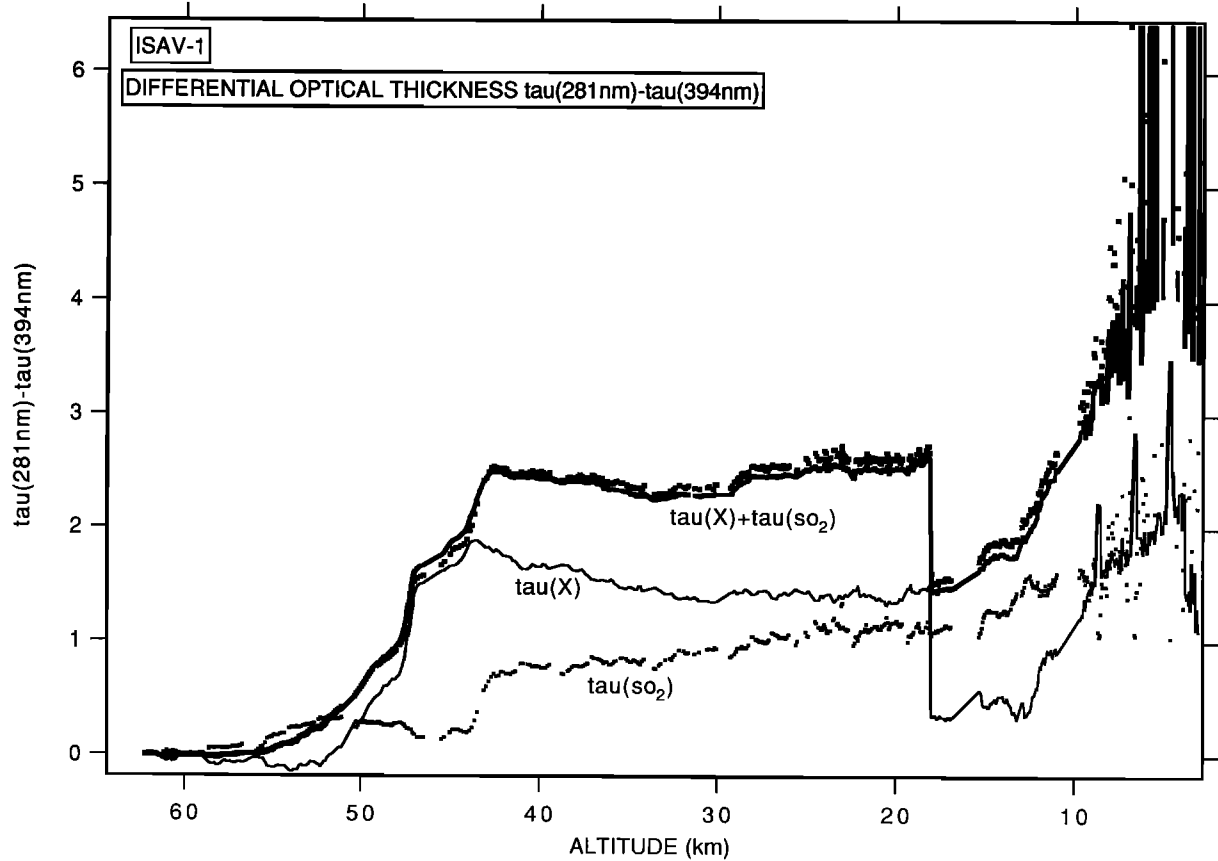


Figure 18. Individual data points representing the measurements of ISAV 1 differential optical thickness $\tau(281 \text{ nm}) - \tau(394 \text{ nm})$. They are compared with the recalculated differential optical thickness (between 281 and 394 nm) for the retrieved SO_2 , for the absorber X, and for the sum $X + \text{SO}_2$. This last curve fits the data points quite well, showing that most of the differential absorption (281 nm – 394 nm) can be explained by the sum absorber $X + \text{SO}_2$.

The other two radiometers, with bandwidths $0.4\text{--}1 \mu\text{m}$ and $0.4\text{--}1.8 \mu\text{m}$, are both sensitive to the material responsible for the albedo (in the region $0.4\text{--}0.55 \mu\text{m}$) and to the thermal radiation. The first one shows a net flux decreasing from 60 to 57 km, then reaching a plateau, interpreted as proof that there is no absorption, with nearly conservative scatterers in the region where the thickest clouds exist. In fact, the net flux curve shows a small increase by 1 W/m^2 below 57 km, which in principle, is the signature of some local emission. Would it be possible that the thermal emission of Venus is responsible for this small increase, and once corrected from the thermal emission, would the net flux curve still show the same plateau, totally excluding in the middle and lower cloud the presence of the visible Venus absorber which is found in the upper cloud and is responsible for the albedo? The answers to these questions may need a full radiative transfer model of Venus, since the thermal radiation measured from outside the atmosphere (ground-based and Galileo) is anyway strongly reduced, and even a crude estimate is beyond the scope of this paper.

Near-Infrared Features on the Venus Nightside

The 1990 Galileo Venus flyby allowed us to collect a unique sample of near-infrared images of the nightside at a variety of wavelengths from 0.7 to $5.2 \mu\text{m}$. Very large intensity contrasts of 20:1 were found at $2.3 \mu\text{m}$ between bright areas and dark areas [Carlson *et al.*, 1991], requiring however, only a modest

25% decrease in cloud opacity ($\tau = 45\text{--}34$) and implying the same variation in cloud number density or extinction cross section (or both) from bright areas. Carlson *et al.* produced convincing evidence that this change in opacity is restricted to the lower cloud levels (48–52 km) because, otherwise, their images at $3.71 \mu\text{m}$ (a wavelength at which the emerging radiation is very sensitive to upper cloud optical thickness) would also show an important contrast, which they do not exhibit.

It is exactly in this range of altitude, 48–52 km, that ISAV instruments collected the cloud particles as shown by Figure 13. Therefore, it is quite likely that the same cloud particles which were collected by ISAV and show a UV absorption by a contaminant of H_2SO_4 droplets, also control the quantity of IR radiation emerging at $2.3 \mu\text{m}$ on the nightside of Venus. The IR contrasts could be related to the amount of contaminant X if it has some absorption at $2.3 \mu\text{m}$ (which would await its formal identification for verification) or simply to the number of particles acting as scatterers.

The quantity of X component (or likely number of droplets) collected by ISAV 1 and ISAV 2 as measured at 40 km altitude by its differential optical thickness $\tau(281 \text{ nm}) - \tau(394 \text{ nm})$ was 1.66 and 0.84, respectively. The quantities differ by a factor of 2, though the two probes were separated by only 2100 km. In view of the high sensitivity of the IR emerging at $2.3 \mu\text{m}$ and the horizontal scale of features as observed by NIMS at this wavelength, the horizontal gradient of cloud particles experi-

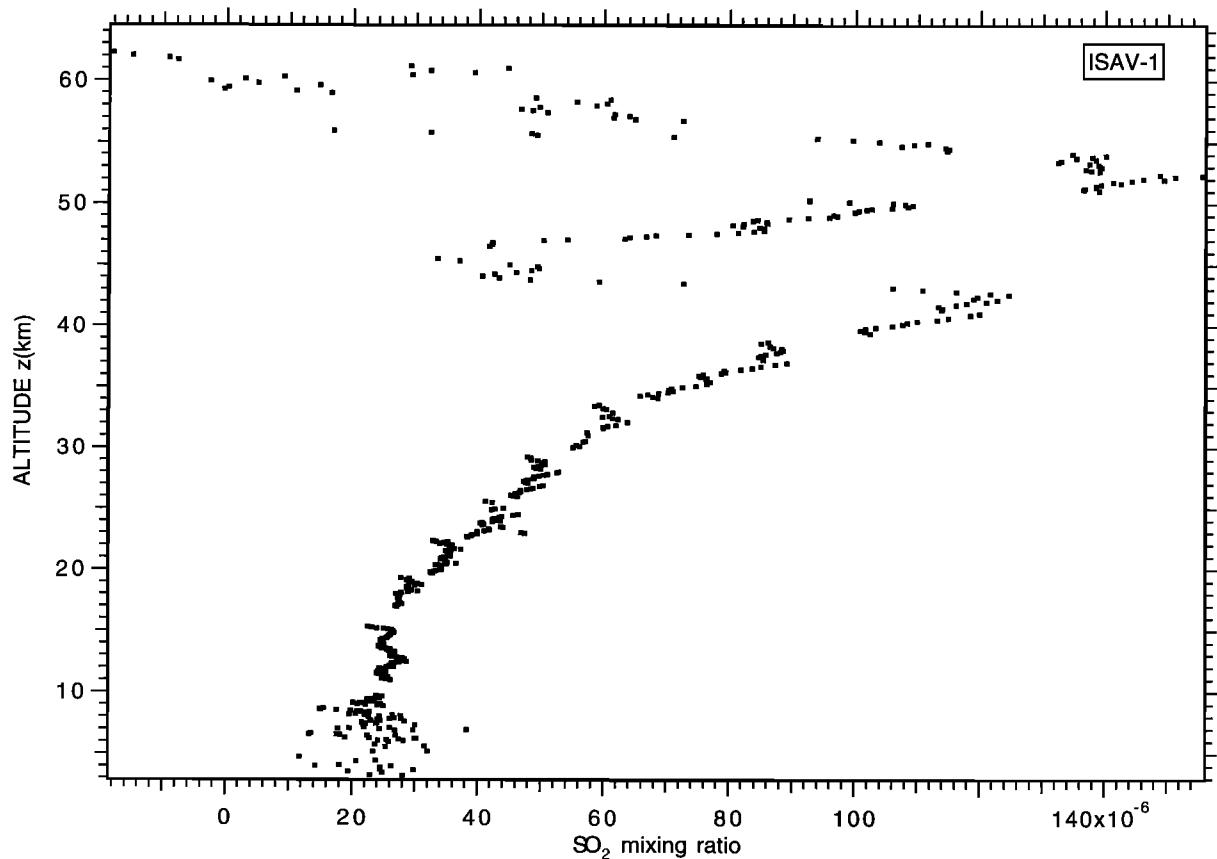


Figure 19. SO_2 mixing ratio measured by ISAV 1 (derived from n_{SO_2} and the atmosphere profile of *Linkin et al.* [1987]). A few points are spurious (instrumental effect of new switch-on at 50 and 56 km). Below 40 km, the mixing ratio is constantly decreasing with altitude, implying a strong downward flux of SO_2 .

enced by ISAV is more than enough to explain the NIMS IR horizontal variations. This factor of 2 is also comparable with the variations of the lower cloud optical depth measured by the Venera and Pioneer Venus probes, and by radio occultations.

7. Vertical Cloud Structure

Though we have relied only on the differential optical thickness with $\lambda = 394$ nm, it is interesting to examine in some detail the light curves at 394 nm. They are displayed for both ISAV 1 and ISAV 2 in Figure 17, in the region above 30 km to enhance the vertical structure showing the layers a–d discovered by ISAV. The solid line is an attempt for ISAV 1 to estimate what the evolution of the light curve would be at 394 nm I_0 (394 nm) in the absence of any absorber. This curve was built with the following reasonable assumptions: (1) above layer b (50 km), the absorption at 394 nm is negligible; (2) it is also assumed to be zero at the peak intensity between layers b and c; and (3) the light increase experienced above 50 km is assumed to continue below 50 km in a smooth fashion, and below the bottom of layer d (42 km), in a parallel way (different only by a scaling factor) with the light curve at 394 nm down to the ground. The building of this curve allows us to determine an estimate of the optical thickness at 394 nm, which would also have to be added to the differential optical thickness measured at all other wavelengths in order to get the true optical thickness at these wavelengths.

As mentioned in section 3, the tiny layer a seen by ISAV 2 does not exist on ISAV 1. Layers b–d are clearly seen on both instruments, separated by two peaks of enhanced transparency of the atmosphere. There is a slight difference of altitude (≈ 1 km lower for ISAV 1 than for ISAV 2) of these peaks (see Table 3).

At the top of Figure 17 is represented the data collected by two nephelometers placed on the large probe (sounding probe) and the night probe of Pioneer Venus [*Regent and Blamont*, 1980]. Both indicate a lower cloud boundary (LCB) at 47 km altitude. This altitude corresponds clearly to several features of ISAV measurements: (1) the bottom of layer b (or peak transparency between layer b and layer c), and (2) the major buildup of absorber X (ISAV 1) and absorber Y (ISAV 2), as shown on Figures 13 and 22, respectively, stops precisely at this altitude of 47 km, with a small secondary enhancement between 47 and 43 km.

However, it is also quite important to note that below the LCB, ISAV 1 and 2 experience severe drops of the intensity with the two episodes of layers b and c between 48 and 42 km, in a region which was measured as free of particles by Pioneer Venus probes, except for very thin layers. We note also that for layers a and b, which are inside the lower cloud, apparently the transmission of the instrument is totally recovered at 394 nm at the bottom of the layer. This can be understood if the absorber at this wavelength is gaseous, or if it is under the form of liquid droplets which evaporate quickly, letting no absorption at 394

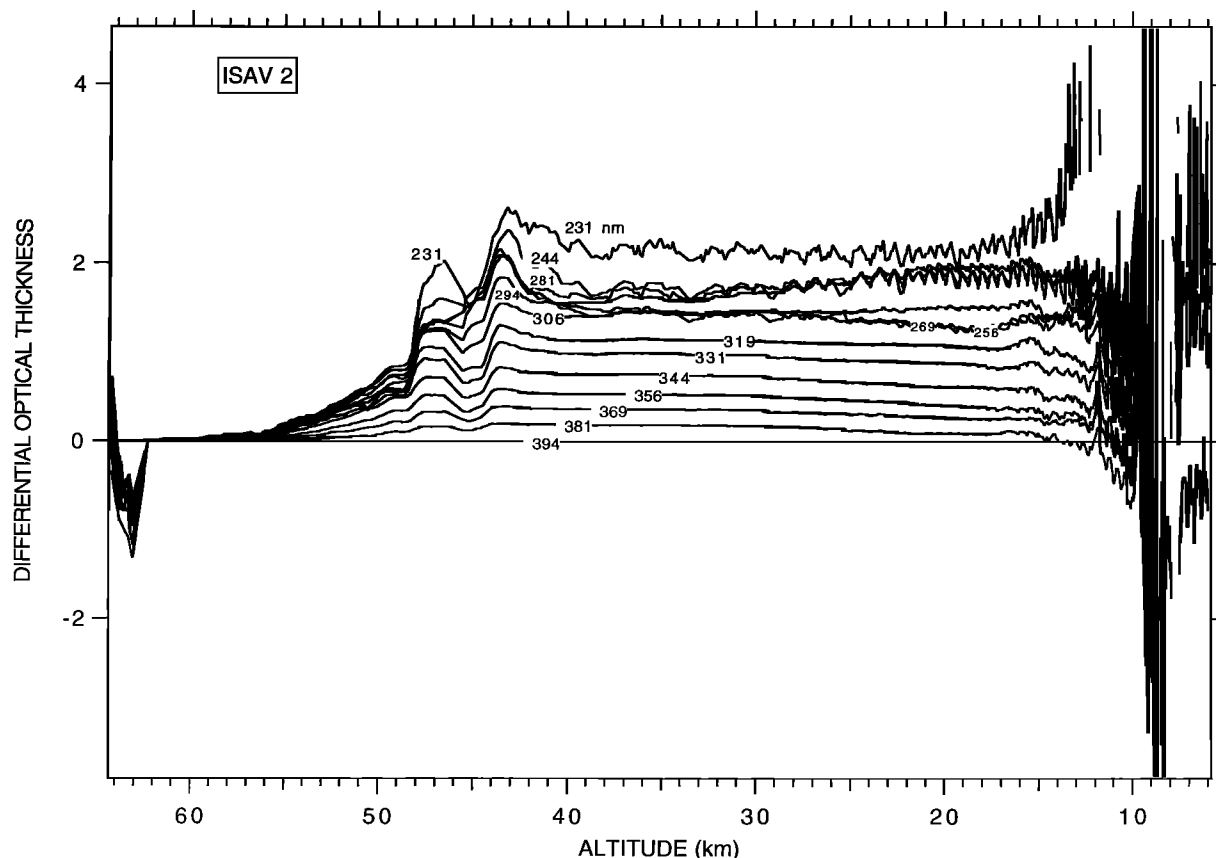


Figure 20. Differential optical thickness $\tau(\lambda_j) - \tau(394 \text{ nm})$ for ISAV 2 as a function of altitude for all the wavelength bins. Wiggles present around 20 km are probably spurious. The optical thickness increases from zero for $\lambda_j = 394 \text{ nm}$ to about 2 for 231 nm in the region 18–40 km.

nm (at variance with other shorter UV wavelengths). Evaporation/sublimation was also invoked to explain the X ray analysis of collected aerosols [Andreychukov *et al.*, 1987].

On the contrary, layers c and d, which are below the clouds, show a decrease of transmission, which is not fully recovered at the bottom of the layer. This is difficult to explain with gaseous absorption alone, and probably requires the presence of droplets well below the clouds which can be deposited on the mirrors on the upper half of the layer and evaporate again during the lower half of the layer. This time, some material absorbing at 394 nm remains on the mirrors of the instrument. These observations seem compatible with the presence of liquid droplets below the clouds, a phenomenon called rain in the atmosphere of the Earth.

8. SO₂ Vertical Distribution

ISAV 1 SO₂ Vertical Profile

The concentration $n_{\text{SO}_2}(z)$ measured by ISAV 1 is displayed in Figure 15. Reliable measurements were obtained between 60 and 10 km, with n_{SO_2} varying between 5×10^{14} and 13×10^{15} molecules cm^{-3} . Below 10 km the data are too noisy to extract reliable estimates of SO₂. With these absolute SO₂ concentrations, the optical thickness in the path light can be computed. Figure 18 is a comparison plot of the differential optical thicknesses $\tau(281) - \tau(394)$ for SO₂, for absorber X, for the data (solid points), and for the sum SO₂ + X. It clearly shows that most of the measured differential absorption can be

accounted solely by these two absorbers. The concentration $n_{\text{SO}_2}(z)$ steadily increases with decreasing altitude, except for a pronounced trough between 50 and 44 km for ISAV 1.

The mixing ratio $[\text{SO}_2]/[M]$ displayed on Figure 19 for ISAV 1 was computed from data of Figure 15 and the atmospheric profile as given by Linkin *et al.* [1987] ($[M]$ is the total number of molecules at each altitude derived from $p = n kT$). This profile is unprecedented and unique up to now, both in the altitude coverage (down to 10 km) and the altitude resolution. It is mainly characterized by a double peak at 52.5 and 42.5 km, separated by a deep valley, with a steady mixing ratio decrease below 42 km, and reaches an apparent plateau of $\cong 25$ ppmv at 10 km.

In the highest peak, a part of the vertical structure is spurious, and linked to one instrumental effect mentioned in section 2, namely, the higher than normal signal after a new switch-on of the xenon flash in some spectral bins. Just above 50 km and 56 km, about five points are affected and should be discarded, eliminating some of the vertical structure. Otherwise, the scattering of data gives an idea of the accuracy of the measurements. The SO₂ mixing ratio peaks at 150 ppmv at 51.5 km and at 125 ppmv at 42.5 km, while it drops severely down to 30 ppmv in the deep valley at 45.6 km.

ISAV 2 Analysis

From Figure 6, representing all data for ISAV 2, the differential optical thickness $\tau(\lambda_j, z) - \tau(394, z)$ can be computed and is plotted as a function of altitude z in Figure 20. All the

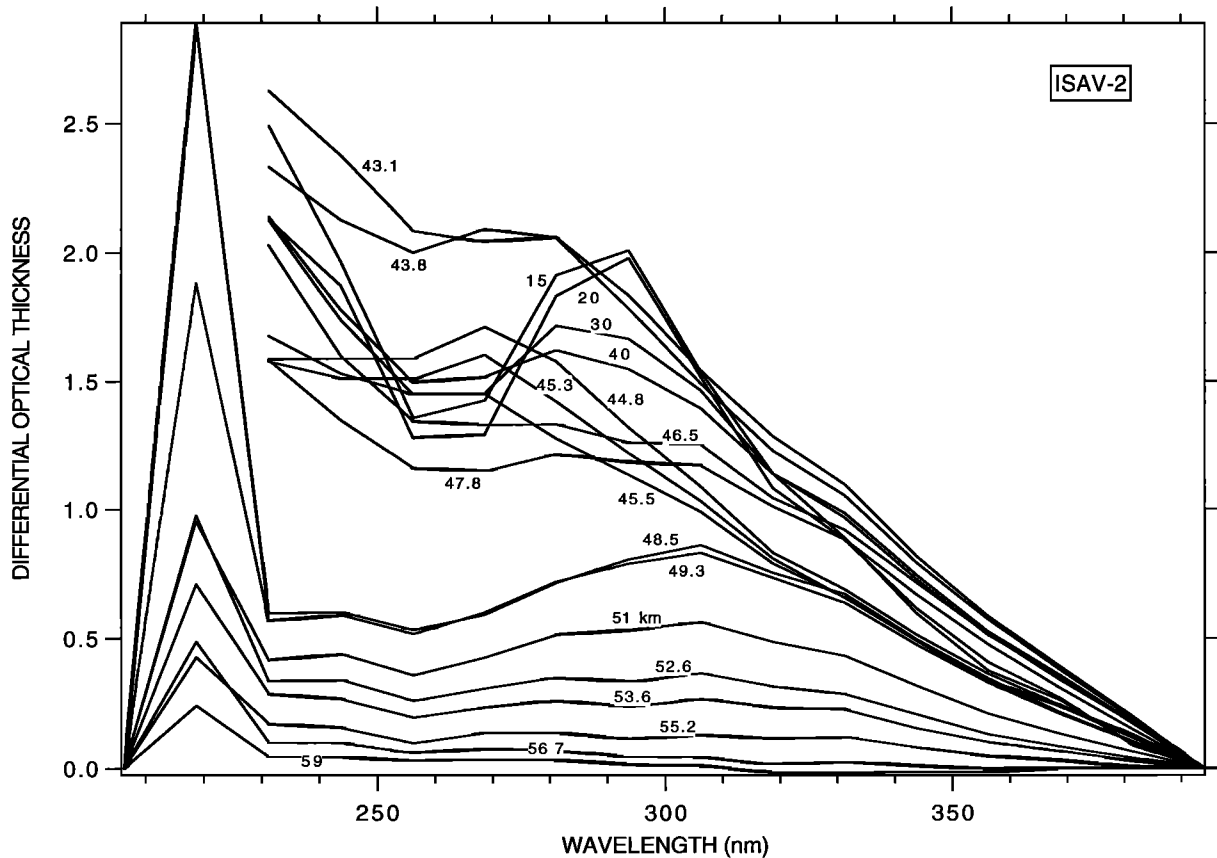


Figure 21. Differential optical thickness $\tau(\lambda_i) - \tau(394 \text{ nm})$ for ISAV 2 as a function of wavelength for various altitude levels. The SO_2 bump at 281–294 nm is clearly seen at low altitudes.

curves increase during the descent down to 43 km altitude, below which they stay more or less constant, except for those wavelengths particularly sensitive to SO_2 . This scenario is much like the one for ISAV 1, showing that, also for ISAV 2, some material must have deposited on the mirrors during the crossing of the cloud decks. Since there were no shocks to kick off the material from the ISAV 2 mirrors, we had to rely on a slightly different approach for the analysis of ISAV 2 data.

The spectra of the differential optical thicknesses obtained at various altitudes for ISAV 2 are shown in Figure 21. They show a somewhat similar shape above 331 nm (no SO_2 absorption), consistent with the idea that an absorber that we call Y has deposited during the cloud deck crossing. The whole spectral signature of Y may be obtained from a spectrum at high altitude. We have selected spectrum 55, obtained at 53.6 km. However, we must account for the fact that at this altitude, a part of the absorption is already due to SO_2 gas. The quantity of SO_2 present at this altitude was determined from the light curve for wavelength $\lambda_2 = 219 \text{ nm}$, where the SO_2 cross section averaged over 12.5 nm is $3.03 \times 10^{-18} \text{ cm}^{-2}$, ≈ 4 times larger than at 281 nm. Though the signal from the xenon flash at 219 nm is very low (not shown in Figure 6) and disappears below 50 km, it is still large enough to estimate the SO_2 concentration at 53.6 km at $0.5 \times 10^{15} \text{ cm}^{-3}$. Therefore the spectrum of absorber Y was obtained by subtracting from the measured spectrum $\tau(\lambda_i, 53.6 \text{ km})$ the spectrum of the optical thickness of SO_2 along a path of 170 cm.

The quantity of absorber Y collected along the descent of ISAV 2 was determined similarly to ISAV 1 for absorber X,

and is displayed in Figure 22. It must be noted that only the six wavelength bins from 331 to 394 nm, where there is no SO_2 absorption, were used (as for ISAV 1), and therefore the quantity $\alpha(Y)$ of Y absorber is totally independent of the quantity of SO_2 present at 53.6 km.

Again, similar to the ISAV 1 analysis, the whole spectrum of Y multiplied by $\alpha(Y)$ was subtracted from the differential optical thickness data. From the remaining spectra, an amount of SO_2 was calculated at each altitude using wavelengths 281–331 nm. The absolute concentration of SO_2 is shown in Figure 23, while the ISAV 2 SO_2 mixing ratio is displayed in Figure 24 as data points. The ISAV 1 SO_2 mixing ratio is also shown as a solid line for comparison. Above 40 km of altitude, the vertical structure of SO_2 for ISAV 2 is different from that for ISAV 1. There is no double peak, but rather a single peak at 43 km altitude, reaching 210 ppm.

Below 40 km altitude, the two curves derived from ISAV 1 and ISAV 2 are strikingly similar, showing the same decrease of mixing ratio with altitude. Apparently, the SO_2 mixing ratio for ISAV 2 becomes lower than that for ISAV 1 below 14 km; however, we estimate that this is most likely an artifact of our method of estimate of SO_2 , which assumes that only SO_2 and absorber Y are present to explain all the data for $\lambda > 281 \text{ nm}$. Indeed, the behavior of differential optical thickness curves below $\approx 15 \text{ km}$ as shown by Figure 20 indicates that this assumption is certainly no longer valid below 15 km, and the low values of SO_2 derived below 14 km for ISAV 2 should be disregarded.

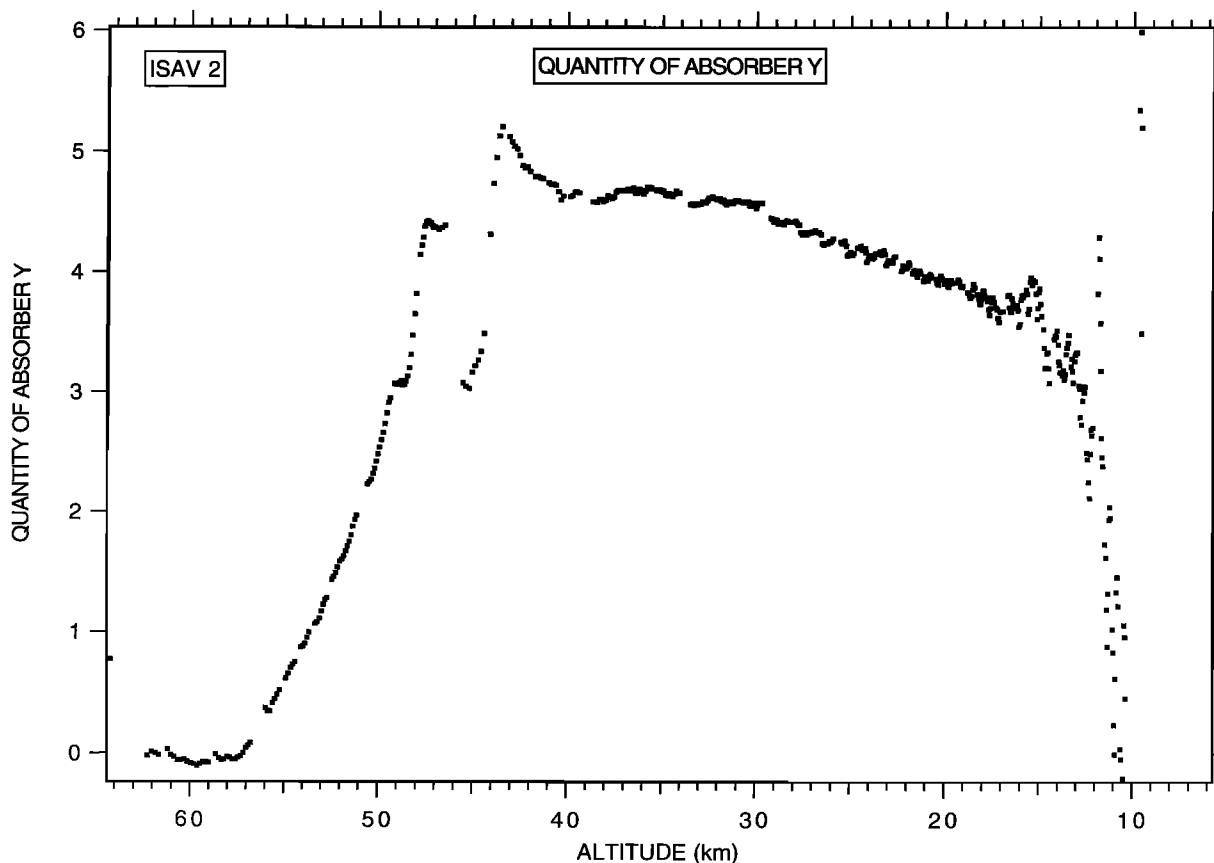


Figure 22. Quantity of absorber Y determined as a function of altitude in ISAV 2 data. The spectrum of this absorber is the one experienced at 53.63 km, minus a small contribution of SO₂. It builds up mainly in the range 57–47 km, which corresponds to middle cloud and lower cloud decks. Variations in the range 44–47 km correspond to the ISAV 2 layer c (see Figures 8 and 20).

Comparison With Previous SO₂ Measurements

Table 4 gives a summary of previous measurements of SO₂ below 60 km (measurements made by UV spectroscopy from outside are not considered because they are relevant to the layer where SO₂ is destroyed photochemically, at higher altitudes than 60 km, where the ISAV measurements begin). These include previous in situ measurements: Pioneer Venus large probe gas chromatograph [Oyama *et al.*, 1980] and mass spectrometer [Hoffman *et al.*, 1980] and Venera 11 and Venera 12 landers gas chromatographs [Gel'man *et al.*, 1979]. At $z = 42$ km, an altitude where Oyama *et al.* [1980] have measured with a gas chromatograph a lower limit of n_{SO_2} of 176 ppm, we have values of 125 ppm for ISAV 1 and 140 ppm for ISAV 2 in a region of strong vertical gradient.

Between $z = 42$ and 15 km, both ISAV 1 and 2 show steadily decreasing values of the measured sulfur dioxide concentration in the lower atmosphere of Venus, in conflict with data from the other in situ experiments (Table 4). At an altitude of $z = 22$ km, the Pioneer Venus large probe gas chromatograph and the Venera 12 lander gas chromatograph measured a concentration above 130 ppm: (130 ± 35) ppm for Venera 12 [Gel'man *et al.*, 1979] and (185 ± 43) ppm for Pioneer Venus [Oyama *et al.*, 1980] (Table 4). At 22 km the ISAV experiment obtains $n_{\text{SO}_2}(z) = 38$ ppm for both ISAV 1 and ISAV 2.

Table 4 also includes more recent measurements obtained from Earth through high-resolution spectroscopy of the IR

light emerging on the nightside through the clouds of Venus [Bézard *et al.*, 1993; Pollack *et al.*, 1993]. They have interpreted their superb spectra with a mixing ratio (abundance) of 130 ± 40 ppmv in the altitude range of 35–45 km, quite compatible with our ISAV 1 value of 125 ppmv at the peak at 42 km. It could be noted, however, that the ISAV 1 average over the range 35–45 km is rather 90–100 ppmv because of the deep valley, a value still compatible with Bézard *et al.*'s estimate. The analysis of lower resolution spectra around $2.46 \mu\text{m}$ also yielded an independent estimate of 180 ± 70 ppm at 42 km, also quite compatible with ISAV results.

It can be observed, as an important verification of our method of determination, that no significant change occurs in the mathematical retrieval of $n_{\text{SO}_2}(z)$ before and after the 18.0-km transition for ISAV 1, when the mechanical shock affecting several spacecraft instruments shakes the dried absorber X out of the ISAV mirrors. The final region between $z = 25$ and 10 km is the most precisely retrieved for SO₂ in the case of ISAV 1. At 10 km the deepest SO₂ concentration measurement ever obtained in Venus gives (25 ± 2) ppm for ISAV 1 and 15 ppm for ISAV 2, but this lower value might be due to an artifact as mentioned above. We are more confident in ISAV 1 estimates at this altitude.

The fact that ISAV SO₂ data are in good agreement with ground-based spectroscopy in the region 35–45 km makes us quite confident of our SO₂ retrieval algorithm and also our optical thickness measurements in the entire range 10–60 km.

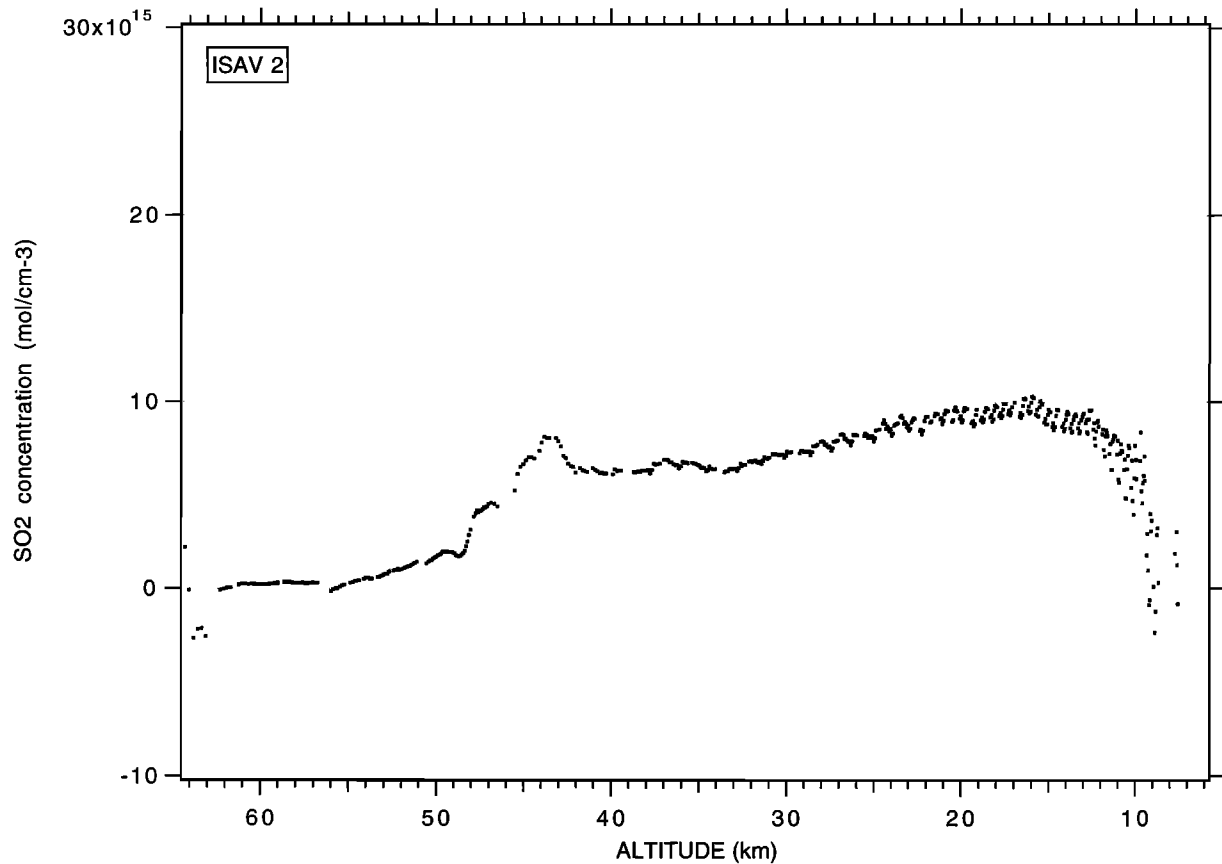


Figure 23. Absolute concentration of SO_2 retrieved from ISAV 2 data. The decrease below 13 km is probably spurious because the assumption that only absorber Y and SO_2 absorb becomes invalid.

Therefore we consider that the low values that we are measuring in the lower atmosphere of Venus are real. It can be checked also on Figure 18 that, if the SO_2 concentration were 185 ppmv at 22 km, as derived from Pioneer Venus instead of 38 ppmv with ISAV, the optical thickness $\tau(281) - \tau(394)$ should have been 6 instead of the 1.2 actually measured, and practically no light would have reached the ISAV detector, while the signal is indeed still quite significant at this altitude.

This is even better illustrated on Figure 25, where the actual light curves for ISAV 1 at 281 nm (maximum SO_2 absorption) and 394 nm (no SO_2 absorption) are plotted as a function of altitude in a log scale, and compared to model computations assuming constant mixing ratios of 50, 100, and 200 ppmv of SO_2 (solid lines). The upper solid line is an estimate of the xenon flash intensity I_0 in the absence of all absorption, based on the assumption that it follows the light curve for 394 nm down to 51 km (upper boundary of our absorbing layer b). It continues to increase as before in region 3, and increases again in region 4 down to 33 km in a parallel fashion as $I(394 \text{ nm})$, and then becomes constant down to the ground as explained in section 7. The absorptions by constant mixing ratio of SO_2 are computed from this solid curve labeled “unabsorbed light curve.”

The data for the light curve at 281 nm indicates that, even if all absorption measured at 281 nm were attributed to SO_2 , the mixing ratio in the range 15–18 km would only be just above 50 ppm, say, ≈ 60 ppm. It is more than likely that what is absorbing at 394 nm, as measured by the difference between I_0 and $I(394 \text{ nm})$, must also have some absorption at 281 nm. Below

15 km, the light curve $I(394 \text{ nm})$ displays a strong decrease, indicating that a substantial fraction of the decrease of the light curve at 281 nm is indeed due to something other than SO_2 . Our ISAV 1 analysis with the differential absorption between 394 nm and lower wavelengths represents our best guess to account for the contribution of material other than SO_2 .

One referee (L. Esposito) pointed out a potential shortcoming in our analysis. The SO_2 cross section varies quite rapidly with wavelength, and our spectral bins cover several features (see Figure A1). Therefore one might expect a nonexponential curve of growth for SO_2 , so that more light is transmitted than would be calculated for the average cross section in the band pass. This question is addressed in the appendix: the detailed calculation of the transmission, with a high-resolution spectrum of SO_2 cross section, shows that this effect is negligible at 281 nm; its maximum amplitude is at 306 nm, where the averaging over 12.5 nm of the cross section would yield an underestimate of 10% of the SO_2 concentration for $[\text{SO}_2] = 10 \times 10^{15}$ molecules cm^{-3} , as measured at 13 km for ISAV 1. Therefore, our derived concentrations, based on several λ , (not only at 306 nm), are certainly within $\approx 5\%$ of what would be retrieved if the whole SO_2 structure were used instead of the wavelength bins.

The arguments of Belton [1982] for a possible nonlinear curve of growth for SO_2 , because of saturation of the hundreds of individual narrow lines, were developed for the upper atmosphere of Venus and for the SO_2 atmosphere of I_0 [Bertaux and Belton, 1979]. As shown in the appendix, these arguments are irrelevant for the lower atmosphere of Venus ($z < 54 \text{ km}$).

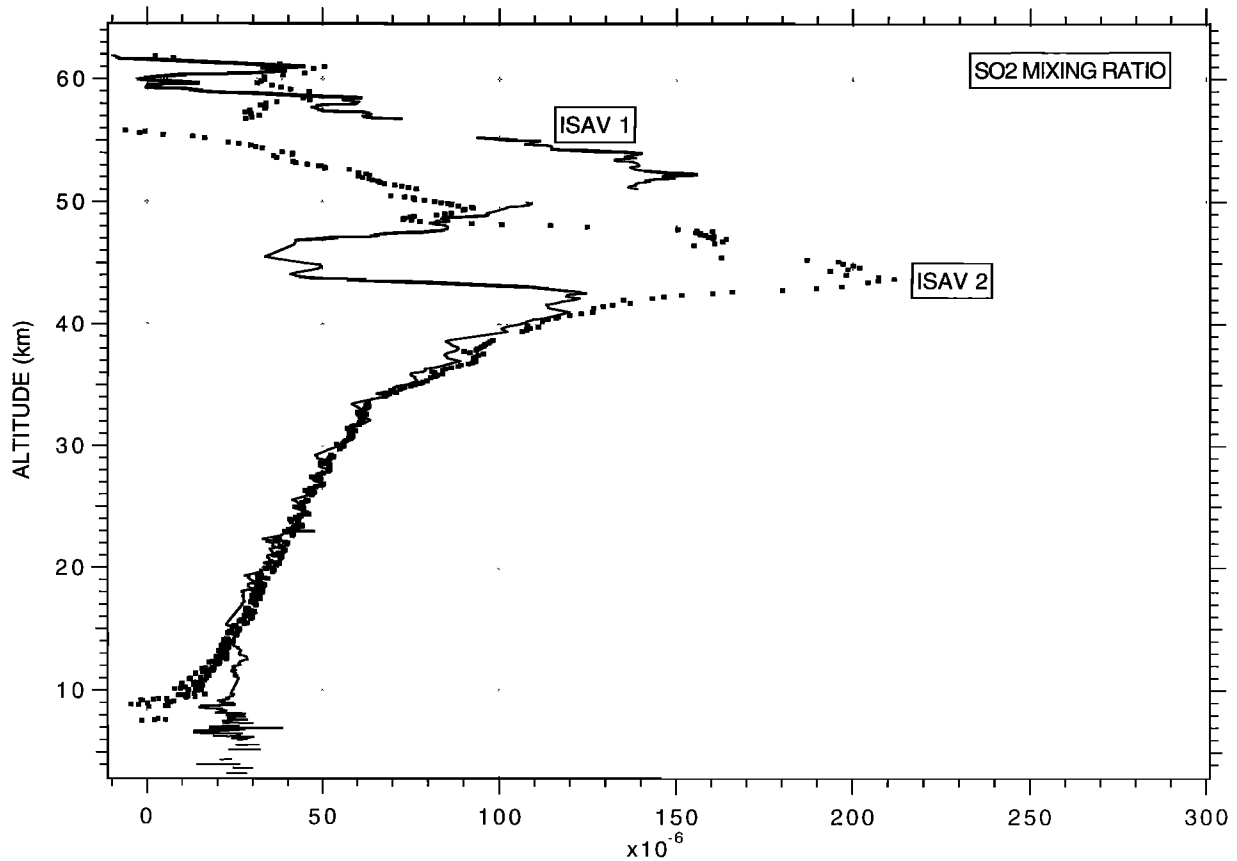


Figure 24. The SO_2 mixing ratio vertical profile retrieved for ISAV 2 (data points) is compared to that determined for ISAV 1. There is a large difference of structure above 40 km, while the profiles are nearly identical below 40 km. A peak of 210 ppm is observed at 43 km in the ISAV 2 data.

Discussion of SO_2 Vertical Profile

Here we concentrate on ISAV 1 data, which show a somewhat more complex structure than ISAV 2.

In order to make a quantitative analysis of the ISAV 1 vertical profile of the SO_2 mixing ratio, we have first eliminated two blocks of five points at 56 and 50 km due to the instrumental “new switch-on effect.” Then we have built a smooth curve $\mu(z)$ to fit the SO_2 data by a series of polynomials (degree 3–5) and resampled every 0.5 km of altitude (Figure 26). This smooth curve was first multiplied by $[M](z)$ to get the absolute concentration $[\text{SO}_2]$, and then integrated to get the SO_2 column density $\int_3^z [\text{SO}_2] dz$ displayed in Figure 27.

Including a small contribution from 0 to 3 km estimated at 5×10^{21} molecules cm^{-2} , we find that the total SO_2 column density in the atmosphere of Venus is 4×10^{22} molecules cm^{-2} , or 4.2 g cm^{-2} of SO_2 , about 5 times less than previously estimated on the basis of earlier data.

A gradient $d\mu/dz$ implies that eddy diffusion will transport SO_2 molecules in the vertical direction. The flux $\phi(\text{SO}_2)$ is

$$\phi(\text{SO}_2) = -K[M] \frac{d\mu}{dz} \quad (12)$$

Values of the eddy diffusion coefficient K are not well known in the lower atmosphere of Venus, but K is probably in the

Table 4. Summary of SO_2 Measurements in the Atmosphere of Venus Below 60 km

Reference	12 km	22 km	42 km	52 km	Instrument, Observations
In situ					
<i>Oyama et al.</i> [1980]		185 ± 43	>176	<600	PV large probe gas chromatograph
<i>Hoffman et al.</i> [1980]		<300		<10	PV large probe mass spectrometer
<i>Gel'man et al.</i> [1979]			130 ± 35 (0–42 km)		Venera 12 lander gas chromatograph
This work					
ISAV 1	25 ± 2	38	125	150	VEGA 1 and 2 lander
ISAV 2	20	38	140	65	UV spectroscopy
Earth based					
<i>Bézar et al.</i> [1993]			130 ± 40 (35–45 km)		IR night spectra
<i>Pollack et al.</i> [1993]			180 ± 70 (37–52 km)		IR night spectra

PV, Pioneer Venus.

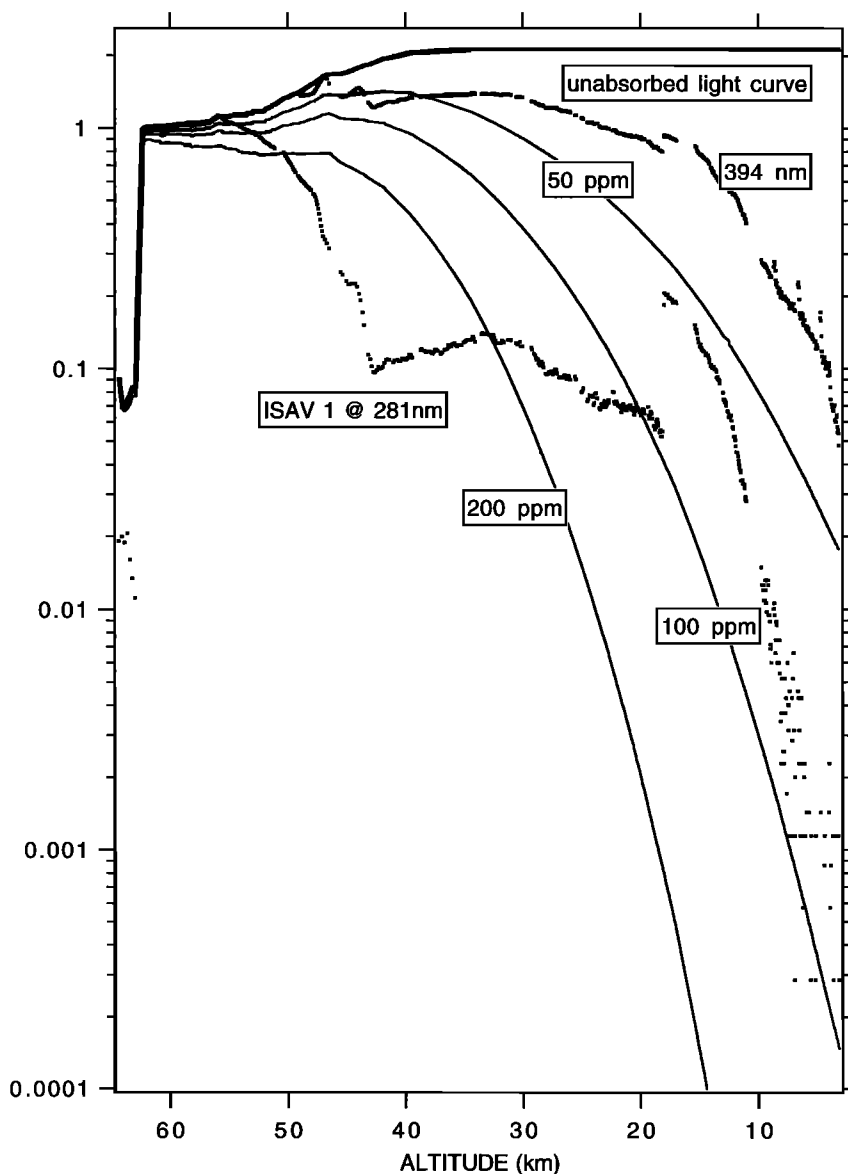


Figure 25. The signal recorded by ISAV 1 at 281 nm (maximum SO_2 absorption) and 394 nm (no SO_2 absorption) are compared on a log scale with a model calculation of how the signal at 281 nm should vary, if only SO_2 were absorbing at 281 nm, for three constant mixing ratios of SO_2 : 50, 100, and 200 ppm. The model assumes that the overall unabsorbed intensity increases, as indicated by the upper solid line. It shows that an extreme upper limit of ≈ 60 ppm of SO_2 at 15–18 km can be derived. Since it is likely that the material absorbing at 394 nm is also absorbing at 281 nm, the real value of SO_2 is below that extreme.

range 10^4 – 10^6 $\text{cm}^2 \text{s}^{-1}$ [Kranospol'sky, 1985]. The flux $\phi(\text{SO}_2)$ is displayed in Figure 28 as a function of altitude, for the lower limit of $K = 10^4$ $\text{cm}^2 \text{s}^{-1}$. The flux is always negative (downward transport) except at the narrow altitude range 43–47 km and above ≈ 53 km.

At 10 km the downward flux is 16×10^{12} molecules $\text{cm}^{-2} \text{s}^{-1}$. Therefore the time to empty the SO_2 column above 10 km would be $t \approx 1.87 \times 10^9$ s, or 60 years (assuming $K = 10^4$ $\text{cm}^2 \text{s}^{-1}$). Neglecting the details of the structure of $\phi(\text{SO}_2)$ below 40 km (which are due to our selection of polynomials), it is found that $\phi(\text{SO}_2)$ is not constant below 40 km. Rather, the flux decreases (in absolute value) when going deeper in the atmosphere. This can only be interpreted as the result of a chemical transformation of SO_2 to another sulfur-bearing chemical species, whose production in the lower atmosphere

(10–40 km) would provoke an upward flux equivalent to the SO_2 downward flux. We note in this respect that the H_2O distributions measured by Moroz [1983] and Moroz *et al.* [1979, 1983] show a behavior similar to our SO_2 vertical profile, the H_2O mixing ratio going down from ≈ 200 ppmv at 50 km to 20 ppmv at 0 km. It is therefore tempting to propose H_2SO_3 or H_2SO_4 as possible gases. However, known thermochemical properties of these gases contradict this hypothesis.

Whatever is the species produced from SO_2 , its rate of formation can be estimated from the divergence of the flux $d\phi(\text{SO}_2)/dz = 1.3 \times 10^7$ molecules $\text{cm}^{-3} \text{s}^{-1}$ averaged in the range 10–40 km. This estimate (to be increased if K were larger than 10^4 $\text{cm}^2 \text{s}^{-1}$) is an important constraint to any thermochemical model of the low atmosphere of Venus. This analysis is also supported by ISAV 2 results.

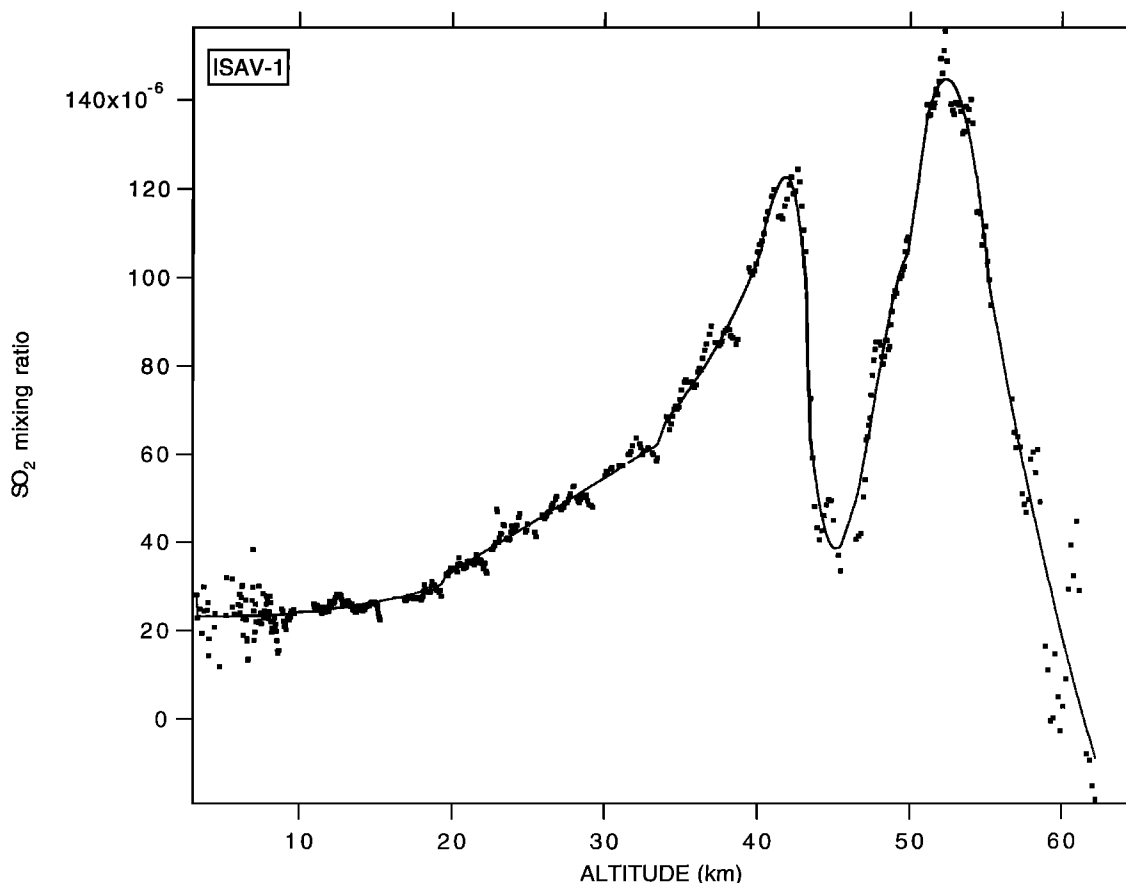


Figure 26. The solid line represents a polynomial fit to the SO_2 mixing ratio $\mu(\text{SO}_2)$ (several polynomials fitting different portions of curves), which is used as a smooth fit to the data, either for integration or for derivation.

Above 40 km altitude, three main regions in ISAV 1 data can be identified as source or sink regions, according to the sign of $d\phi/dz$ ($d\phi/dz > 0$ indicates a source region; $d\phi/dz < 0$ indicates a sink region). The altitude limits of these regions, as can be seen in Figure 28, are as follows.

1. From 41.7 to 44.7 km, a strong source region totaling a production rate of 2.3×10^{14} molecules s^{-1} extends below the classical lower cloud boundary and covers fully our so-called layer d and half of layer c.

2. From 44.8 to 48.8 km, a strong sink region extends, totaling a loss rate of $\approx 2.2 \times 10^{14}$ molecules s^{-1} . It extends from the center of our so-called layer c to the top of our layer b in the lower cloud layer.

3. From 49 to 56.5 km, a source region totaling 0.7×10^{14} molecules s^{-1} (all these estimates depend on the value assumed for K ; here, $10^4 \text{ cm}^2 \text{ s}^{-1}$). This layer is just above our so-called cloud layer b, in the middle cloud layer.

This structure of SO_2 vertical profiles, correlated with the various cloud layers, illustrates the complexity of the SO_2 relationship with the materials of the Venus cloud droplets.

SO_2 : Volcanism and Equilibrium with Surface Minerals

In this section we will discuss briefly the significance of our new value of SO_2 in the lower atmosphere, in the context of volcanism and chemical equilibrium with Venus surface minerals.

Clearly, the arguments that were developed when a value of 180 ppmv in the lower atmosphere (22 km) was believed must

be now revisited with the present ISAV value of 25 ppmv at 10 km. We will rely heavily on the recent and excellent study of *Fegley and Treiman* [1992] on the chemistry of atmosphere-surface interactions on Venus and Mars. On Earth, recent volcanic eruptions are the source of SO_2 in the atmosphere. During major volcanic eruptions on Earth, emission of SO_2 can reach the stratosphere with other volcanic gases and aerosols, where it chemically interacts with stratospheric H_2O to form the Junge layer of H_2SO_4 aerosols droplets at ≈ 22 km. Therefore it is a natural analogy to link the presence of SO_2 in the atmosphere of Venus with volcanic activity on Venus, either presently occurring or very recently having occurred. The questions are, Is the Venus SO_2 of volcanic origin, and if so, When were the latest volcanic episodes?

Two lines of arguments linking SO_2 to volcanism have been developed since the first SO_2 measurements on Venus. Using data from the Pioneer Venus orbiting ultraviolet spectrometer (PVOUVS), *Esposito* [1984] has observed a gradual decrease of n_{SO_2} at the top of the clouds from ≈ 100 ppb at the end of 1978 to ≈ 10 ppb at the end of 1982, along with a slight increase of SO_2 scale height. *Esposito* [1984] has interpreted this rapid diminution of $n_{\text{SO}_2}(z)$ as the consequence of a recent injection of sulfur dioxide into the atmosphere as a result of presently active volcanism. On this subject, ISAV SO_2 measurements, performed well below PVOUVS observations, cannot really be definitive. We note, however, that the highly structured SO_2 vertical profile of mixing ratio found here near 60 km probably

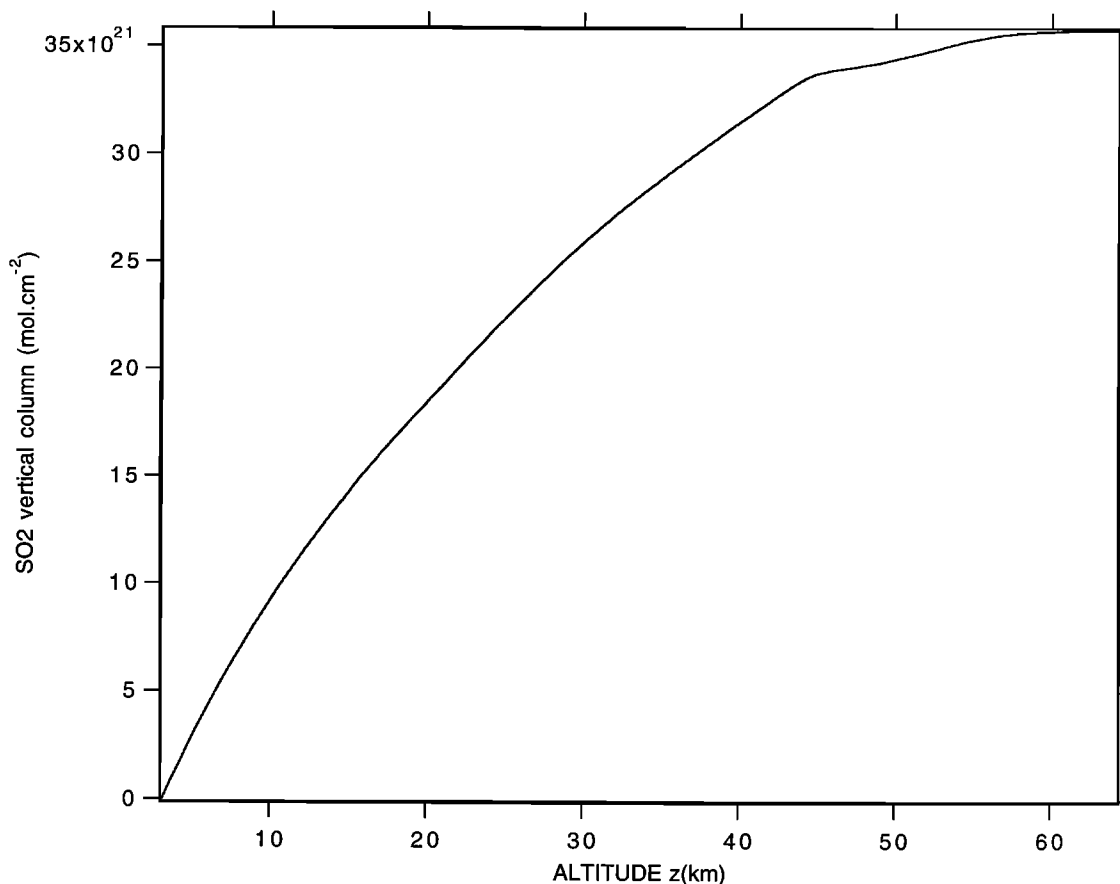


Figure 27. Integrated vertical column density from altitude 3 km up to altitude z , as a function of altitude (molecules cm^{-2}). This curve is derived from the integration of the smooth curve of Figure 18 for ISAV 1 data (after multiplication of atmospheric density). Including a small contribution below 3 km, which can be extrapolated from the graph, the total SO_2 column density is found to be 4×10^{22} molecules cm^{-2} , 5 times lower than previous estimates.

provides room for at least horizontal variations of what can be observed from the top, in the region of photodestruction of SO_2 , as a result of atmospheric dynamics.

The second line of argument concerns the surface reaction between SO_2 , COS, and H_2S , with minerals like pyrite and calcite at a temperature of 740 K, representative of the average of Venus surface (the lowest is the altitude, the highest is the temperature).

The reaction with calcite is, for instance,



for which *Fegley and Treiman* [1992] have measured, in the laboratory, a rate of 4.6×10^{10} SO_2 molecules $\text{cm}^{-2} \text{s}^{-1}$ at 740 K. Early studies of these reactions with minerals [Lewis, 1970] had indicated an SO_2 mixing ratio equilibrium value of about 0.3 ppmv. Therefore the high values of 180 ppmv measured by Pioneer Venus gas chromatograph at 22 km were taken as a proof of a disequilibrium situation, with the large excess of SO_2 in the atmosphere of Venus being attributed to "recent" volcanic injections, maybe not directly in the form of SO_2 , but rather in the form of OCS and H_2S and later transformed to SO_2 [Prinn, 1985].

Our new value of 25 ppmv is much above the range that was at one time believed to be in equilibrium with surface reactions. However, the new study of *Fegley and Treiman* [1992]

indicates that the SO_2 equilibrium value with calcite CaCO_3 and anhydrite CaSO_4 is about 3 ppmv, at 740 K, increasing with temperature T . Therefore, though ISAV values indicate an SO_2 situation much nearer equilibrium than previously believed, it is still $\cong 8$ times higher than that calculated by *Fegley and Treiman* [1992].

It is beyond the scope of this paper to develop a detailed discussion of the chemistry of SO_2 in the lower atmosphere of Venus. However, a few remarks may be of interest here.

1. The SO_2 equilibrium value for reaction (13) depends directly on the mixing ratio of CO at ground level, which has not really been measured near the ground. Therefore, if the CO mixing ratio were higher than assumed by *Fegley and Treiman* [1992], the SO_2 equilibrium mixing ratio would increase accordingly.

2. The presence of a mineral like MgSO_4 on the surface of Venus was discarded by *Fegley and Treiman* on the grounds that it would produce amounts of SO_2 that were too large. However, there would remain the possibility that some quantity of such a material would have been "recently" exposed to the atmosphere, bringing a certain amount of SO_2 in the atmosphere which is now slowly reincorporated into the ground through reaction (13) with calcite. By "recently," we mean some 10^5 – 10^6 years: though the Magellan radar has not seen any trace of presently active volcanism, it is difficult to discard

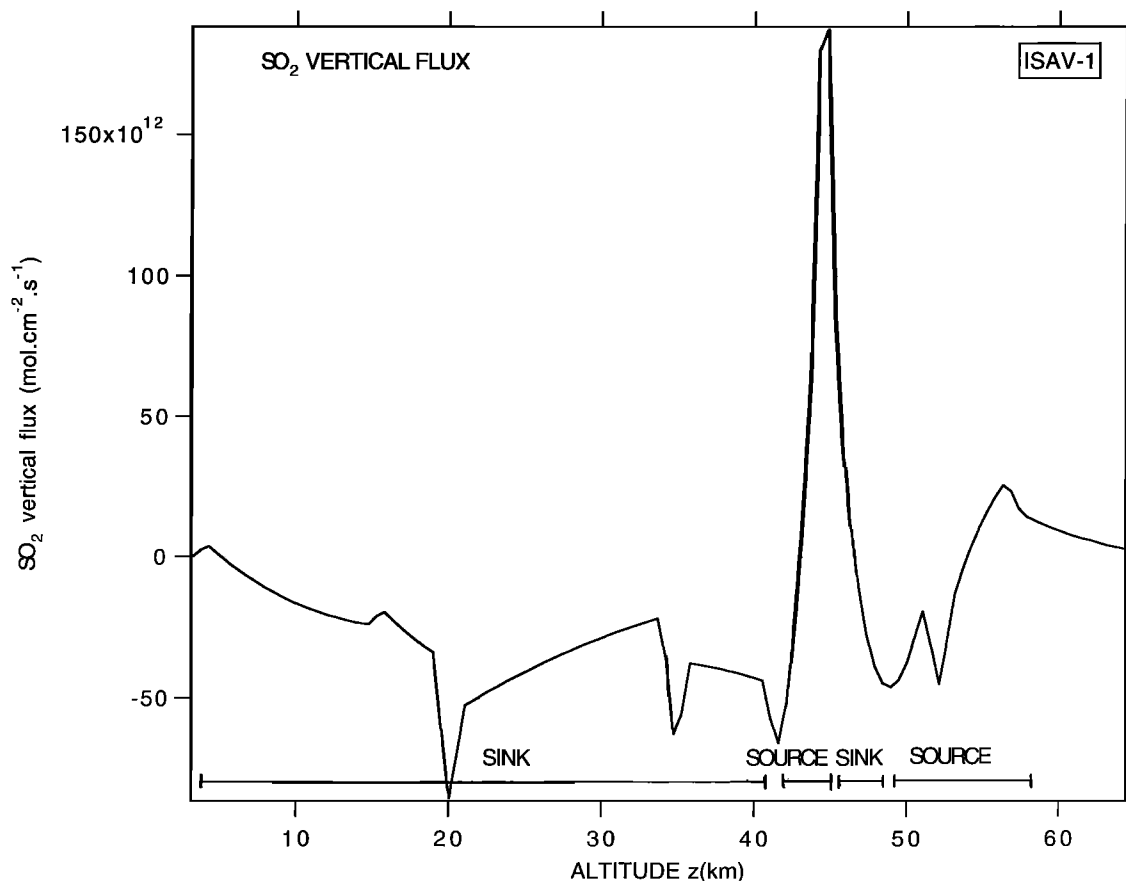


Figure 28. Variation of the SO_2 mixing ratio implies a vertical transport of SO_2 , $\phi(\text{SO}_2) = -K[M]d\mu/dz$, which is represented (solid line) as a function of altitude, for $K = 10^4 \text{ cm}^2 \text{ s}^{-1}$. The fine structure of the curve is an artifact of the polynomial fit, except for the strong peak at 44 km. Four regions where $d\phi/dz$ has a constant sign are identified as source or sink regions, the magnitudes of which correspond to the variation of ϕ between the boundaries of these regions.

the possibility of exposing new material to the surface, through lava flows or through impact cratering in this time frame before present.

3. All reaction rates between SO_2 and minerals are strongly dependent on temperature, and vary with height at the surface Venus. Therefore, the possibility should be considered that the hottest point of Venus, or the coldest point, is controlling the entire SO_2 content of the lower atmosphere. This situation would be somewhat analogous to the distribution of water vapor in the Earth's stratosphere, controlled by the coldest temperature at the tropopause.

4. It is interesting to compare the reaction of SO_2 with calcite estimated by *Fegley and Treiman* [1992], taking into account the distribution of Venus area and temperature: $4.6 \times 10^{10} \text{ molecules cm}^{-2} \text{ s}^{-1}$, with the SO_2 downward flux at 10 km estimated from ISAV measurements at $16 \times 10^{12} \text{ molecules cm}^{-2} \text{ s}^{-1}$ for the lowest range of $K = 10^4 \text{ cm}^2 \text{ s}^{-1}$ and 1.6×10^{15} if $K = 10^6 \text{ cm}^2 \text{ s}^{-1}$. Clearly, downward transport is not a limiting factor for the progressive fixation of SO_2 in the minerals of Venus. Since the calcite reaction (13) can accommodate $4.6 \times 10^{10} \text{ molecules cm}^{-2} \text{ s}^{-1}$, the time required to completely empty the SO_2 atmospheric content would be 27×10^3 years if calcite were present everywhere. Therefore the presence of SO_2 and associated ubiquitous cloud cover may be only a transient phenomenon in the life of Venus, triggered by

rare episodes of volcanic activity or impact cratering revealing sulfur-rich material at the surface.

Our SO_2 lifetime of 27×10^3 years is much shorter than the value estimated earlier by *Fegley and Prinn* [1989] of 1.9 m.y. The difference arises, first, because our total SO_2 column is 5 times less than previously estimated, and second, because they have estimated that calcite would be present only on a small fraction of the surface of Venus ($\cong 8\%$). In such a likely case, the SO_2 lifetime would instead be about 3×10^5 years. Since the rate of reaction (13) is very much temperature dependent, the actual distribution of calcite is quite important.

9. Conclusion

In this paper we have presented the data obtained at high vertical resolution with ISAV 1 and ISAV 2 on the in situ absorption of the atmosphere of Venus. In our minds, the most important result is the lower than previously thought SO_2 mixing ratio in the lower atmosphere, a result related to the existence of clouds. If indeed, reaction with calcite is the dominating one at ground level, it appears that the SO_2 should disappear quickly (a few 10^5 years), unless there is a replenishment catastrophic mechanism: volcanoes or impact cratering, or a constant crustal outgassing of OCS , S_2 , and H_2S coming from pyrite FeS_2 .

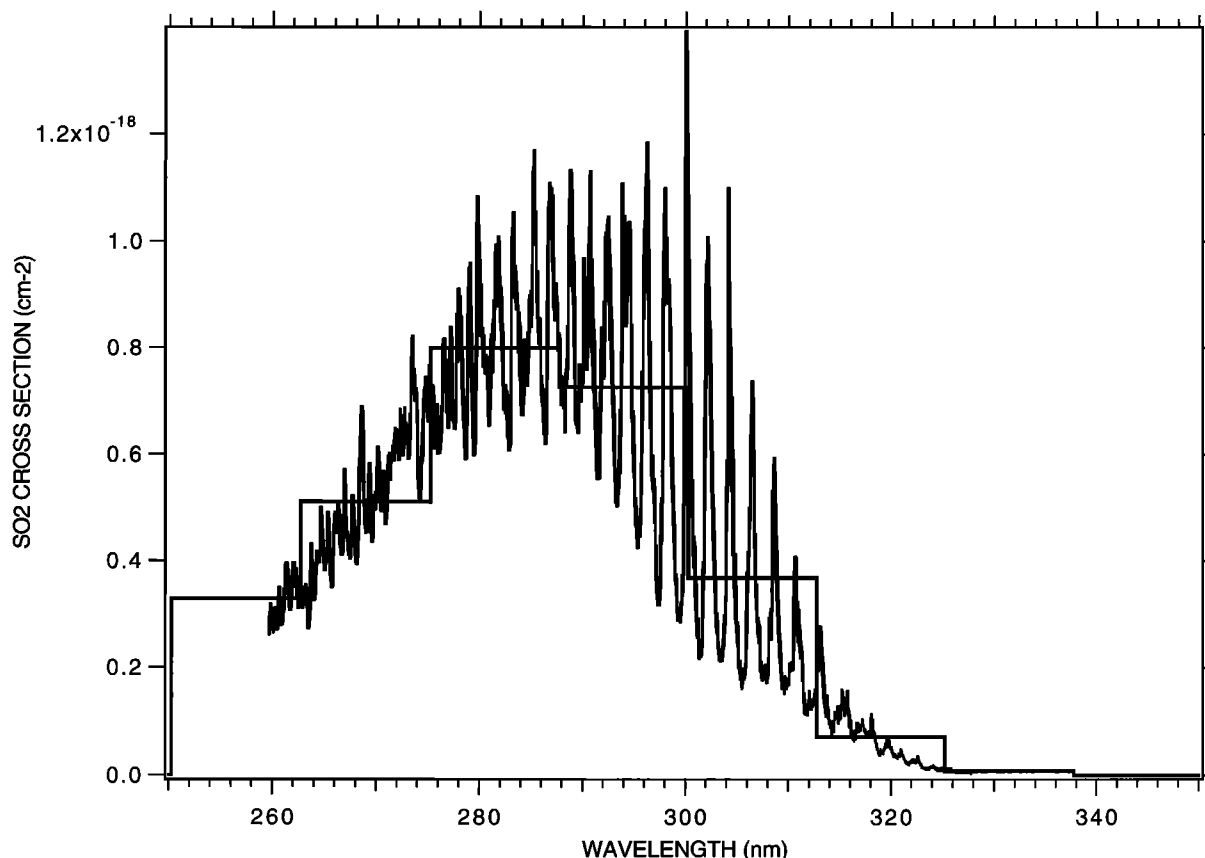


Figure A1. High-resolution cross section of SO₂ between 260 and 328 nm measured by UV Fourier transform spectroscopy at $T = 296$ K. Cross sections have been averaged in 12.5-nm spectral bins corresponding to ISAV.

In the course of this analysis, we had to make some assumptions, which could be criticized or questioned. However, we felt an obligation to the scientific community to present the details of the measurements obtained with ISAV 1 and ISAV 2, along with a comprehensive data analysis scheme, because of the uniqueness of this type of measurement with “active spectroscopy.” Indeed, there is at present no possibility to repeat this kind of measurement in the foreseeable future. We felt confident in our analysis and the underlying assumptions, both by the general consistency of ISAV 1 and ISAV 2 results, and by the remarkable agreement with SO₂ measurements obtained from ground-based observations in the range 35–45 km.

If some reader would be interested in personally testing the ISAV data with other sets of assumptions, we would be glad to communicate the data on the basis of a sort of “guest investigator” program.

Appendix

Here we address following question. Because of the fine structure with a wavelength characteristic scale of 2 nm of SO₂ cross section in the UV, the modeled transmission of a parcel of gas will be different if the true SO₂ fine structure is taken into account or if the SO₂ cross section is averaged over bins of 12.5 nm, as was done in the present ISAV analysis.

In Figure A1 is plotted the detailed cross section of SO₂, with an overlay of the cross sections σ_m averaged over bins of 12.5 nm. The high-resolution measurements were made with a

UV Fourier transform spectrometer at $T = 296$ K and a pressure of 1.02 hPa [Vandaele *et al.*, 1994]. In Figure A2 are compared, for five wavelengths, the results of two different computations, when n_{SO_2} is varied: first, the calculated transmission with the average cross section σ_m , (solid lines),

$$T = \exp(-n_{\text{SO}_2} L \sigma_m)$$

where $L = 170$ cm is the path length of the ISAV cell, and second, the transmission calculated with the same quantity of SO₂, for all wavelengths, and then averaged over the 12.5-nm bins (symbols),

$$T_{\text{moy}} = \frac{1}{12.5} \int \exp[-\sigma(\lambda) n_{\text{SO}_2} L] d\lambda$$

at points every $2 \times 10^{15} \text{ cm}^{-3}$. The curve at 306 nm is where there is the largest difference between solid points and the approximate calculation of the solid curve (something which could be predicted by examining Figure A1). For a density of $1.2 \times 10^{16} \text{ cm}^{-3}$, the exact transmission is 0.515, and the same value of the transmission is found on the approximate curve for a density of $1.07 \times 10^{16} \text{ cm}^{-3}$.

The difference of density for the same transmission is even smaller for wavelength bins 294 and 281 nm, which are the ones with the largest weight in our retrieval of SO₂. Therefore the SO₂ densities retrieved with averaged cross sections in the present paper cannot be underestimated by more than $\approx 5\%$ by the saturation effect of large- σ spikes.

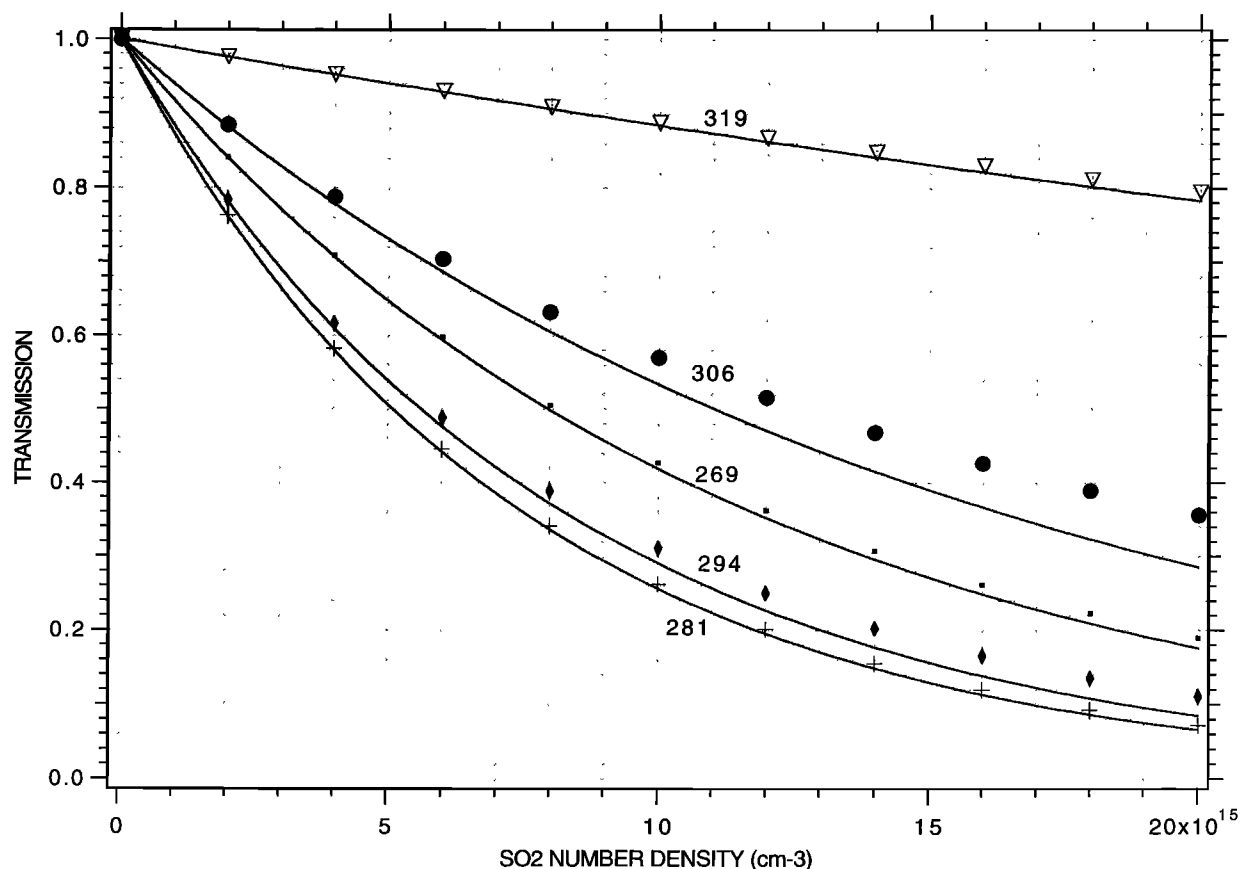


Figure A2. UV transmission at various wavelengths computed for the ISAV path length of $L = 170$ cm for various SO_2 concentrations experienced by ISAV. Computations were made with averaged cross sections of Figure A1 (solid lines with wavelength indicated), or with the full detailed spectrum of Figure A1 and then by averaging the transmission over the 12.5-nm line (solid points). The largest difference occurs for 306 nm, yielding a slight underestimate of SO_2 concentration by using binned cross sections.

In the present analysis, the SO_2 cross sections were those measured at room temperature, while the Venus temperature is constantly increasing with decreasing altitude, reaching 300 K at 55 km. To our knowledge, there are no measurements of SO_2 cross sections at higher temperatures relevant to the lower atmosphere of Venus. However, there were measurements between 200 and 300 K [Hicks *et al.*, 1979], showing an increase of cross sections at all wavelengths between 281 and 313 nm, by a factor varying from 2 to 6 from cold to warm temperatures. The factor is larger for small cross sections than for large cross sections. Therefore the contrast of the cross section decreases with temperature increase, making the problem addressed above less and less critical when altitude decreases. In addition, our choice of 296 K cross sections is likely to yield an overestimate of SO_2 densities in the lower atmosphere, rather than an underestimate. If the increased rate of SO_2 cross section experienced between 200 and 300 K was the same above 300 K, it would mean that the mixing ratio found in the lower atmosphere would have to be lowered, possibly down to the point of equilibrium with calcite, namely, 3 ppm at 740 K.

Belton [1982] questioned the validity of the Beer Lambert law for SO_2 in the UV (the absorption is computed as for continuum) on the ground that each of the 2-nm spectral features of SO_2 (Figure A2) is, in fact, made up of a large number of individual lines, very narrow, which may saturate. His work was stimulated by the problem of SO_2 on Io [Bertaux

and Belton, 1979] and SO_2 in the upper atmosphere of Venus, as can be observed from outside. His objection is perhaps valid for these conditions, but because of the high pressure and high temperature of the lower atmosphere of Venus, it is not relevant to ISAV measurements. Belton [1982] quotes a pressure/temperature effect for the linewidth a_L of individual lines of

$$\alpha_L = 0.28 \pm 0.13p \left(\frac{T}{300}\right)^{1/2} \text{ cm}^{-1}$$

while the mean spacing between individual lines is $d = 0.15 \text{ cm}^{-1}$. Therefore $\alpha_L > \delta$ everywhere below the altitude of 54 km in the atmosphere of Venus, and the Beer Lambert law may be used confidently.

Acknowledgments. This work was supported by the French Centre National d'Etudes Spatiales, the INSU-CNRS Programme National de Planétologie, the former Academy of Sciences of USSR, and the Academy of Sciences of Russia. We wish to thank the technical team at Service d'Aéronomie du CNRS who built the instrument: Bernard Mege, Gilbert Souchon, Christian Taulemesse, Jacques Porteneuve, and Michel Leclère. We thank Jean Claude Lebrun for data management. We would like also to recognize the huge task performed at IKI (Moscow) and in Frundze (now Bishkek in Kirgistan), under the direction of Sultan Tabaldaev. We also are indebted to Eric Chassefière for useful scientific discussions, Sylvie Mascle for fruitful discussions on the singular value decomposition method, Alain Abergel for participation in the early phases of this project, and Marie-Françoise

Leveau for typing the many successive versions of the paper. Finally, we wish to acknowledge very useful remarks of referees Larry Esposito and Vladimir Krasnopolsky, and stimulating discussions with Bruce Fegley. Most of the analysis was made on a MacIntosh with IGOR commercial software.

References

- Allen, D. A., and J. W. Crawford, Cloud structure on the dark side of Venus, *Nature*, 307, 222–224, 1984.
- Andreychikov, B. M., Chemical composition and structure of the clouds of Venus inferred from the results of X-ray fluorescent analysis on descent probes VEGA 1 and 2 (in Russian), *Kosm. Issled.*, 25, 721–736, 1987. (*Cosmic Res.*, Engl. Transl., 25, 568, 1987.)
- Andreychikov, B. M., O. K. Akhmetshin, B. N. Korchuganov, L. M. Mukhin, B. T. Ogorodnikov, I. V. Peterianov, and V. I. Skitovich, X-ray radiometric analysis of aerosols in Venusian clouds aboard VEGA 1 and VEGA 2 (in Russian), *Kosm. Issled.*, 25, 721–736, 1987. (*Cosmic Res.*, Engl. Transl., 25, 554, 1987.)
- Barker, E. S., Detection of SO₂ in the UV spectrum of Venus, *Geophys. Res. Lett.*, 6, 117–120, 1979.
- Belton, M. J. S., An interpretation of the near-ultraviolet absorption spectrum of SO₂: Implications for Venus, Io, and laboratory measurements, *Icarus*, 52, 149–165, 1982.
- Bertaux, J. L., and M. J. S. Belton, Evidence of SO₂ on Io from UV observations, *Nature*, 282, 813–814, 1979.
- Bertaux, J. L., et al., Active spectrometry of the ultraviolet absorption within the Venus atmosphere, *Sov. Astron. Lett.*, 12, 78–84, 1986.
- Bertaux, J. L., et al., Study of the absorption of ultraviolet radiation in the atmosphere of Venus on the descending spacecraft VEGA 1 and VEGA 2 (in Russian), *Kosm. Issled.*, 25(5), 691–706, 1987. (*Cosmic Res.*, Engl. Transl., 25(5), 528, 1987.)
- Bézar, B., C. de Bergh, B. Fegley, J. P. Maillard, D. Crisp, T. Owen, J. B. Pollack, and D. Grinspoon, The abundance of sulfur dioxide below the clouds of Venus, *Geophys. Res. Lett.*, 20(15), 1587–1590, 1993.
- Carlson, R. W., et al., Galileo infrared imaging spectroscopy measurements at Venus, *Science*, 253, 1541–1548, 1991.
- Crisp, D., Radiative forcing of the Venus mesosphere, I, Solar fluxes and heating rates, *Icarus*, 67, 484–514, 1986.
- Deryugin, V. A., V. P. Dolgoplov, V. P. Karyagin, V. M. Kovtunenkov, R. S. Kremnev, K. M. Pichkhadze, G. N. Rogovskii, and R. Z. Sagdeev, VEGA 1 and VEGA 2 spacecraft: Operation of landers in Venusian atmosphere (in Russian), *Kosm. Issled.*, 25(5), 649–654, 1987. (*Cosmic Res.*, Engl. Transl., 25(5), 494, 1987.)
- Ekonomov, A. P., B. E. Moshkin, V. I. Moroz, Y. M. Golovin, V. I. Gnedykh, and A. V. Grigorev, UV photometry experiment on descent probes Venera 13 and Venera 14 (in Russian), *Kosm. Issled.*, 21, 254–268, 1983. (*Cosmic Res.*, Engl. Transl., 21, 554, 1983.)
- Ekonomov, A. P., V. I. Moroz, B. E. Moshkin, V. I. Gnedykh, Y. M. Golovin, and A. V. Grigorev, Scattered UV solar radiation within the clouds of Venus, *Nature*, 307, 345–346, 1984.
- Esposito, L. W., Sulfur dioxide: Episodic injection shows evidence for active Venus volcanism, *Science*, 223, 1072–1074, 1984.
- Fegley, B., Jr., and R. G. Prinn, Estimation of the rate of volcanism on Venus from reaction rate measurements, *Nature*, 337, 55–58, 1989.
- Fegley, B., Jr., and A. H. Treiman, Chemistry of atmosphere-surface interactions on Venus and Mars, in *Venus and Mars: Atmospheres, Ionospheres and Solar Wind Interactions*, *Geophys. Monogr.*, vol. 66, edited by J. Luhmann, M. Tatrallyay, and R. Pepin, pp. 7–71, AGU, Washington, D. C., 1992.
- Gel'man, B. G., V. G. Zolotukhin, L. M. Mukhin, N. I. Lamonov, B. V. Levchuk, D. F. Nenarokov, B. P. Okhotnikov, V. A. Rotin, and A. N. Lipatov, Gas chromatograph analysis of the chemical composition of the Venus atmosphere, *Space Res.*, 20, 219, 1979.
- Gnedykh, V. I., L. V. Zasova, V. I. Moroz, B. E. Moshkin, and A. P. Ekonomov, Vertical structure of the Venus cloud layer at the VEGA 1 and VEGA 2 landing points (in Russian), *Kosm. Issled.*, 25(5), 707–714, 1987. (*Cosmic Res.*, Engl. Transl., 25, 542, 1987.)
- Hapke, B., and F. Graham, Disulfur monoxide and the spectra of Venus and Io (abstract), *Lunar Planet. Sci.*, XVI, 316–317, 1985.
- Hapke, B., and R. Nelson, Evidence for an elemental sulfur component of the clouds from Venus spectrophotometry, *J. Atmos. Sci.*, 32, 1212–1218, 1975.
- Hartley, K. H., A. R. Wolff, and L. D. Travis, Croconic acid: An absorber in the Venus clouds?, *Icarus*, 77, 382–390, 1989.
- Hicks, E., B. Leroy, P. Rigaud, J. L. Jourdain, and G. Le Bras, Spectres d'absorption dans le proche UV et le visible des composés minoritaires atmosphériques NO₂ et SO₂ entre 200 and 300 K, *J. Chim. Phys.*, 76, 693–698, 1979.
- Hoffman, J. H., R. R. Hodges Jr., T. M. Donahue, and M. B. McElroy, Composition of the Venus lower atmosphere from the Pioneer Venus mass spectrometer, *J. Geophys. Res.*, 85, 7882–7890, 1980.
- Kamp, L. W., and F. W. Taylor, Radiative transfer models of the nightside of Venus, *Icarus*, 86, 510–529, 1990.
- Knollenberg, R. G., A reexamination of the evidence for large, solid particles in the clouds of Venus, *Icarus*, 57, 161–183, 1984.
- Knollenberg, R. G., and D. M. Hunten, The microphysics of the clouds of Venus: Results of the Pioneer Venus Particle Size Spectrometer Experiment, *J. Geophys. Res.*, 85, 8039–8058, 1980.
- Krasnopolsky, V. A., *Photochemistry of the Atmospheres of Venus and Mars*, Springer-Verlag, New York, 1985.
- Krasnopolsky, V. A., VEGA mission results and chemical composition of Venus clouds, *Icarus*, 80, 202–210, 1989.
- Krasnopolsky, V. A., and J. B. Pollack, H₂O-H₂SO₄ system in Venus' clouds and OCS, CO, and H₂SO₄ profiles in Venus' troposphere, *Icarus*, 109, 58–78, 1994.
- Lewis, J. S., Venus: Atmospheric and lithospheric composition, *Earth Planet. Sci. Lett.*, 10, 73–80, 1970.
- Linkin, V. M., et al., Thermal structure of the atmosphere of Venus from the results of measurements taken by landing vehicle Vega 2 (in Russian), *Kosm. Issled.*, 25, 659–672, 1987. (*Cosmic Res.*, Engl. Transl., 25, 501–512, 1987.)
- Moroz, V. I., Summary of preliminary results of the Venera 13 and 14 missions, in *Venus*, edited by D. M. Hunten, T. M. Donahue, and V. I. Moroz, pp. 45–68, Univ. of Ariz. Press, Tucson, 1983.
- Moroz, V. I., Scientific results from the VEGA mission (in Russian), *Kosm. Issled.*, 25(5), 643–648, 1987. (*Cosmic Res.*, Engl. Transl., 25(5), 489, 1987.)
- Moroz, V. I., N. A. Parfen'ev, and N. F. San'ko, Spectrophotometric experiment on the Venera 11 and 12 descent modules, 2, Analysis of Venera 11 spectra by layer-addition method, *Cosmic Res.*, 17, 601–614, 1979.
- Moroz, V. I., A. P. Ekonomov, Yu. M. Golovin, B. E. Moshkin, and N. F. San'ko, Solar radiation scattered in the Venus atmosphere: The Venera 11, 12 data, *Icarus*, 53, 509–537, 1983.
- Moroz, V. I., A. P. Ekonomov, B. E. Moshkin, H. E. Revercomb, L. A. Stromovsky, J. T. Schofield, F. W. Taylor, and M. G. Tomasko, Solar and thermal radiation in the Venus atmospheres, *Adv. Space Res.*, 5, 197–232, 1985.
- Moshkin, B. E., V. I. Moroz, V. I. Gnedykh, A. V. Grigorev, L. V. Zasova, and A. P. Ekonomov, Vega 1, 2 optical spectrometry of Venus atmospheric aerosol at the 60–30 km levels: Preliminary results (in Russian), *Pis'ma Astron. Zh.*, 12, 85–93, 1986. (*Sov. Astron. Lett.*, Engl. Transl., 12, 36, 1986.)
- Oyama, V. I., G. C. Carle, F. Woeller, J. B. Pollack, R. T. Reynolds, and R. A. Craig, Pioneer Venus gas chromatography of the lower atmosphere of Venus, *J. Geophys. Res.*, 85, 7891–7902, 1980.
- Pollack, J. B., O. B. Toon, R. C. Whitten, R. Boese, B. Ragent, M. G. Tomasko, L. W. Esposito, L. D. Travis, and D. Wiedman, Distribution and source of the UV absorption in Venus atmosphere, *J. Geophys. Res.*, 85, 8141–8150, 1980.
- Pollack, J. B., et al., Near-infrared light from Venus' nightside: A spectroscopic analysis, *Icarus*, 103, 1–42, 1993.
- Porshnev, N. V., L. M. Mukhin, B. G. Gelman, D. F. Nenarokov, V. A. Rotin, A. V. Dyachkov, and V. B. Bondarev, Gas-chromatographic analysis of products of the thermochemical processing of aerosols in the Venus clouds on VEGA 1 and 2 probes (in Russian), *Kosm. Issled.*, 25, 715–720, 1987. (*Cosmic Res.*, Engl. Transl., 25, 549–553, 1987.)
- Prinn, R. G., *The Photochemistry of the Atmosphere of Venus*, in *The Photochemistry of Atmospheres*, edited by J. S. Levine, pp. 281–336, Academic, San Diego, Calif., 1985.
- Ragent, B., and J. Blamont, Structure of the clouds of Venus: Results of the Pioneer Venus nephelometer experiment, *J. Geophys. Res.*, 85, 8089–8105, 1980.
- Titov, D. V., On the possibility of aerosol formation by the reaction between SO₂ and NH₃ in the atmosphere of Venus, *Cosmic Res.*, 21, 401, 1983.
- Tomasko, M. G., L. R. Doose, P. H. Smith, and A. P. Odell, Measurements of the flux of sunlight in the atmosphere of Venus, *J. Geophys. Res.*, 85, 8167–8186, 1980.

- Toon, O. B., R. P. Turco, and J. B. Pollack, The ultraviolet absorber on Venus: Amorphous sulphur, *Icarus*, 51, 358–373, 1982.
- Toon, O. B., B. Ragent, D. Colburn, J. Blamont, and C. Cot, Large, solid particles in the clouds of Venus: Do they exist?, *Icarus*, 57, 143–160, 1984.
- Vandaele, A. C., P. C. Simon, J. M. Guilmot, M. Carleer, and R. Colin, *J. Geophys. Res.*, 99, 25,599–25,605, 1994.
- Weitz, C. M., and A. T. Basilevsky, Magellan observations of the Venera and Vega landing site regions, *J. Geophys. Res.*, 98(E9), 17,069–17,097, 1993.

J.-L. Bertaux, A. Hauchecorne, and T. Widemann, Service d'Aeronomie du CNRS, B.P. 3, F-91371 Verrières-le-Buisson, France.
A. P. Ekonomov and V. I. Moroz, Space Research Institute, Prof-soyouzraya 88, Moscow 117810, Russia.

(Received May 8, 1995; revised January 23, 1996;
accepted January 30, 1996.)